N83-22086

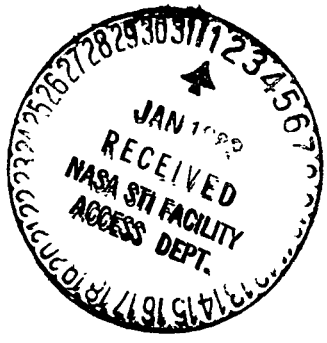

MCR-82-626
Contract NASw-3108

Final
Report November 1982

COMET COMPOSITION AND DENSITY ANALYZER

Prepared by

Benton C. Clark
Senior Research Scientist
Payloads, Sensors, and Instruments

MARTIN MARIETTA AEROSPACE
DENVER AEROSPACE
P. O. Box 179
Denver, Colorado 80201

X-RAY COMPOSITION ANALYZER FOR COMET MISSIONS

Final Report

August 1982

Prepared by:
Benton C. Clark

With Contributions by
B.J. Cook

Martin Marietta Corporation
P.O. Box 179
Denver, CO 80201

This work was performed for the National Aeronautics and Space Administration under contract NASw-3108.

Table of Contents

I. INTRODUCTION

This study was begun in response to more general studies sponsored by the National Aeronautics and Space Administration into deep-space missions to selected comets. Scientific investigation of cometary objects is of exceeding interest because of the assumed role of such bodies in planetesimal evolution, and in particular their contribution of volatile-rich materials during late-stage accretion of the planets. As singled out by the Comet Science Working Group, the measurement of the chemical composition of the cometary nucleus ranks in the highest priority of experiments for such missions.

In the following studies, we have sought by laboratory experimentation and concept analysis to arrive at an experiment of demonstratable practicality, yet with performance at accuracy and sensitivity levels adequate to make sophisticated distinctions between cometary material and other extraterrestrial materials (meteorite suites and stratospherically-captured cosmic dust). Much of this work involves the technique of x-ray fluorescence (XRF) for analysis of elemental composition. Concomitant with these investigations, we have solved the problem of collecting representative samples of comet dust (for rendezvous missions), and also evaluated several related techniques such as mineralogic analysis (x-ray diffraction), direct analysis of the nucleus without docking (electron macroprobe), dust flux rate measurement, and test sample preparation. An explicit experiment concept based upon x-ray fluorescence analysis of biased and unbiased sample collections has been scoped and proposed for a future rendezvous mission with a short-period comet.

Toward the end of this study, the emphasis was shifted to include certain engineering and scientific aspects of a time-of-flight mass spectrometer analysis of ions extracted from the plasma cloud of high-speed particle impact events. These studies pertain to future Comet Halley fast-encounter missions.

Two New Technology Disclosures were written as a result of these studies and are also described within this report.

II. STUDIES

A. X-ray Techniques for Composition and Density Analysis

Background. X-ray fluorescence spectroscopy is a commonly used laboratory method for determining the elemental composition of samples. Typically, a sample is irradiated with x-rays produced by a radioisotope source or x-ray tube, causing electrons to be ejected from one of the inner shells of atoms in the sample. As electrons drop from outer shells to fill the vacancies, they emit fluorescent x-rays at discrete energies characteristic of the elements in the sample. These fluorescent x-rays are then analyzed by an energy-sensitive detector.

Although laboratory equipment is usually large and heavy, the fundamental geometrical arrangement is quite simple, as can be seen in Figure A-1. None of the angles or distances are critical, but for the best analytical accuracy they should be kept constant. Certain other factors of geometry are important to minimize the amount of scattered radiation reaching the detector; collimators and sample holder must be given careful consideration to prevent interfering secondary fluorescences. Even trace elements in these materials can affect the performance of the system.

Note that the physical state of the sample is of little or no importance. Thus, liquids and even gases can be analyzed via the fluorescence of constituent atoms. Cross-sections of the more tightly bound electrons are larger than outer shell electrons, so that the stronger x-ray emissions are the K lines (from K-shell ejections), then L lines (L shell electrons), and then M lines. Absorption phenomena usually dictate the use of K lines for elements in the first third of the Periodic Table, and then L lines for the remaining elements. In these cases, the energy of the x-ray is typically much higher than inter- and intra- molecular bonding energies, so that neither the chemical nor the physical state affects the x-ray fluorescent emission energies to a discernable degree; neither is the cross-section importantly affected, so that both identification and quantification of the constituent elements is unambiguous. This property of fluorescence analysis has the advantage that bulk elemental composition can be determined with little or no

PRINCIPLE OF OPERATION

X-ray Fluorescence

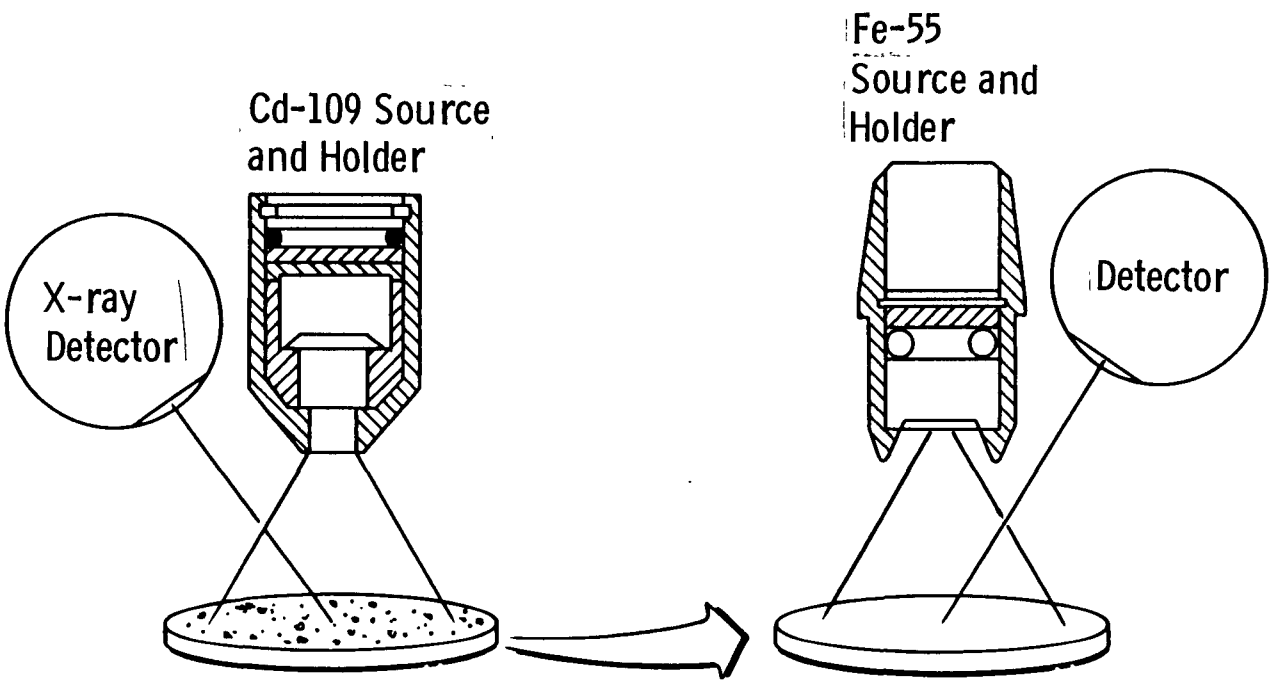

Figure A-1
X-Ray Analysis Technique

sample preparation or characterization by other techniques. On the other hand, it entails the disadvantage that little or nothing can be learned about the chemical state of the elements present. For this, other techniques such as x-ray diffraction, optical and electron microscopy, or microprobe analysis are necessary.

Excitation Methods. It was decided early on in the course of this study that three types of sources should be considered for achieving excitation of the fluorescence response. These three types are x-ray tubes, radioisotope sources, and electron beams. As will be seen in the discussion which follows, the radioisotopes allow quite adequate analytical capability for the problem at hand, and do not entail the requirements for high voltage power supplies, filaments, and filament power supplies as do the x-ray tube and electron gun. They are thus simpler to implement. The chief drawback of the isotope sources is that their excitation flux is generally much lower, so that the intensity of fluorescent x-rays generated is much less. For comet missions, this is of no particular detriment since analysis times of hours to even several days would be considered acceptable in view of the long-term nature of the mission itself. A limiting factor would be signal-to-background ratio, i.e., the counting rate in the detector of fluorescent x-rays relative to the spectrum and counting rate of cosmic ray interaction events. This can be adjusted by raising the source strength to sufficiently high levels that the cosmic-induced background is either negligible or calibratable compared to sample signals. Another way by which signal can be raised is to increase the amount of sample collected. Good signal-to-background is, in practice, readily achievable since background counting rates for the smaller detectors are less than 1 count per second.

X-ray Tube Excitation. Miniature x-ray tubes are now available with typical dimensions of 5 cm long by 2 cm diameter. Once they are packaged within a shielded case with high voltage connector and "miniature" high voltage power supply, the overall device assembly is typically 15 x 15 x 7 cm and weighs over one kilogram. Compared to radioisotope excitation assemblies, they are thus much larger, heavier and more complicated. The potential advantages are (1) a much higher flux, permitting very rapid analysis (seconds, compared to

hours), and (2) versatility in the selection of source energies. The latter is possible by using secondary targets, where primary x-rays from the tube target are projected not at the sample but rather at a second target. Fluorescent x-rays from the second target are then used as the excitation source for the sample. Since the secondary target can be any element or combination of elements desired, it becomes feasible to precisely select the optimum excitation for various groups of elements in the sample. X-ray tubes can also be used to produce a beam of polarized x-rays which, when employed in the optimal viewing geometry, can reduce the background interference from x-rays Compton-scattered from the sample. The method for producing the polarized beam (crystal diffraction at 45^{o} incidence) results in an output flux considerably weaker than the fluxes from radioisotope sources. As will be seen in the following sections, a comet mission is compatible with the use of the weaker, but simpler isotope sources. X-ray tubes are certainly feasible, but not required to meet scientific objectives of this mission.

Electron Beam Excitation. X-ray fluorescence analysis of samples is often done in the laboratory by exciting the surface of the sample with a high-energy electron beam. This method is particularly useful for determining the element composition of small samples, such as mineral grains. The laboratory instruments used are the scanning electron microscope (SEM) and the electron microprobe. In principle, it is within the realm of possibility to miniaturize such instruments for space application. At least two separate proposals for miniature SEM's, one by Albee et. al. and another by King et. al., were submitted to NASA in 1980, in response to the Announcement of Opportunity for International Comet Mission. We provided certain technical input to these proposals. The chief advantage of the SEM approach is that compositional heterogeneity on the microscale can be studied. Mineralogic make-up might be inferred if it turned out that comet dust is composed of a variety of minerals, such as olivine, metallic, and sulfide grains. Also, very small quantities of comet dust (theoretically, down to a single grain) can be analyzed. On the other hand, a significant disadvantage is that the accuracy of elemental analysis is typically less for electron excitation of grains than for X-ray excitation of a bulk sample. This is of extreme importance when attempting to diagnose departure from primitive nebular concentration of the elements or classifying the material chemically with

respect to the known meteorite classes. Furthermore, the SEM analysis of small grains is unlikely to be successful in detecting the presence of a number of scientifically interesting trace elements.

Apart from microbeam analysis of collected grains, there is another potential application of electron-beam excited X-ray fluorescence. This would be for direct analysis of the nucleus itself by directing a high-powered beam from the spacecraft itself to the nucleus. We call this scheme the "electron macroprobe".

Radioisotope Source Excitation. Most radioactive isotopes can stimulate x-ray emission, but for greatest yield, lowest background, and for radiation safety reasons, the best excitation source for elements above sodium are electron capture (EC) isotopes. These isotopes decay via removal of an electron from inner shall into the nucleus, thereby creating a vacancy whose subsequent filling is attended by emission of a fluorescent x-ray. These x-rays may then be used to create vacancies, via the photoelectric effect, in the material being irradiated, resulting in x-ray fluorescence of the material. To stimulate fluorescence, the impinging x-ray must be of an energy higher than the binding energy of the electron in its shell - these critical energies are called the "absorption edges". Ideally, for greatest sensitivity and accuracy, there would be a large number of excitation sources, each with an emission energy optimum for exciting one to three neighboring elements. Unfortunately, the available isotopes are dictated by the physics of the nucleus, and only a few suitable EC isotopes exist. For analysis of comet dust, the isotopes of choice are cadmium-109 and iron-55.

For sodium and other elements below sodium in the periodic table, none of the EC sources are satisfactory. Fortunately, light elements can be stimulated very readily by heavy ionizing particles, such as alpha particles. Several alpha emitters could be used; we have selected curium-244. In the following paragraphs, we discuss in detail the application and some of the results of using these three isotope sources. Table A-I summarizes important characteristics of these sources.

Table A-I Radioisotope Characteristics

Isotope	Half-Life, yr	Decay Mode	Principal Emissions
Curium-244	17.6	Alpha Emission	5.8 MeV alpha
Iron-55	2.6	Electron Capture	5.9 keV x-ray
Cadmium-109	1.24	Electron Capture	22.2 keV x-ray
			87.7 keV gamma-ray

Iron-55 Radioisotope Excitation. This source is particularly appropriate for exciting elements between Mg and Mn in the Periodic Table. These elements include many of those most important for diagnostic discrimination among meteorite types and also the "solar composition". As seen in Fig. A-2, in the Orgueil meteorite (Type 1 Carbonaceous Chondrite) the elements Mg, Al, Si, S, Cl, K, Ca, Ti, and Cr are all readily detected under Fe-55 excitation. For two of the stronger lines, Ca and Ti, the less intense K-beta peaks (marked CB and TB, respectively) are seen in addition to the K-alpha emission lines. It is important to note that this sample is a very sparse deposit of Orgueil powder grains onto a polycarbonate foil (Kimfol) which has been coated with a one micrometer layer of "sticky" material. The meteorite dust is only 200 ug/Cm, or about one-half monolayer thickness equivalence for cometary dust.

Cadmium-109 Radioisotope Excitation. The elements principally susceptible to excitation by this source may be seen by inspection of Fig. A-3. They mainly include the elements from Cr to Mo in the Periodic Table. For meteoritic material, such as the Allende carbonaceous chondrite, the emissions of Cr, Fe, and Ni are most prominent. Also detected, however, are Ca, Mn, Zn, and Cu (as a shoulder on the Ni K-beta peak). In addition, if adequate sample is available, heavier trace elements such as Sr and Zr become apparent.

Curium-244 Radioisotope Excitation. Although this source can excite elements as high as iron or nickel in the Periodic Table, its main utility is the alpha-particle excitation of very light elements such as carbon, oxygen, nitrogen, sodium, and magnesium. Figure A-4 is an excellent example of the

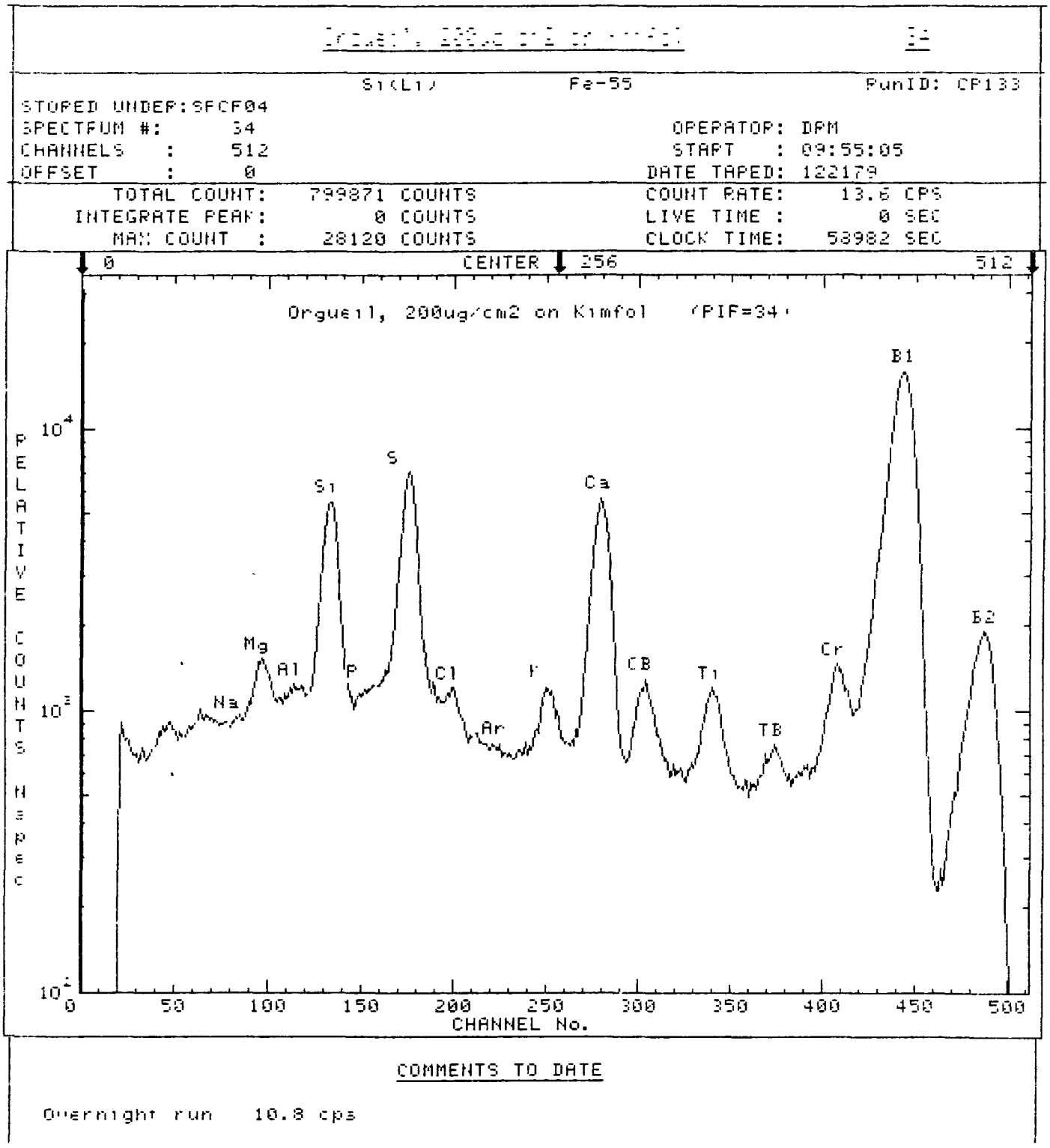

Figure A-2 Elements detected by Fe-55 excitation of a thin sample of Orgueil meteorite.
CB and TB are Ca and Ti
beta peaks, respectively.

ALLENDE PELLET, Cd-109

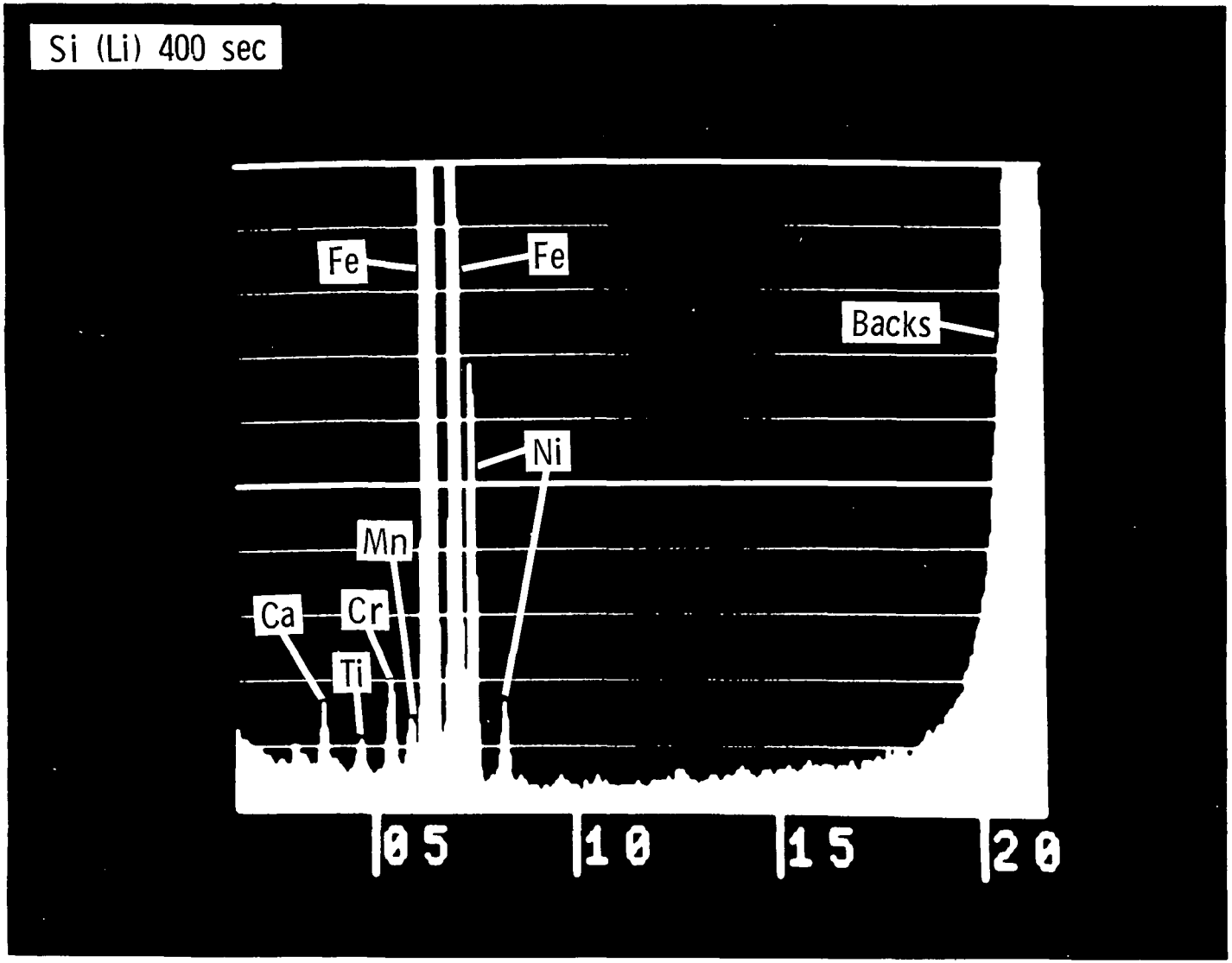

Figure A-3

Detection by Windowless Si(Li) Detector of Light Elements (including C, O, Na, Mg) in Allende Meteorite--Sample on Gallium

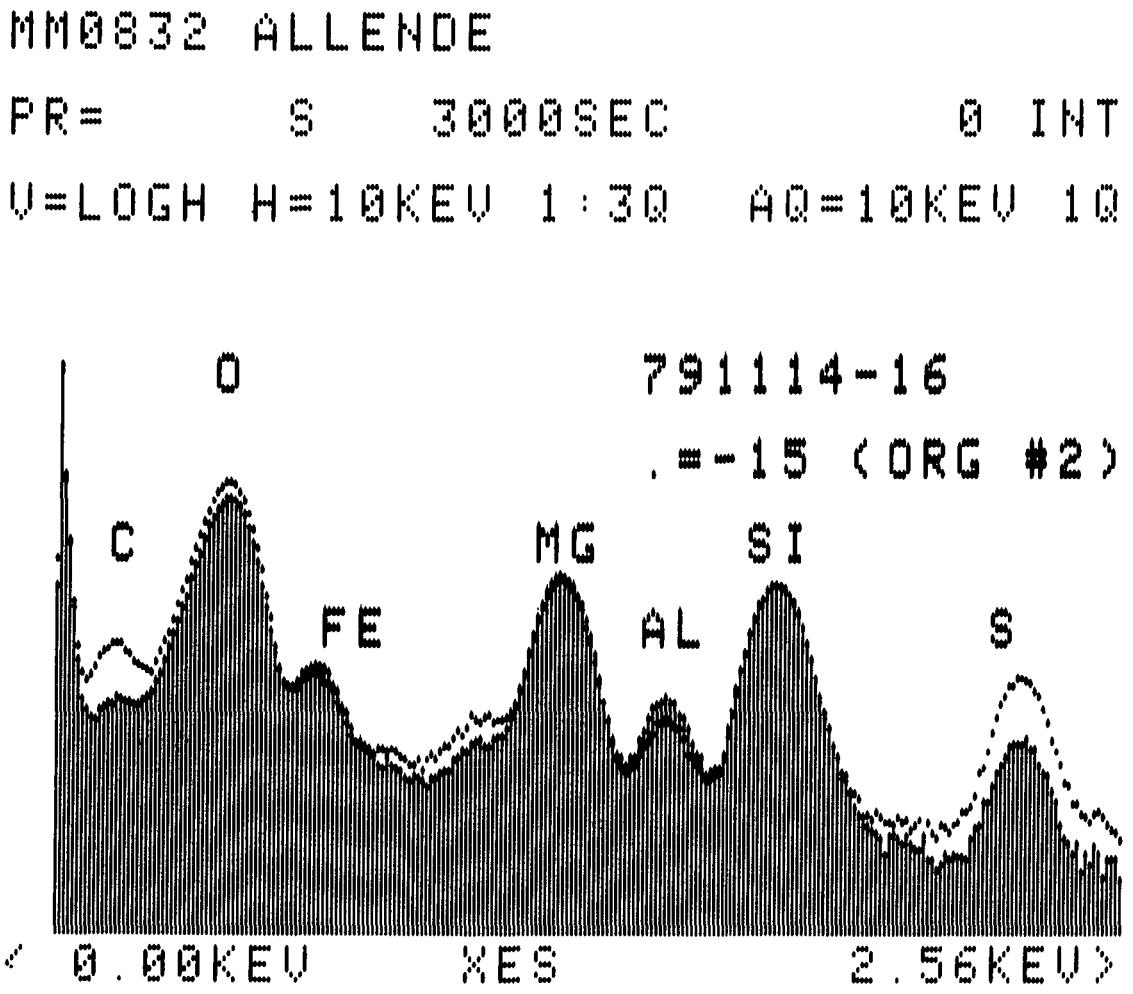

Figure A-4 Comparison of Allende and Orgueil meteorites under heavy particle excitation (Cm-244 source).

capabilities of this source when combined with a high performance cryogenically-cooled silicon detector. By normalizing the spectra of the Allende and Orgueil meteorite at the silicon peak, differences in C, O, Al, and S content are readily apparent. The significantly higher carbon and oxygen concentrations in the Orgueil sample are strikingly revealed. Even though the peak at carbon in the Allende spectrum is relatively weak, it is nonetheless real and statistically significant. This is borne out by the magnified comparison in Fig. A-5 between Allende and the ordinary chondrite Leedey, whose C content is less than 0.1%. This comparison shows the clear detection of the 0.3% carbon in Allende. These samples are on gallium mounts.

Detection of sodium is accomplished by exciting the sample with the alpha source, but using an inorganic viscid material for collection rather than gallium. This is because the Ga L lines overlap the Na K line. In Fig. A-6 the relatively high Na of Orgueil is revealed relative to the lower Na in Allende.

Methods for Detection. In addition to selecting the excitation source, careful consideration should also be given to the detector. Although many varieties are available for laboratory and research work, only three types are suitable for this application: the miniature proportional counter (PC), the mercuric iodide solid state detector (HgI_2), and the silicon solid-state detector, Si(Li). As shown in Table A-II, there is about a factor of three improvement in resolution for each step that one moves up this sequence. Detectors are chosen according to the characteristics of the sample, including which specific metals are present and what their concentrations are relative to one another.

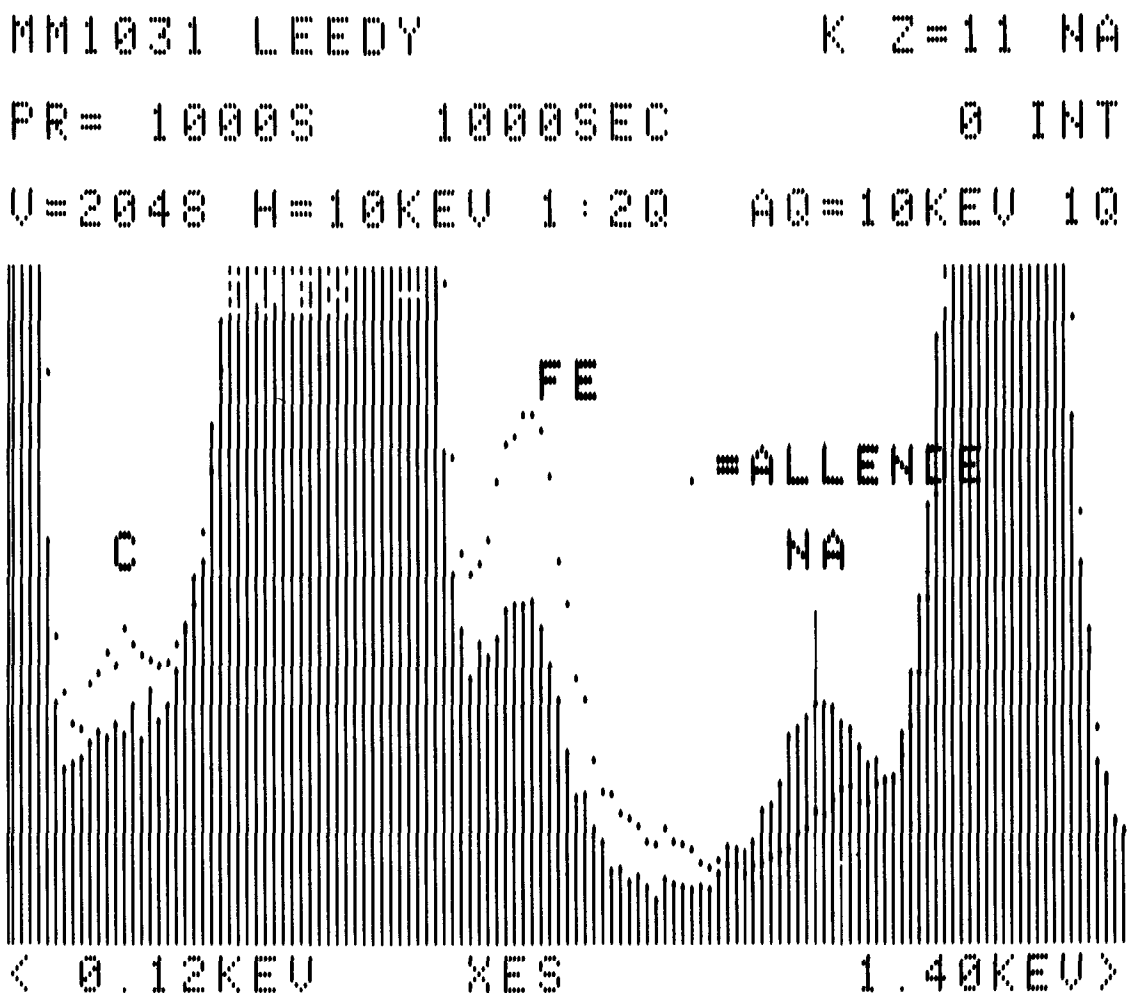

Figure A-5 Detection of carbon in Allende meteorite sample, compared to Leedey meteorite (<0.05% C)

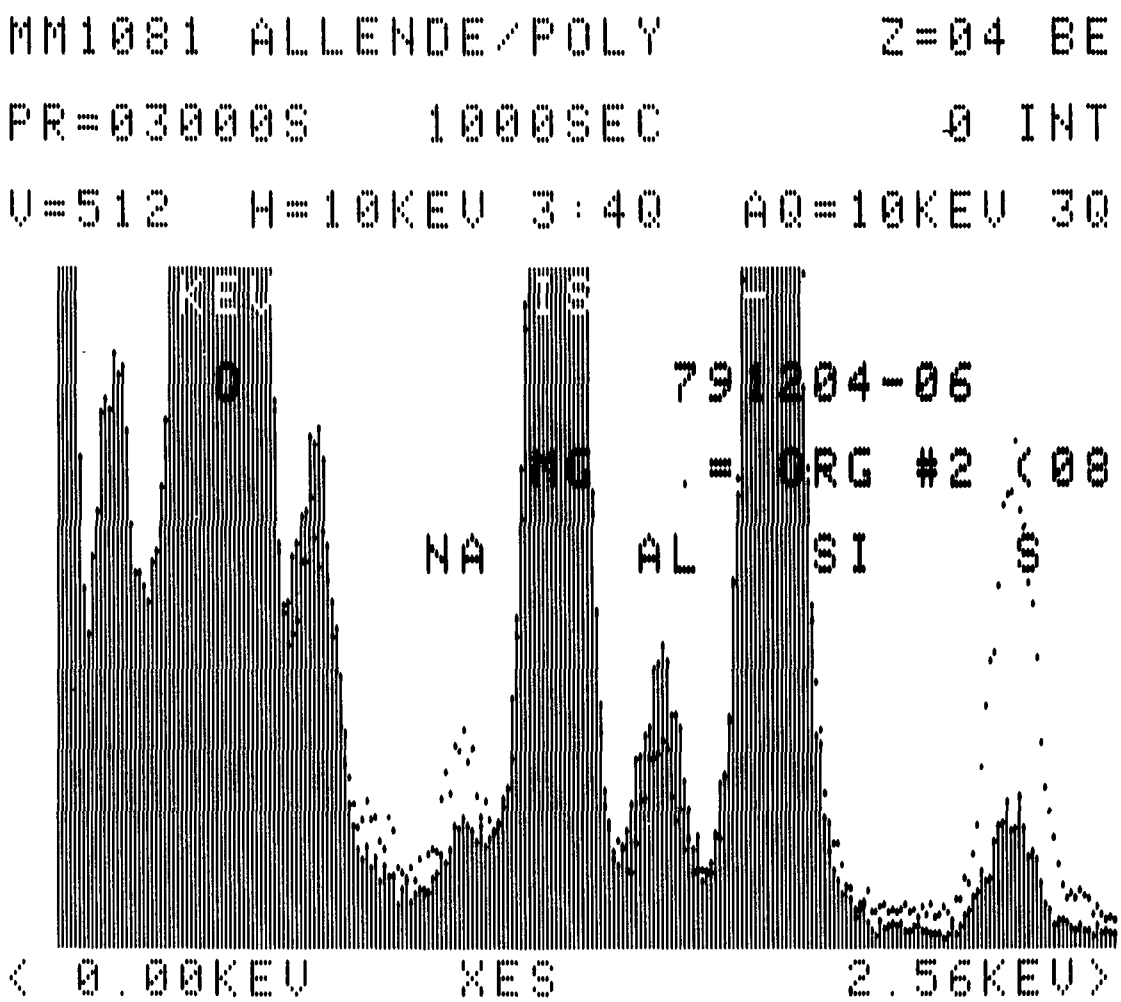

Figure A-6 Detection of sodium in Orgueil (dots) and Allende (bars) meteorite samples.

Table A-II COMPARISON OF DETECTORS

DETECTOR	TYPE	ABBREVIATION	TYPICAL RESOLUTION	COMMENTS
Proportional Counter	Gas Filled	PC	1100 ev	Requires 1000 VDC Bias
Mercuric Iodide	Solid State	HgI_2	400 eV	R & D Devices Only
Silicon (Lithium drifted)	Solid State	Si(Li)	160 eV	Requires Cryogenic Operating Temperature

* For 5.9 keV X-rays (Fe-55 source)

Proportional Counter (PC) Detector. The PC tube has the advantage of being a simple, proven device (Viking mission) for this application, but has the drawback of relatively poor resolution: about 1000 eV for ^{55}Fe radiation. With new techniques of enhancing PC tube resolution, the FWHM could be reduced to 630 eV. A very noteworthy improvement is the mercuric iodide detector, which has recently achieved 295 eV for ^{55}Fe. This type of solid-state device does not require cooling for operation, unlike the silicon detector which, when operated cryogenically, achieves 146 eV resolution.

Mercuric Iodide Detector. In a collaborative effort with a group of researchers in the Medical Imaging Science Group at the University of Southern California (USC), the feasibility for using mercuric iodide detectors for practical x-ray fluorescence analysis has been evaluated. This work involved a 7-mm^2, 400-mm-thick HgI_2 detector coupled to a selected FET and a modified Tennelec 161D preamplifier. Resolution was 380 eV for the iron-55 K line. Spectra were taken using both Fe-55 and Cd-109 excitation on pure and mixed-element standards, geochemical standards (BCR), and certain meteorites. Comparisons of spectra between proportional counter, HgI_2 and Si(Li) spectra are given in the published results. The great advantage of HgI_2 detectors over Si(Li) devices is, of course, their ability to operate at room temperature with good resolution. This eliminates the need for

complex thermal control systems to achieve the cryogenic temperature required for acceptable Si(Li) operation.

However, the excellent results achieved to date cannot be counted on to assure proper operation of an HgI_2 detector for a comet mission whose rendezvous occurs 3 years after launch. A number of specific developments must take place before the reliability of these devices can be assured. Considerable uncertainly also surrounds their production, because yields of both usable crystals and ultralow-noise FETs are very low. Two methods of growing crystals are available -- oscillating temperature vapor deposition and organic polymer-controlled growth. Both techniques have at one time or another produced usable crystals, but neither is consistently reliable. Long-term survivability of detectors is also an uncertainty. Table A-III summarizes required development studies. Space limitations do not permit in-depth discussion of these items.

Table A-III. Advanced Development Required for Mercuric Iodide Detector

Reliable method of production of quality HgI_2 crystals
Apparent limitations in detector lifetime and reliability
Low-noise FET selection (1 in 50)
Dead layer thickness minimization
Thin conductive layer for low-attentuation entrance window
Collimator and/or guard ring to avoid fringing fields
Cosmic ray background due to thick depletion region
Escape peak interferences
Overpulse ringing
Pre-amp optimization
Amplifier optimization relative to pre-amp
Low-temperature performance and survivability
Vacuum survivability
Environment effects (shock, acceleration, acoustic noise)

Silicon Detector. The Si(Li) detector is by itself very small (the size of a large transistor), but accessory electronics and mounting hardware are much larger. The major operating consideration is that the detector must be at

cryogenic temperatures in order to reduce thermal noise and produce a satisfactory signal-to-noise ratio. In conventional technique, a liquid nitrogen dewar is hard-mounted to the detector assembly via a cold finger. Condensation is prevented by thermally isolating the detector and cold finger in a vacuum. X-rays reach the detector through a thin beryllium window sealed to the vacuum jacket. Several different companies now manufacture Si(Li) detector systems for laboratory use. Normally, these laboratory units incorporate large dewars, and the detectors are such that they cannot be allowed to reach room temperature without the possibility of being damaged. The problems associated with maintaining this detector at cryogenic temperatures using space-borne techniques is addressed in sections G and K below.

As will be seen in the material presented in section G, the silicon solid state detector can be accommodated into a flight experiment. Thus, the excellent peak definition and separation evident in Figures A-2 through A-6 will allow detection and assay of all the major, minor, and several of the trace elements expected in comet dust material. Sensitivity of detection for various elements is considered in detail under section E below. Predicted accuracy of analysis is given in section F. Sampling schemes are covered in section C.

Non-Sampling (Direct Excitation) Scheme. As brought out in the original proposal, it is quite possible to directly excite ambient dust and gas without explicit sample collection, per the arrangement portrayed in A-7. This has excellent scientific advantages, not the least of which are direct measurements of dust/gas ratio, absolute mass loss rate, and dynamical measurement of these and chemical composition parameters. The chief drawback is that lower sensitivity limits the technique to close encounters (tens of km or less) as compared to hundreds or thousands of km for a dust collection method. Nonetheless, during the latter and terminal phases of the mission, this method could be of substantial scientific merit, provided the comet was still active. The estimated minimum density required of comet dust and gas to allow detection is 10^{-10} g/Cm^3.

PRINCIPLE OF OPERATION

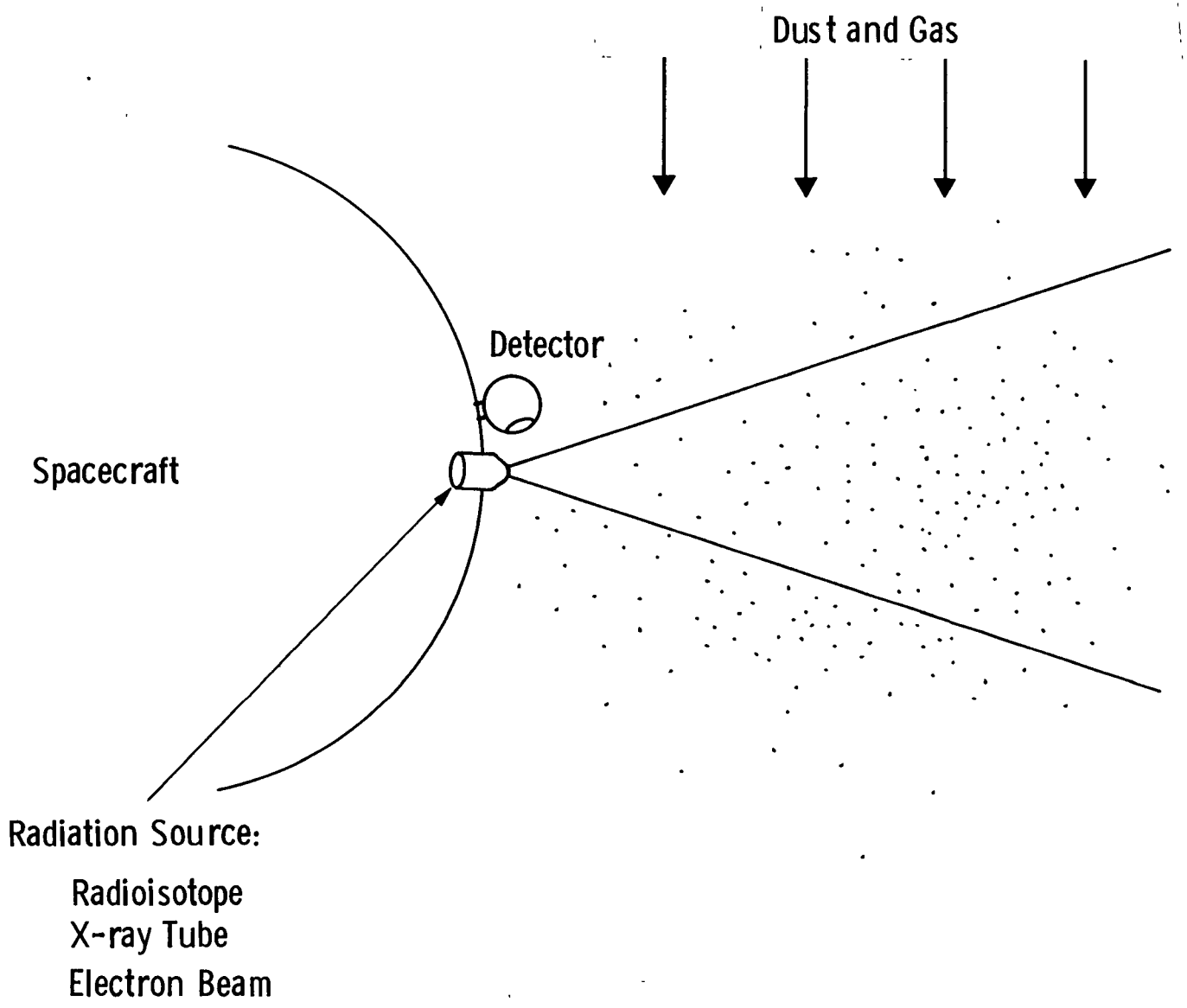

Figure A-7
Direct Excitation Method

B. Sample Simulation Methods

An important aspect of any spaceborne scientific experiment is to provide pre-flight calibration of the instrument and a method of evaluating performance under controlled laboratory conditions. In this case, the ideal calibration would involve the use of actual cometary dust. No bulk sample of unaltered cometary material is known to exist on earth. Brownlee particles, the particles collected in the stratosphere by special high-attitude airplanes, may be cometary debris. However, the sum total of all Brownlee particles collected to date are not enough bulk material for calibration and at any rate are much too valuable for such use.

At the outset of this study, we conducted certain experiments using thin wires and foils of various pure elements (mostly metals) to evaluate sensitivity of source-detector geometry parameters. Beyond this, it was realized that exact methods of simulating the physical size distribution as well as chemical composition of cometary particles would be critical for evaluation of any of the proposed analytical techniques, whether x-ray fluorescence or other instruments. This is not a trivial task, as is well known to anyone who has tried quantitative manipulation of particles in the micron and submicron ranges.

We have developed several approaches for preparing standards and test samples. These specimens have been used to find detection limits, evaluate accuracy, and optimize experiment design. Briefly summarizing, we have prepared quantitative deposits of submicron nontronite (iron-rich smectite clay) over a 10^3 range in thickness; employed APDC chelating agent to prepare thin standards of selected metals; developed the use of liquid gallium as a substrate for fixing powder deposits with no organic or oxygen interferences (NASA New Technology Report 696); deposited various meteorite samples as thin powder layers on Kimfol substrates coated with 2 um of a viscid material; and "shot" precise thicknesses of dust materials onto a collection substrate using a real-time microbalance (in collaboration with G. Rupprecht) to monitor mass accumulation. A long term objective is to evolve methods of producing microparticles with precise predetermined multielement compositions. One approach is impulse-heating for formation of glasses.

Element Precipitates. Quantitative precipitation of selected cations onto thin filters was undertaken in preparation of standards for measurements of detection limits and analysis accuracies. The precipitations are done by the APDC (ammonium pyrrolidinedithiocarbamate) method onto Gelman membrane filters. Standards have been prepared for Fe, S, Pb, Ni, and Zn, from levels of 1 to 100 ug in about 1.5 cm diameter circles.

Deposition of Materials on Nuclepore Filters. It became desirable to physically and hold certain materials on Nuclepore filters. This was accomplished for non water-soluble materials by suspending them in a 20% glycerol solution. Starting with an amount of material determined gravimetrically, we make a series of dilutions, then deposit the contents of aliquots from these dilution flasks by vacuum filtration. The materials were generally deposited in 15 milliliters of the 20% glycerol solution, followed by a rinse of prefiltered 20% glycerol solution.

Using this method, Pennsylvania Nontronite (Wards Scientific Establishment) was applied to Nuclepore filters at several different concentrations ranging from 1,000 to 0.3 ug/Cm^2. The nontronite was first purified by dispersing with sodium hexametaphosphate (sonicated), and cleaning by repeated centrifuge separations and washings with distilled water.

For materials that contain water-soluble components, it was found possible to use Freon TF as the liquid carrier. However, this method does not produce the same adherence to the filter as the 20% glycerol solution.

Thin Layers of Viscid Materials. Very thin layers of "sticky" materials were prepared on a variety of substrates. Among the substrates were Kapton (polyimide), Kimfol (polycarbonate), Mylar (polyethelene terephthalate), and aluminum foil. The "sticky" material that produced the best result was Poly-A-103, a polyamide. The thin layer was produced by applying 200 ul of a solution of Poly A in xylene solvent (5.4 mg/ml of Poly A) to the substrate. Using this method, it was possible to produce a layer about 2 um thick (200 ug/cm^2

of Poly A). One method for application of the powder was to spread it uniformly on the Teflon plate, then invert the substrate with the sticky layer on top of the powder. If the powder is not cohesive, only a monolayer adheres to the substrate.

Dry Mixing Analog Samples. Some analog samples are prepared by weighing specific amounts of pure chemical components (mostly oxides of the elements) and combining them. These are then placed in a mixing jar that contains a slotted paddle to provide a constantly changing mixing path. After several hours of tumbling in this jar, the sample is transferred to an automatic mortar and pestle where it is ground for 8 hours to produce an intimate mixture. Some samples are also prepared in a commercial ball mill (SPEX 5100 Mixermill) using tungsten-carbide balls and end caps.

Gallium on Copper. This method was developed because of the need to hold a powdered sample against gravitational or other disruptive forces during chemical analysis. One requirement was that the material not completely cover the sample. Another requirement, unique to our application, was that the substrate have no K, L, or M x-ray emission lines in the light-element emission range (0.1 to 0.8 keV). The "standard" method is to prepare a pellet or thin wafer of the material in a hydraulic press. In many cases, including ours, the materials to be used cannot be made into satisfactory pellets because of poor consolidation. Likewise, use of a binder agent is highly undesirable because of interferences and changes in the matrix characteristics. Our solution to this problem was to find a low-melting metal suitable for fixing the powder in the molten material, then cooling below the melting point. Gallium metal proves to be nearly ideal because it is a solid at room temperature, but melts at only a few degrees above room temperature. It is free from x-ray interferences (In and Hg are not), and has an extraordinarily low vapor pressure, even at 500°C. The gallium is adhered to a copper backing by the following procedure. A copper foil is wiped with acetone (or ethanol), rinsed with distilled water, cleaned in 5% HCl for 5 minutes, and again rinsed with distilled water. The cleaned dry copper is heated in air to 200°C for 30 minutes to form an oxide layer on

its surface. Gallium heated to slightly above its melting point (30°C) is then applied with a glass rod to the copper sheet maintained at a temperature of about 40°C by a hot plate. The sample is then affixed by inverting the prepared foil onto a thin layer of powder on a Teflon sheet and applying appropriate pressure.

Preparation of Salt Mixtures. Certain salt mixtures were prepared by putting each individual component, including a suite of trace elements, into solution. When all components achieve solution, they become perfectly mixed. Small portions of this solution are evaporated sequentially until the entire solution has been dehydrated. The resulting droplets are thoroughly mixed by grinding.

C. Collection Materials and Mechanisms

The problem of sampling comet dust during a rendezvous mission has been addressed during this study in order to make preliminary evaluations of the magnitude of the problem and to investigate possible solutions. Two specific studies were performed by Dr. F. Vandrey on problems suggested by this author. In the first of these, methods of concentrating particles for collection were examined critically. It was concluded that narrow-angle cone concentrators should successfully concentrate, via single-bounce collection, with concentration factors of around 8 to 10. On the other hand, it was determined that electrostatic concentration techniques are most probably quite impractical from the volume, weight and complexity standpoint. In the second study, the penetration of high-velocity dust particles into thick and thin "sticky", viscous coatings was examined. It was concluded that only very thin coatings should suffice to produce the required minimum stopping thickness.

Realizing that many viscid (sticky) materials would not retain the desired properties under high vacuum, an effort was made to find suitable materials with low intrinsic vapor pressure. Investigated were vacuum greases, diffusion pump oils, space lubricants, and organic stationary phases for high temperature gas chromatography. Also at this time, a technique for acceleration of particles to typical comet dust velocities (3 to 100 meters/second relative to the nucleus) was conceived. Because of the need by other investigators as well as by this experiment to collect dust for analysis during a rendezvous mission, it was decided by NASA to sponsor additional work in this area. Under contract JPL 955180, entitled "Comet Dust Collection Techniques," this work was carried on to a much further extent than could have been accomplished here. These studies have been completed. The interested reader can find detailed information on these results in Acta Astronautics (Volume 7, pages 531-541, 1982; article by B. Clark and D. Clair), and in NASA publication MCR-81-574o (May, 1981; 116 pages). Mechanisms for collection of comet dust are discussed in section G below.

D. Engineering Feasibility

The engineering challenges associated with designing flight-worthy sensors (x-ray detectors), excitation sources, and a comet dust collector mechanism have been examined in sufficient detail to ascertain overall feasibility of such an experiment. Using the fundamental criteria of scientific performance, size, mass, power requirement, data production, complexity, and probable spacecraft operating environment and mission mode, we have selected an optimum approach to elemental analysis of comet dust by x-ray fluorescence. In this section, we discuss the engineering aspects and trade-offs of these three major component subsystems. In section G will be found a description of the recommended experiment, including other pertinent subsystems.

Sensors. As brought out above (section A), the state-of-the-art laboratory device is the silicon solid-state detector (coupled to a low-noise FET transistor). Such units are operated at cryogenic temperatures. In spite of the complexity of implementing cryogenic cooling of the Si detector and FET, we propose its use because of its outstanding performance. However, to minimize possible effects on mission operations and to back up this high-resolution (HiRes) device, we also would recommend a lower-resolution (LoRes) detector to use as a monitor to provide continuous, albeit less sophisticated analysis capability, and to serve as back-up of the primary HiRes device.

The high resolution (HiRes) device selected is a lithium-drifted silicon detector of special design and construction, and a 10-mm^2 effective area. Its resolution (FWHM) at 100-cps counting rate represents the state of the art: 146 eV for Fe-55 105 eV for Al K, and 99 eV for carbon K x-ray. The undesirable tailing phenomenon found in intrinsic Ge and Ge(Li) detectors at low x-ray energies is not present in this Si(Li) device. Resolution of the

Si(Li) + FET system depends on operating temperature. We have conducted experimental measurements of this effect using a prototype system equipped with built-in monitoring thermocouples. The results indicate optimum performance at temperatures below 135° K. At 155° K, the resolution for ^{55}Fe degrades to 160 eV, and at 175° K (ca. -100°C), the resolution is 180 eV. At higher temperatures, degradation is much more rapid, and the system probably cannot be operated profitably above about -80°C. As discussed below (section G), we have designed a combined active/passive thermal control system that can provide the necessary cryocooling. Commercial Si(Li) units are kept cooled not only for operation but also to prevent damage caused by outdrifting of the Li dopant and migration of contaminants onto sensitive surfaces. These two adverse effects can be avoided during periods when the detector must be allowed to be warmed by: (1) keeping the detector under bias at all times; (2) Continously operating an appendage ion pump to maintain vacuum cleanliness.

Many Si(Li) detectors have been flown in space in the past 18 years--this author was one of the first to fly a charged-particle telescope of such devices (in 1963). However, only in recent years was a cryogenically cooled detector flown in the windowless mode. This application, an x-ray astronomy experiment on HEAO-B, used a very similar detector but cooled with a passive stored-cryogen system. The detector worked extremely well for the 1-year cryogen lifetime and showed no evidence of cosmic ray damage, in contrast to Ge detectors. Cosmic ray background was less than 0.3 cps over the 0.5- to 5-keV analysis range (S. S. Holt, private communication, 1979).

The primary purpose of the low-resolution (LoRes) detector is to monitor the progress of dust collection and analyze samples when it is either undesirable or not possible to achieve full cryogenic cooling of the HiRes detector. The LoRes sensor is also a back-up device in the low-probability event that the HiRes unit malfunctions. As indicated above there is good reason to leave open the option of what type of x-ray sensor should be selected to serve as the LoRes device. This is because of continuing development being undertaken on the mercuric iodide detector. Indeed, if the long-term stability and other problems associated with this detector could

be solved in time for a comet mission, then it would be the ideal choice. On the other hand, the proven reliability of the miniature proportional counter could make it the best choice for this measurement function.

The x-ray sensors themselves are very small, i.e., less than 15 cubic centimeters each. However, each requires associated pre-amplifier electronics and, in the case of the solid-state detectors, a sealed protective housing. Design estimates indicate the HiRes housing could be as small as 4 cm diameter by 10 cm long, exclusive of the ion pump. The mass estimate is 0.5 kg for the HiRes detector assembly, and 0.2 kg for the LoRes detector assembly. Less than 50 milliwatts is consumed by the detectors themselves. Data rates from the detectors will not exceed 100 pulses per second, which when digitized translates into less than one kilobit per second. Extensive data compression within the experiment will be accomplished by multichannel pulse-height analysis, and in certain modes by peak selection. This will reduce raw data rates by factors of 100 to 1000.

Excitation sources. After considering the relative merits of x-ray tube, electron beam, beta ray, charged-particle beam, and radioisotope excitation, we have concluded that the latter provides adequate performance for this application, and suffers none of the drawbacks of the other techniques. In particular, an electron beam produces bremsstrahlung background that limits ultimate sensitivity. Both miniature electron guns and x-ray tubes are available, but inclusion of either would cause significant increases in instrument mass and cost, and a decrease in reliability.

Five sealed radioactive sources (Table D-I) are recommended. Each source is made from one of the three isotopes: curium-244, iron-55, or cadmium-109.

The purpose of the ^{244}Cm source is to provide energetic alpha particles to efficiently excite low-Z elements. Although originally suggested for the Viking x-ray experiment, an alpha source was not included because the Viking heat sterilization constrained the type of detectors used. As proposed here, this source will be particularly useful in analysis for the light elements: C, N, O, Mg, Al, and Si. This source also emits Pu L x-rays

Table D-I Radioisotope Excitation Sources

Source	Configuration	Isotope	Source strength, mCi at Launch	Source strength, mCi at Rendezvous*
A	Annular	Cm-244	3	2.7
B	Annular	Cd-109	300	48
C	Annular	Fe-55	800	335
D	Collimated Disk	Cd-109	150	24
E	Collimated Disk	Fe-55	400	165

* Assumes three year cruise phase before reaching comet.

(principally at 14.3 and 18.3 keV), which provides less-efficient, but useful excitation of Ca, Cr, Mn, Fe, and Ni. It should be pointed out that this use of an alpha source is totally distinct from the so-called "alpha backscatter" method of analysis, which requires an extremely mono-energetic and high-level alpha source, and consequently must be of the unsealed, hazardous type. The well-known aggregate recoil mechanism tends to cause such a source to disintegrate with time. If only a small particle then migrates into the view of the detector array, the experiment is compromised. This source contains only 3 mCi of ^{244}Cm, which is electrodeposited, then overcoated and edge bonded by proprietary techniques. It is approved by the NRC as a sealed source. One such unit with a heavy use factor in high vacuum for more than 2 years has shown no evidence of leakage.

The isotope Fe-55 is used in two different configurations: disk and annular (Table D-I). Each source is triply sealed by electroplating the active material onto high-purity nickel foil, diffusion bonding, and sealing into a capsule by electron beam welding (disk) or epoxy bonding (annulus). The disk source is the same as that used in the Viking XRFS instruments. Annular sources are 2.5-cm OD, and 1.2-cm ID foils with a thin strip (3 mm wide) of electrodeposited active material. The Fe-55 source is particularly well suited for excitation of the elements Mg, Al, Si, P, Cl, K, Ca, Ti, and Cr.

The Cd-109 sources are constructed similar to the Fe-55 capsules. They are especially suited for excitation of higher-Z elements, including Ca, Ti, Cr, Mn, Fe, Co, Ni, Cu, Zn, Ge, Se, Br, Sr, Zr, and Hg. Of the approximately 50 elements above Zr in the periodic table, only In and Hg can be expected to occur above the few part-per-million level. For this reason, an Am-241 source was not incorporated into the design because only a single element, indium, is at a plausible detection level. However, it should be noted that all elements are in fact excited by the three sources, and unusually high concentrations of any element above boron would be detectable by L and/or M line emissions.

Each radioisotopic source is a separate assembly, enclosed within its respective collimator. The largest of these assemblies would be approximately 5 cm in diameter by 2 cm long. The aggregate weight of all five assemblies can be as light as 0.1 kg. No power and no data allocation is required by the excitation sources themselves.

Dust collector mechanism. The dust collection devices themselves are recommended to consist of a large number of small plaques, each 1 or 2 cm in diameter, so that a number of samples can be taken during different active phases of the comet, and so that different types of collectors can be used in an attempt for both total, representative collection, and biased collection of particles with certain physical characteristics. Based upon a carousel design, the collection assembly would occupy 20-30% of the total instrument volume. Although the power to move the carousel would be trivially small since collection periods are long, there would probably be an average power consumption of up to one watt needed to thermally control the collection substrates to their optimum temperature for collection (i.e., to maintain viscid materials in the "sticky" state, and to keep gallium above its freezing point). Approximately 64-bit data packets would be generated with each motion of the carousel, and 24 bits every 200 seconds would be used to monitor the thermal control function. A more detailed description of a mechanism for carousel collector and isotope source positioning is provided in section G.

E. Minimum Detection Limits

From analysis of a number of thin-sample meteorite samples and series of standards using our laboratory mock-up of the recommended x-ray fluorescence system, it has been possible to estimate scientific performance in terms of element detection for various models of comet dust. In Table E-I, we list the "probable" concentration by weight for each element of interest, based on solar abundances (CI meteorite composition), while the "range" encompasses variations among meteorite groups that may be representative of primitive material. For certain volatile elements, upper limits have been raised, based on the high volatile content of certain material ("mysterite") thought to be a late accretionary component (according to Ganapathy and Larimer) and possibly an important constituent of cometary nuclei. Also included is a summary of the optimum excitation method and the expected minimum detection levels. Potential overlapping interferences are pointed out where applicable. It is important to note that intrinsic sensitivities are extremely good, especially for transition metals and other elements, but that the anticipated high abundance of Fe and, to a lesser extent, Ni will mask the presence of some of these elements at their most probable abundance levels.

[TABLE E-I]

Table E-I. Detection Sensitivity for Elements at Levels Expected in Cometary Dust *

Si. Probable concentration: 12% (range 10 to 20%). Minimum detectable thickness (MDT) is 0.05 ug/cm^2 (0.0005 monolayer) for Fe-55 excitation. Peak-to-background ratio for one monolayer is 20 to 1. Absolute concentration is diagnostic of silicate-to-volatile ratio.

Fe. Probable 20% (range 17 to 30%). Excitation of K lines requires Cd-109 source. Minimum detection limit of 0.1 ug/cm^2 (0.001 monolayer). All particle sizes less than 10 um are "thin." L lines excited efficiently by Cm-244, allowing accurate measurement of highly diagnostic O:Fe ratio in "thick" approximation.

[TABLE E-I, continued]

O. Probable 43% (range 30 to 50%). Detection in windowless mode under Cm-244 excitation only. MDT is 0.2 ug/cm^2 (0.001 monolayer). Peak asymmetry possibly indicative of chemical state. All particle sizes greater than 7 um are "thick." Requires oxygen-free substrate (e.g., liquid gallium or hydrocarbon).

Mg. Probable 10% (range 9 to 15%). Excitation by Fe-55, but even better with Cm-244.

S. Probable 5% (range 1 to 7%). Detected under all excitations. MDT with Fe-55 excitation is 0.1 ug/cm^2. S/Si ratio of great importance. Potential masking by Hg (M-beta line) and Mo (L-alpha line) contaminants, but such contamination is detectable as peak broadening.

Ca. Probable 1.2% (range 0.7 to 2%). Excited by all sources. MDT with Fe-55 excitation is 0.1 ug/cm^2. Both K peaks are observed.

C. Probable 3% (range 0.1 to 10%). Detection limit Cm-244 and windowless mode = 0.1 ug/cm^2 for the pure element and 0.13% by weight in chondritic matrix.

Ni. Probable 1% (range 0.7 to 2%). Excitation by Cd-109. No interferences. MDT only slightly greater than for Fe.

Na. Probable 0.4% (range 0.3 to 0.9%). Of high diagnostic value. Requires Cm-244 excitation. Interference from Ga and Cu L lines; hence requires organic collection substrate. MDL better than 0.08% at one monolayer thickness.

Al. Probable 0.9% (range 0.7 to 1.6%). Accurate measurement requires careful stripping of tail of neighboring Si peak.

Cr. Probable 0.24% (range 0.2 to 0.4%). Excited by all sources; readily detected. MDT only slightly greater than for Fe.

[TABLE E-I, continued]

Mn. Probable 0.2% (range 0.1 to 0.4%). Mn/Fe ratio highly diagnostic and nearly independent of sample loading. Requires Cd-109 excitation.

N. Probable 0.2% (range 0 to 0.5%). Detection unlikely unless N/C and N/O ratios unexpectedly high, because of interference from flanking C and O peak. Mercuric iodide detector of inadequate resolution to detect N even at high abundance.

P. Probable 0.1% (range 0.08 to 0.2%). Obscured by strong flanking Si and S peaks.

Co. Probable 500 ppm (range 400 to 900). Obscured by Fe and Ni peaks. Probably not detectable in chondritic material.

Cl. Probable 500 ppm (range 50 to 800). Of high diagnostic value. Detection limit in one monolayer of CI material ~100 ppm (under Fe-55 excitation). Requires careful control of substrate cleanliness.

K. Probable 500 ppm (range 400 to 800). Best detection under Fe-55 excitation. MDL better than 100 ppm in thick sample.

Ti. Probable 400 ppm (range 300 to 900). Highly efficient excitation by Fe-55 source. Detection limit is 5 ppm for an 11-hour count on a monolayer of CI material on Kimfol substrate.

Zn. Probable 300 ppm (range 100 to 800). Possible maximum up to 1200 ppm based on analysis of two stratospheric particles by Ganapathy and Brownlee. Readily detected in Orgueil. Zn K-alpha is 374 eV upscale and superimposed on the approximately 3-fold more intense Ni K-beta peak. Controls of extraneous interferring radiations include: (1) avoidance of Cu- and Zn-containing aluminum alloys; (2) Ag overcoating of tungsten shielding to attenuate W L-alpha; (3) selection of low-Zn lead shielding.

[TABLE E-I, continued]

Cu. Probable 150 ppm (range 80 to 200). K line sandwiched between Ni K and K-beta, at 217 eV below the approximately 15X higher peak of the latter.

F. Probable 250 ppm (range 50 to 300). Detection not possible because of obscuration by intense Fe L-alpha at only 27-eV higher energy.

V. Probable 50 ppm (range 40 to 100). Can be assayed, but requires careful correction because of major contribution to observed peak by Ti K-beta. (Note: V K-beta completely masked by Cr K-alpha).

Ge. Probable 40 ppm (range 5 to 50). Data require correction for contribution to observed peak by Zn K-beta. Interference possible by mercury contamination (Hg L-alpha is 102 eV upscale. MDL approximately 10 ppm for thick sample.

Se. Probable 20 ppm (range 5 to 30). No interferences, but requires more than 2000 ug/cm^2 of sample for detection.

Ga. Probable 10 ppm (range 5 to 20). No interferences. Expected level near MDL.

Zr & Sr. Probable 10 ppm (range 5 to 15). No significant interferences. MDL is 5 ppm with thick sample.

Br. Probable 5 ppm (range 0.1 to 10). Mercury L-beta only 100 eV downscale. Detection only possible for sample thickness of 9000 ug/cm^2 and if no significant Hg contamination (e.g., from ion engines).

* Abbreviations:

ug = microgram

MDT = minimum detectable thickness, in units of ug/cm^2.

MDL = minimum detectable level (in % or ppm, by weight).

Monitoring dust flux. Even at very low exposures to the Cometary dust, the x-ray fluorescence experiment will be capable of detecting the dust buildup. In Figure E-1 we show the detection of 1 ug of Fe deposited on a Gelman filter by quantitative precipitation from solution using a special organic chelator. Here we clearly see the Fe K-alpha peak in channel 128. The actual detection limit for Fe is about 0.1 ug/cm^2. Since Fe is expected to compose about 20% by weight of the cometary grains' chemical make up, this corresponds to a minimum detection limit of about one one-thousandth of a monolayer of dust. If a funnel concentrator is employed, the instrument should be capable of detecting the point at which the spacecraft has been exposed to a total flux equivalent to only 0.0001 of a monolayer. Monitoring of Fe and other major and efficiently detected elements like Ca, S, and Si, will allow determination of the differential and integrated dust exposures. Of course, measurements of minor and trace elements will require the eventual collection of dust samples to the one monolayer or greater thickness.

Fe 1ug A2 (MM105) 43

Si(Li) Cd-109 RunID: WS-132

STORED UNDER:SPC103
SPECTRUM #: 43
CHANNELS : 512
OFFSET : 0

OPERATOR: DPM
START : 11:14:12
DATE TAPED: 21280

TOTAL COUNT:	232854 COUNTS	COUNT RATE:	4.2 CPS
INTEGRATE PEAK:	0 COUNTS	LIVE TIME :	0 SEC
MAX COUNT :	4373 COUNTS	CLOCK TIME:	55346 SEC

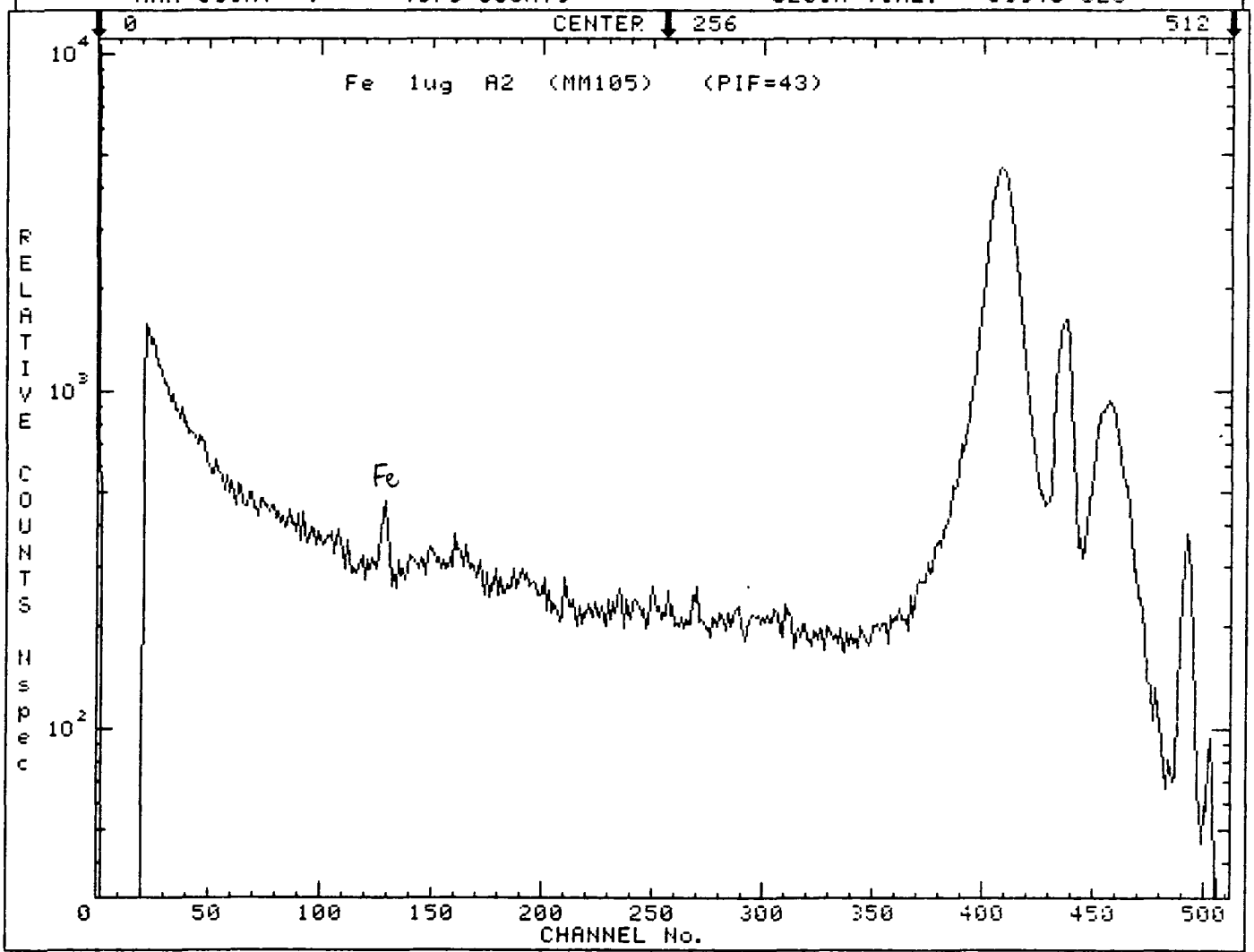

COMMENTS TO DATE

Vac. Filter alone in 16 position carousel ("Q")

Figure E-1
Detection of 1 microgram Fe standard (prepared by NaDDTC precipitation onto a Gelman Filter).

F. Evaluation of Analytical Accuracy

The absolute accuracy of any given analytical technique can be no better than the reproducibility, i.e., "precision," of the measurement. By careful optimization, the precision limit of the method can be made acceptably small.

Several factors are involved: use of custom processed accelerator-grade radioisotopes (high specific activity and radio-chemical purity), long counting times, highly stable electronics, a special (proprietary) collimator design, state-of-the-art detector resolutions, tight temperature control of critical components, multi-element targets for inflight calibrations, and ultrathin collection substrates with minimum backscatter. Combining the planned counting rates with the low background level achieved by these techniques, expected precision would be better than 1% for relatively abundant elements such as Si, S, Ca, and Fe, degrading to only 5% for trace elements such as Al , Cl , K and Ti (conditions: 100 g/cm^2 sample on Kimfol substrate; 10-hour count period).

Besides precision, constraints on absolute accuracy result from uncertainties in exact size distribution and chemical uniformity of the grain population. We have conducted extensive theoretical studies, via our COMETD computer program, (see Section L below) of expected relative x-ray fluorescence intensities from subsaturated samples of comet dust. The modeling in this program permits comparison of differing dust size distributions. Although some sensitivity to the assumed particle-size function does occur, this study has demonstrated by laboratory testing with prepared samples that the accuracy of the method is well within the requirement of discriminating among compositions such as CI, CM, and CO/CV meteorites. Samples used for these tests were ground powders of the Orgueil (Type CI), Murchison (CM), and Allende (CV) meteorites. The detector used was the high-performance (146-eV resolution) silicon device in a flight-prototype mounting configuration operated in vacuum using a special inverted bell jar system especially set up for comet experiment simulations.

The CI carbonaceous chondrite meteorites have a bulk elemental composition closely approximating the relative elemental abundance pattern of the sun. For this reason, they are often taken as the best analog to cometary dust material. Mineralogically, however, they represent extreme alteration from the mineral phases expected during condensation of the gases in the original pre-planetary nebula. Also pertinent are dust particles of extraterrestrial origin collected in the earth's stratosphere by special fly-through techniques. Many of these particles also have a carbonaceous chondrite-like compositional profile. For these reasons, the scientific performance of an element composition analyzer should be judged relative to the known differences between various classes of meteorites.

In Table F-I, some key ratios of elements to Si are listed for ten meteorite classes. Plots of these data and certain elements relative to Fe as well are given in Figures F-1 and F-2. It turns out that by determining these element/Si or element/Fe ratios to $\pm$10 to 25% in cometary dust, one can clearly resolve whether the cometary matter can be classified as a particular chondrite group; in addition, even if comet dust were different from any such classes, the data obtained would provide very tight constraints upon theoretical models of comet formation.

Table F-I.

Composition Properties of the 10 Chondrite Groups-- All Element/Si Ratios Normalized to those in CI Chondrites

Groups	Al/Si	Ca/Si	Mg/Si	Fe/Si	Ni/Si	C/Si*	S/Si
CV	1.36	1.34	1.03	0.87	0.87	0.1	0.24
CO	1.10	1.12	1.00	0.90	0.90	0.1	0.24
CM	1.13	1.11	1.00	0.93	0.92	0.6	0.46
CI	1.00	1.00	1.00	1.00	1.00	1.0	1.00
LL	0.82	0.79	0.88	0.62	0.55	0.02	0.21
L	0.84	0.79	0.88	0.66	0.64	0.02	0.21
H	0.85	0.81	0.92	0.93	1.02	0.02	0.21
IAB	0.76	0.75	0.76	0.7	0.7	?	?
EL	0.68	0.60	0.81	0.76	0.74	0.05	0.30
EH	0.65	0.60	0.71	1.13	1.02	0.07	0.60

* Wide range of C/Si ratios occur in these groups; uncertainties about factor of 2 for all meteorite types except CI and CM.

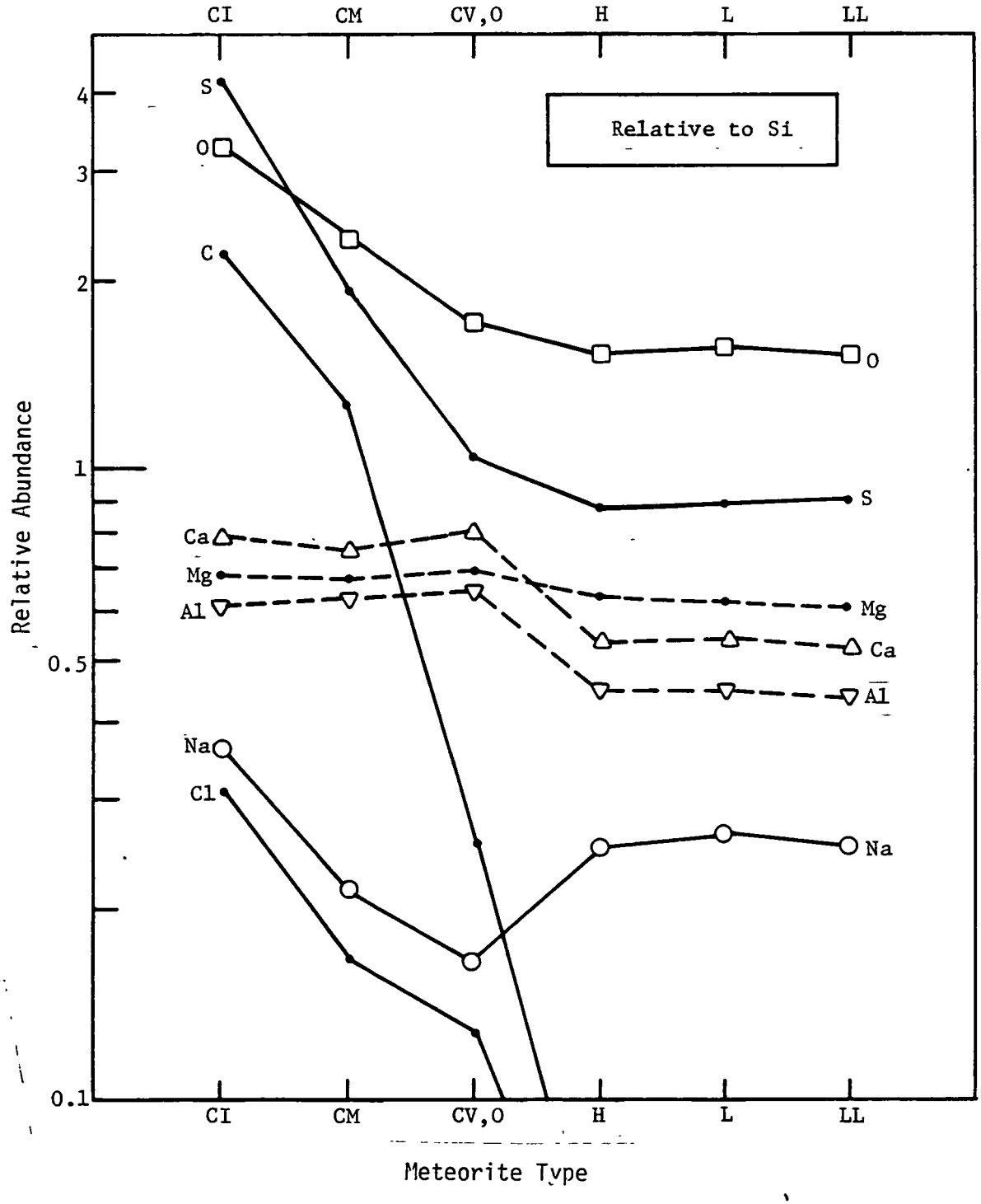

Figure F-1

Relative Abundance Levels of Elements in Various Meteorite Classes

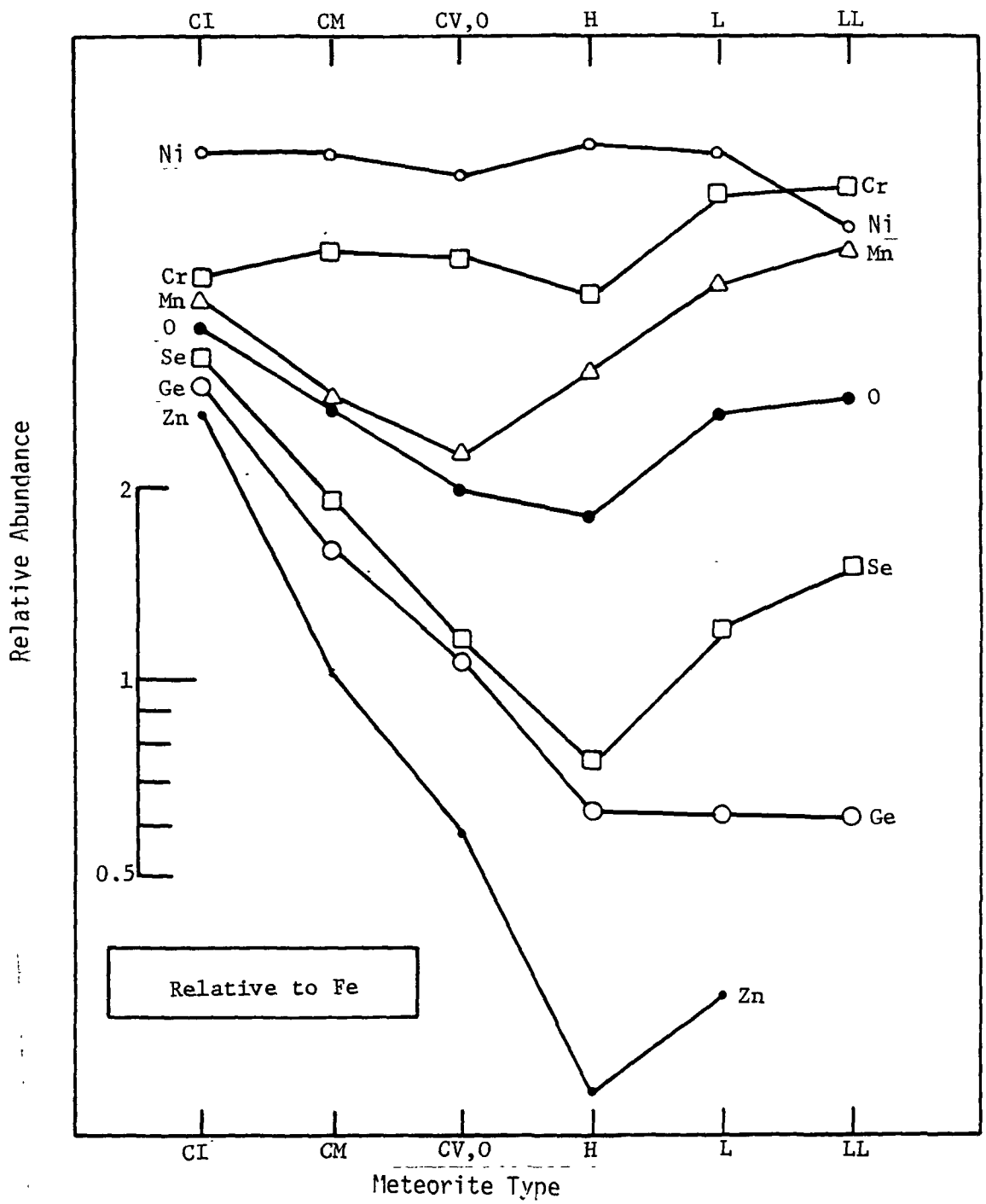

Figure F-2
Relative Abundance Levels of Elements in
Various Meteorite Classes

These data show that certain volatile elements (sulfur, chlorine, zinc, and especially carbon) are highly diagnostic, as is the lithophile (expressed as Mn/Fe ratio) content. The refractory group of elements (Ca, Mg, Al) are less easily used for diagnostic purposes, although more highly refined recent data indicate CV's can be distinguished from CO's by this element triad.

As seen in Figure F-3, even a sparse layer--about one-half of a monolayer--of comet dust analog material permits detection of key elements with excellent signal-to-background ratios. Count times in this case are long (10 to 24 hours), but readily achievable during a comet mission. Note the clean resolution of low K signal from high Ca. (The Cl peak observed for this sample is chiefly caused by a contaminant in the substrate; methods for its removal are under development). The successful detection of Cl in Orgueil may be seen in in Fig. F-5. Excitation by Cd-109 produces strong Ca, Cr, Fe, and Ni lines, as shown in Figure F-4, and demonstrates detection of Mn/Zn, and certain trace elements.

Additional spectra provided in section H below demonstrate unambiguous measurement of C, O, and Na to accuracies capable of resolving the elemental trends among the carbonaceous chondrites. Figure F-5 and F-6 should be compared with Figure F-3. This trio clearly demonstrates the capabilities of distinguishing between the major classes of carbonaceous cosmic material based on key elements such as sulfur.

To summarize, extensive data have been taken with realistic samples, excited and analyzed by flight-configured radioisotope sources and detectors. The data obtained directly show that the technique proposed can not only readily distinguish among the meteorite classes (CI, CM, CV) thought to most likely represent the composition of comet dust, but also provide high-quality data for totally unexpected chemical compositions.

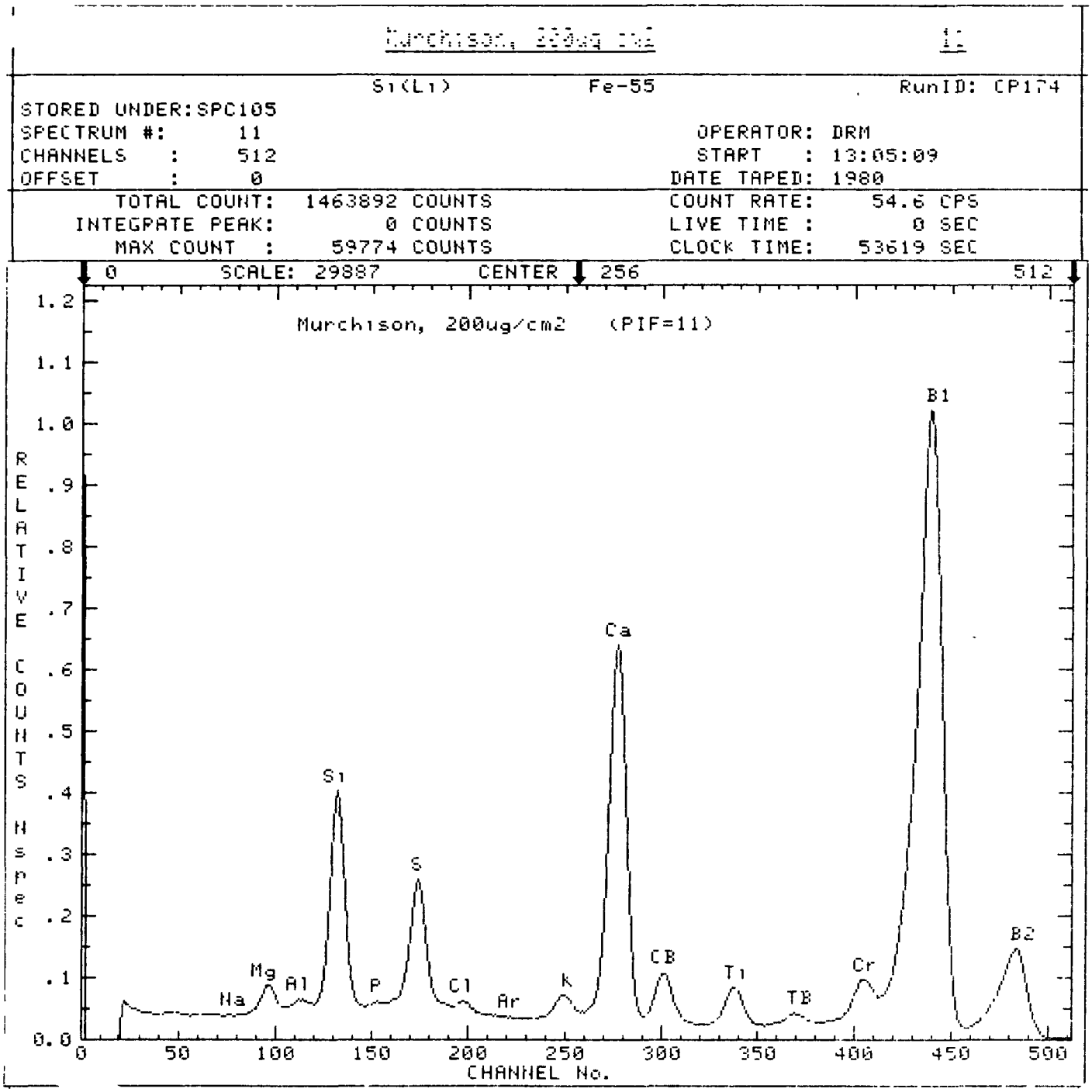

Figure F-3
Spectrum of Thin Layer (0.5 Monolayer) of
Murchison Meteorite

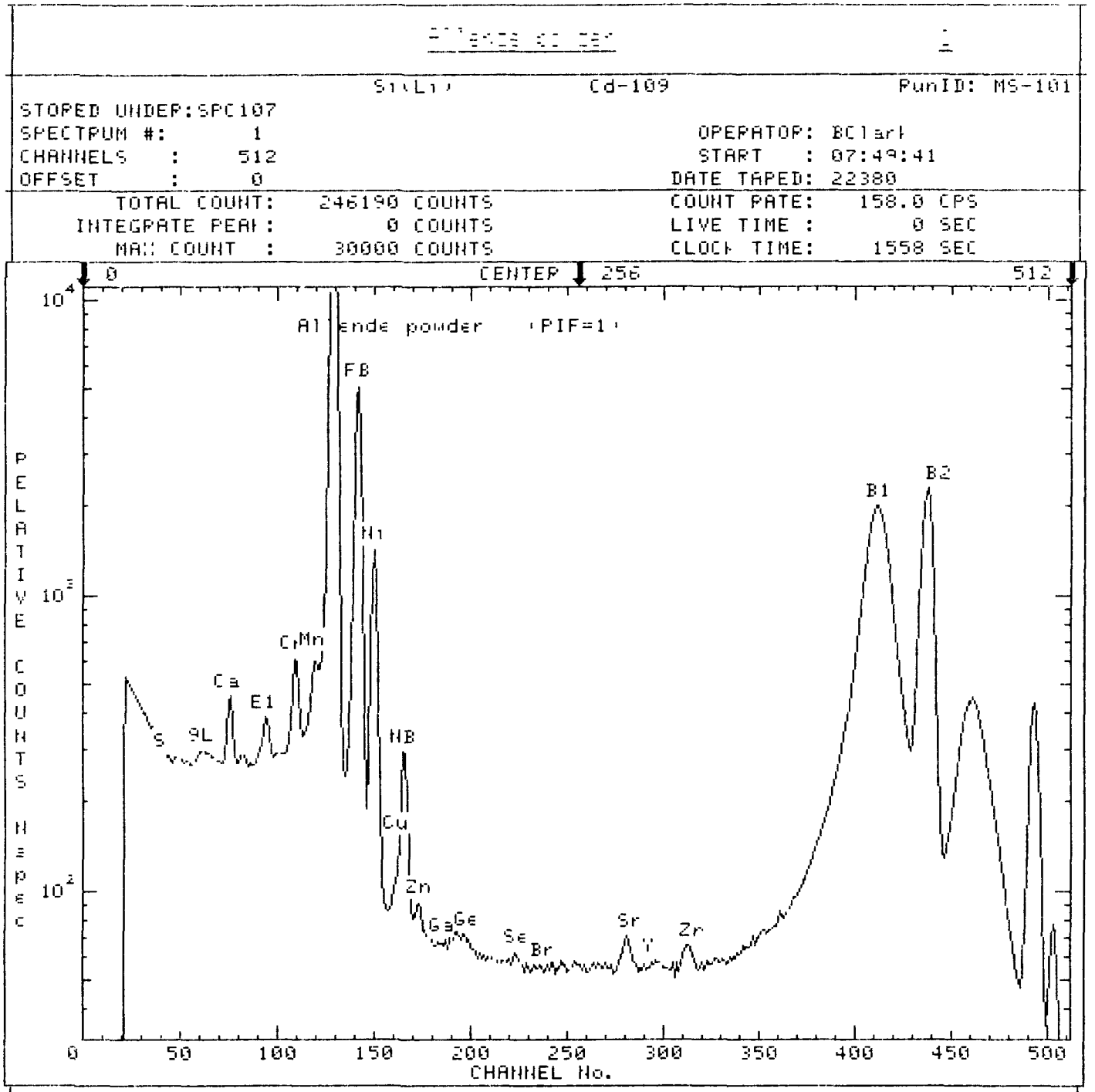

COMMENTS TO DATE

In Air. Powder in polyethylene cap. 54 cps. 46738 second run.

Figure F-4 Heavy and trace elements detected in a "thick" sample of Allende meteorite. The peak off-scale is the Fe K-alpha line. The FB and NB are beta lines from Fe and Ni.

8

Si(Li) Fe-55

STOPED UNDER: SPC104
SPECTRA # : 8
CHANNELS : 512
OFFSET : 0

DATE : 19790, 1979
OPERATOR: BClark
START : 09:32:48
DATE : 121679

SPECTRUM STOP CRITERION: OF 666.67

TOTAL COUNT: 578000 COUNTS
INTEGRATE PEAK : 0 COUNTS
MAX COUNT : 9957 COUNTS

COUNT RATE: 14.5 CPS
LIVE TIME : 0.00 MIN
CLOCK TIME: 666.67 MIN

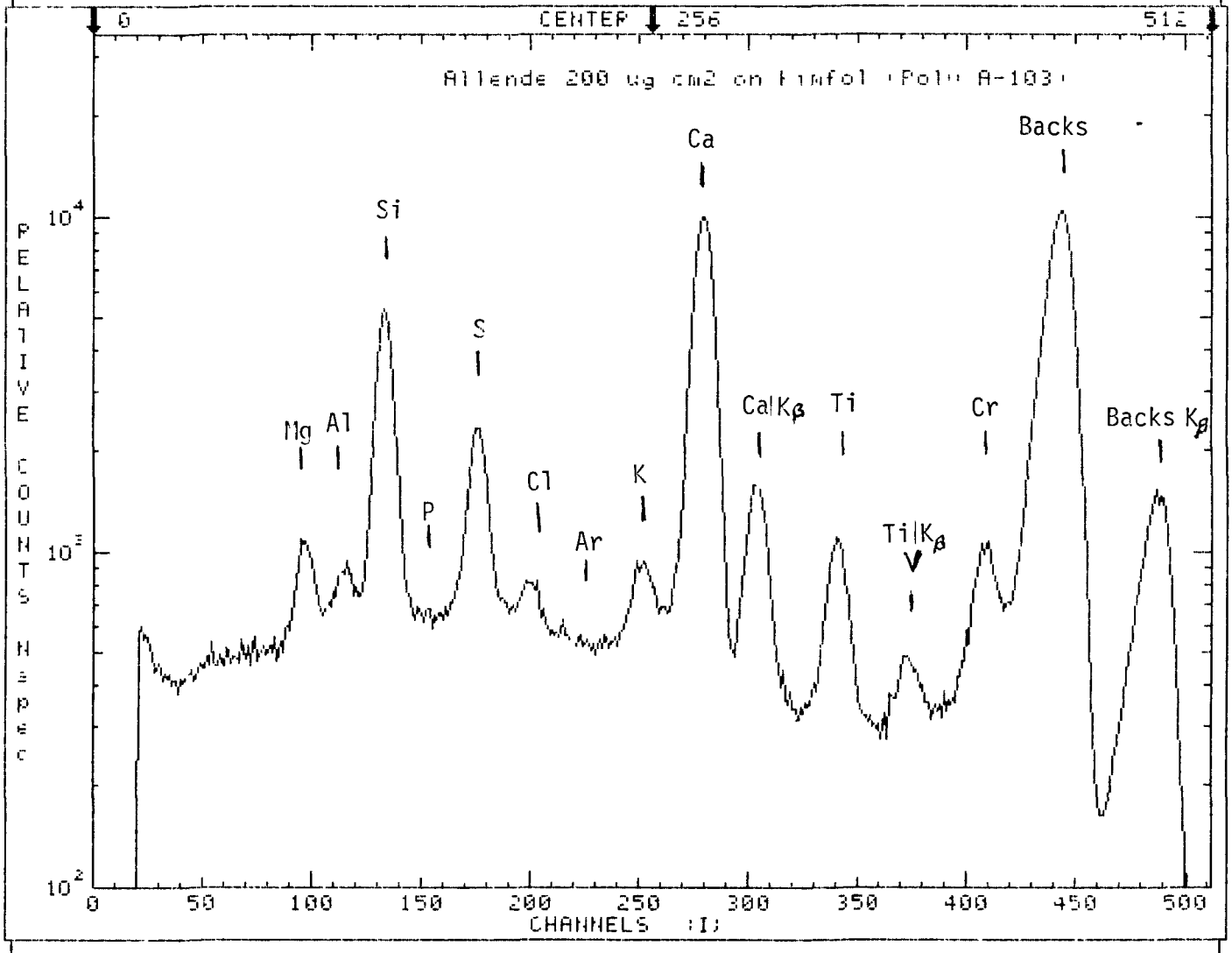

COMMENTS TO DATE

Real= 40000 sec count, but set Nsec(0)=30000. Rate is correct, however.

Figure F-5
Spectrum of Thin Layer (0.5 Monolayer) of
Allende Meteorite

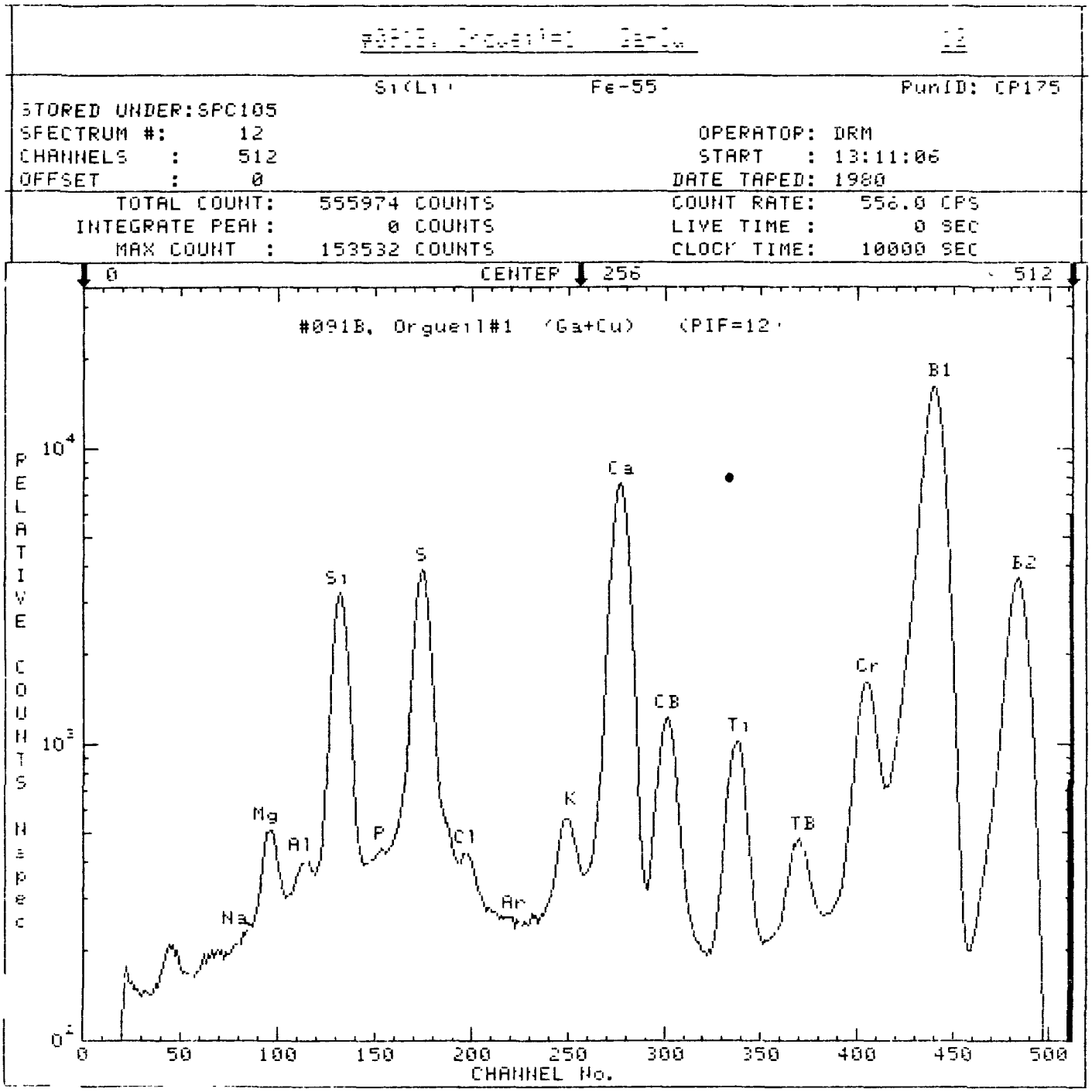

Figure F-6
Elements Detected by Fe-55 excitation of Orgeuil

G. X-ray Analyzer Experiment Description

The concept for a Dust Collection and Analysis by X-ray (DCAX) instrument for a comet rendezvous mission is portrayed in Figure G-1. To summarize, the instrument consists of a collection carousel, two dust inlets, radioisotope source wheel, high and low resolution x-ray detectors, active and passive thermal control subsystem, associated electronics and mechanical subsystem. The collection carousel wheel includes approximately 30 individual collection substrates of different types, including liquid gallium, metal foil, Apolane-87 coated nickel, Martin Marietta Black, and a number of Kimfol films coated with various viscid organic layers. The carousel also would include calibration targets (dolomite slab and two artificial "dust" samples). This collection disk is designed to be driven by dual-redundant, variable-reluctance motors (with three back-up modes of operation). An independent "total dust" collection target would be continuously exposed and inserted in the carousel plate by a rotary solenoid drive near the end of the rendezvous collection phase.

The source wheel is mounted coaxially with and above the collection wheel. It allows for sequentially placing each of the five sources in analysis position next to each detector. An independent dual-drive system (identical in design to that for the collector wheel) positions the sources and, through a mechanically engaged stop, a shutter plate.

The high-resolution detector is a state-of-the-art 10-mm^2 Si(Li) solid-state device in an ion-pumped vacuum housing with a spring-ejectable 9-um beryllium window removable on command after launch. This detector is maintained at cryogenic operating temperature by a two-stage thermal radiator pointed at deep space, connected via a heat pipe and thermal switch. During periods when the radiator views the cometary surface or the Sun, the thermal switch is "open," and a back-up split-cycle Stirling cycle cryorefrigerator is turned on (see below for thermal subsystem description).

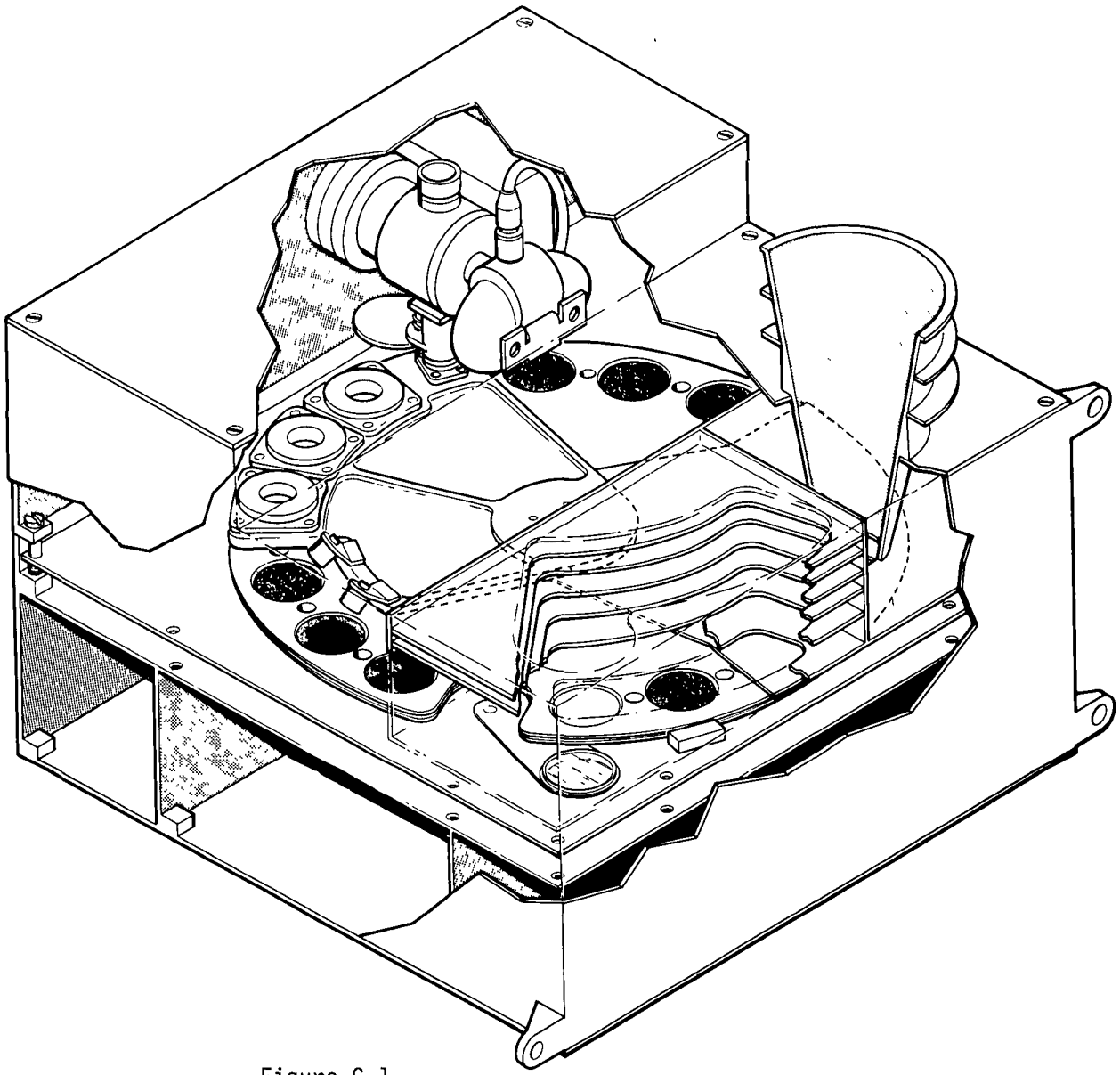

Figure G-1
The recommended Dust Collection and Analysis by X-ray (DCAX) experiment. (Base dimensions are approximately 10" x 10").

The low-resolution detector is selected from one of the options discussed in section D. Electronics are microprocessor-based and include a 4096-channel pulse-height analyzer memory that can be electronically reconfigured on command into submemories down to the 128-channel level for storage of up to 32 different spectra before data transfer. Dust inlet ports consist of: (1) a main port with stacked collimator blades to ensure that stray reflected grains are not collected, and (2) an 8 degree concentrator funnel with an eight-fold enhancement factor. Protection against Hg and Mo contamination, stray sunlight, and comet light is provided by the shutter wheel and internal baffles coated with Martin Marietta Black.

In operation, selected targets and the shutter wheel are positioned to permit collection under the inlet port of interest. Once per hour, the shutter closes the port, and the sample is temporarily rotated to appropriate positions for rapid analyses. However, thorough analytical runs would be delayed until completion of each spacecraft collection sortie.

A number of instrument characteristics and engineering operating parameters are analyzed in Tables G-I and G-II. A detailed mass properties breakdown is in Table G-III. In succeeding paragraphs, the three major engineering subsystems--mechanical/mechanisms, electronics, thermal control--are considered in some detail.

Table G-I. Mass, Size, and Power Requirement Estimates for DCAX.

Item	Mass (kg)	Heritage
A. Structure	1.9	Detailed design layout
(Housing = 1.3)		Layout and mechanical mockup
(Wheels, funnels = 0.6)		
B. Devices	0.5	
(Motors = 0.4)		Existing hardware, Viking
C. Thermal Control	1.8	
(Cryoradiator)		Detailed design
(Croyorefrigerator)		Existing hardware
(Thermal blankets)		Standard multilayer material
D. Cabling	NA	NA
E. Sensors and Sources	0.8	
(HiRes Det Assy = 0.5)		Prototype unit
(LoRes Det Assy = 0.2)		design, Viking
(Radiation sources + coll = 0.1)		
F. Electronics	1.1	Existing units, Viking
		Portable x-ray electronics,
		numerous flight programs
Total	6.1	

Size

Dimensions for main instrument:	25 x 27 x 20 cm
Dimensions of cryoradiator:	30 x 30 x 0.5 cm

Power

Instrument should be powered continuously, at 1 W average and 2 W peak consumption, using 28 VDC. Highest power mode is during operation, if required, of the Stirling-cycle cryocooler, which draws 30 W maximum.

Data Rates

16,384 bits maximum per spectrum, plus 2,048 bits engineering data. Maximum transfer rate: once per 30 minutes.

Command Requirements

50 bytes per new collection or analysis sequence.

Pointing Requirements

Collection-port axis anti-parallel to dust velocity vector within $\pm$ 20°
Concentration funnel axis within $\pm$8°

Table G-II

SUMMARY CHART FOR DCAX EXPERIMENT

Experiment: Dust Collection and Analysis by X-ray Spectrometry (DCAX)

Measurements:
a) Chemical composition (15 to 25 elements) of dust grains and moderately volatile constituents
b) Physical properties of grains (adhesion and rebound)
c) Dust fluence as a function of comet activity
d) Source regions of principal dust emission on Tempel 2
e) Chemical variations among b, c, and d

Instrument: Energy-dispersive x-ray fluorescence spectrometer, including a low-resolution detector and cryogenically cooled high-resolution detector. Excitation by passive radioisotope sources. Instrument includes sample collection device with multiple targets, and a combined passive and active thermal control subsystem.

Dimensions: 25 x 27 x 20 cm (main instrument)
30 x 30 x 0.5 cm (cryo-radiator)

Mass: 6.1 kg (3.7 for analyzer; 0.6 for collection; 1.8 for thermal control)

Power Requirements: 4 W average (28 ± 1 Vdc)
30 W peak at approximately 10% duty cycle

Data Rate: Less than 0.1 kb/s

Uplink Requirements: 100 bytes every second day

Thermal Control Requirements: Sink to spacecraft body at -10 to +40°C

Pointing Requirements: During dust collection only: ±4° toward comet (desired); ±20° toward comet (required)

Deployment Mechanism: None required. Unit is fix-mounted.

Ion Engine Compatibility: Employs baffle shielding and thermal control to protect sensitive surfaces (collection targets, detector windows, thermal radiators) from Hg and Mo contamination.

Radiation Safety: All radiation sources are doubly or triply sealed and extremely rugged. Similar sources previously flown on Viking.

Special Requirements:
a) Radiation source change-out at launch minus 3 months.
b) Continuous power (1 W max) for operation of ion pump during ground checkout, launch, and cruise.
c) Minimum exposure of cryogenic radiator to a direct view of the Sun.

Table G-III
Mass Properties Breakdown (TOTAL = 6114 grams)

C = Calculated from Drawing
W = Actual Weight
S = Manufacturers Specs.
E = Estimated

	BASIS	REV	WEIGHT (grams)	TOTAL (grams)
A. Carousel Assembly				385
1. Sample Wheel (Mg)	C	B	165	
2. Primary motor	S	B	20	
3. Carousel drive				
a. 48 Pitch Worm Wheel (Al)	C	B	38	
b. Bearing (303 CRES)	C	C	36	
4. Back-up motor	S	B	20	
5. Worm gear (303 CRES)	C	C	36	
6. Encoder Disk (Glass)	E	D	20	
7. Motor Mount (Al) [2]	C	B	50	
B. Shutter				45
1. Shutter Wheel (Mg)	C	B	40	
2. Mounting Hardware	E	E	5	
C. Source Wheel				359
1. Source Mount Fan (Mg)	C	B	46	
2. Source Holders				
a. Shield Mounting (Mg) [3]	C	B	12	
b. Annular Shields and Sources (1-W,2-Brass) [3]	C	B	52	
c. Small Shield Mounting	C	A	4	
d. Small shield & Source	C	A	22	
e. Collimated Sources [2]	C	C	20	
3. Source Wheel Axle (Al)	C	B	31	
4. Bearing (303 CRES)	C	C	25	
5. 48 Pitch Worm Wheel (Al)	C	B	51	
6. Worm Gear (303 CRES)	C	B	36	
7. Primary Motor	S	B	20	
8. Back-up Motor	S	B	20	
9. Encoder Disk (Glass)	E	D	20	
D. Base Plate assembly				573
1. Base Plate (Mg)	C	B	342	
2. Cooling coil (Cu)	C	D	20	
3. Solenoid	E	B	100	
4. Heating elements [3]	E	B	50	

Table G-III, Cont.

5. Hub (Al)	C	B	61	
E. Housing and Dividers				950
1. Thermal Blanket	E	B	50	
2. Housing (Mg)	C	B	900	
F. Dust Cover				151
1. Cone Concentrator (Mg)	C	C	61	
2. Stiffner Rings				
a. ring #1	C	C	3	
b. ring #2	C	C	5	
c. ring #3	C	C	7	
3. Baffles (Mg) [6]	C	C	31	
4. Cover (Mg)	C	B	44	
G. High Resolution X-Ray				499
1. Ion Pump	C	D	160	
2. Housing (Mg)	C	D	39	
3. Detector	C	D	164	
4. Pre-Amp Electronics	E	D	92	
5. Electronics Housing (Mg)	C	D	36	
6. Cable	C	E	8	
H. Low Resolution X-Ray				173
1. Detector	C	E	37	
2. Pre-Amp Electronics	E	E	92	
3. Electronics Housing (Mg)	C	E	36	
4. Cable	C	E	8	
I. Cryogenic Thermal Control				1844
1. Radiation Panel St. 2 (Al)	S	B	161	
2. Radiation Panel St. 1 (Al)	S	B	190	
3. Support Panel (Mg)	S	B	405	
4. MLI Bet. Stage 1 & 2	S	B	19	
5. MLI Bet. Stage 1 & Support Panel	S	B	22	
6. Thermal Diode	S	B	50	
7. Thermostats	S	B	45	
8. 1/4" Dia. Heat Pipe [11.8"]	S	C	22	
9. 1/4" Dia. Heat Pipe [18"]	S	C	33	
10. Heat Pipe MLI [18"]	S	C	2	
11. External MLI on Surf.	S	B	31	
12. Active Cryocooler	S	B	864	
J. Hardware, Piece Parts				60
1. 8-32*1 Flat Head [11]	C	A	25	
2. 4-40*1/2 Socket Head [22]	C	A	16	
3. 2-56*1/2 Socket Head [8]	C	A	3	
4. 2-56*1/4 Flat Head [4]	C	A	1	
5. 2-56*1/2 Flat Head [4]	C	A	2	

Table G-III, Cont.

6. 4-40*1/2 Flat Head [24]	C	A	13	
K. Electronics				1075
1. Printed Circuit Boards				
a. Digital Boards [2]	E	C	210	
b. Analog Boards [3]	E	C	405	
2. Spacers [16]	E	B	14	
3. Screws & Mounting Hardware	E	B	12	
4. Power Supply Boards [3]	E	C	162	
5. Power Supply Housing	E	B	212	
6. Potting For Hi Voltage	E	D	60	
		TOTAL		6114 g

Mechanical/mechanisms subsystem. The mechanical portions of the experiment include two fixed detectors (HiRes and LoRes), moveable collector, radioisotope source wheel, shutter, and main mounting structure. A radioisotope source positioner (RSP), a dust sample collector positioner (DSCP), and a exposure shutter would share the same axis of rotation. However, the mechanism for positioning x-ray sources over the samples would operate independently of the sample positioning mechanism.

The RSP is conceived to consist of the five radioisotope sources mounted on a pie-shaped portion of a disk. It also would include an axle, two thin torque-tube ball bearings, a 180-tooth worm wheel with matching worm gear, two variable-reluctance stepper motors, and an optical encoder disc with read head.

The point of the pie-shaped source holder is mounted on the axle (sources are mounted adjacent to the outer radius of the pie shape). The axle passes through the two ball bearings (the outer race of each bearing is fixed to a mounting pedestal that is in turn mounted on top of the aluminum mounting plate). The 180-tooth worm wheel is attached to the end of the axle opposite the source holder (below the aluminum mounting and cooling plate). The worm gear (which meshes with the worm wheel) is mounted on the drive shafts of both stepper motors (one motor at each end of the worm gear); and the stepper motors are mounted on the bottom of the aluminum mounting and cooling plate. An optical encoder disc is mounted on the worm wheel, and the read head of the encoder is fixed to the aluminum plate.

This implementation of the RSP would have several advantages:

1) The simple implementation of a worm-gear/wheel arrangement eliminates the need for gear heads on the motors;

2) The use of variable-reluctance stepper motors permits coupling both drive shafts at the worm gear (these motors display no power-of detent torque, so the driving motor can easily rotate the shaft of the "dead" motor);

3) The variable reluctance motor can be full stepped at 24 steps per revolution or half stepped at 48 steps per revolution, permitting source-wheel positioning resolution to 12 or 24 steps per degree;

4) The opposed motors permit a high degree of redundancy - (a) either motor can drive the RSP, (b) both motors can simultaneously drive the RSP in case of binding, (c) either or both motors can be double torqued (by energizing opposite poles with opposite polarity pulses) to provide up to four times the rated single-motor torque for overriding any binding;

5) The optical encoder prevents loss of wheel position if the stepper motor(s) misstep.

The DSCP mechanism is a duplicate of that used for the RSP in that a dual stepper-motor arrangement is used to drive a worm-gear/worm wheel that in turn rotates a wheel to which the samples are mounted. However, the DSCP also positions the sample exposure shutter, which consists of a pie-shaped piece of magnesium mounted (at the point) to the center rotation pedestal via a plastic bearing. The plastic bearing will load enough friction onto the shutter rotation to prevent drift. The shutter is moved by mating a drive pin on the sample wheel, with a stop on the shutter, and rotating the sample wheel.

Electronics subsystem. Electronics would be a microprocessor-based unit with programmable pulse-height analyzer memory allocation. Much of the electronics could be based upon programs to develop portable x-ray fluorescence spectrometers for use by NASA and the U.S. Bureau of Mines. Also, Martin Marietta Internal Research and Development projects have involved advanced charge-sensitive preamplifier and high-voltage power supplies. The electronics consist of a distributed processing unit (DPU), instrument control system (ICS), pulse-height analyzer (PHA), analog monitor unit (AMU), and appropriate power supplies.

The DPU would converse with the spacecraft Command and Data System (CDS) and instrument control system (ICS), and will pass command sequences, instrument system software modules, and external data from the CDS to the ICS. Conversely, the DPU will accept ICS-generated science and engineering data, external data requests, and external function requests; format these data into packets, and pass the packets to the CDS.

The ICS would control all DCAX system hardware. The ICS could consist of a CMOS microprocessor and appropriate RAM, ROM, addressing, timing, and interface hardware.

The PHA receives its input from either of the high and low-resolution detector preamp outputs. It consists of a peak detection circuit for each detector, a high-speed 10-bit A/D converter for each detector, an access port to the science data RAM's address bus for each A/D converter and the ICS address bus (3 ports), an 8K-byte science data RAM, 16-bit counter, science data output port to the ICS data bus, and digital PHA control circuits.

The temperature sensors, heater currents, and mechanical refrigerator motor current would be monitored with an analog multiplexer-A/D converter monitor unit. The AMU will be controlled by the ICS. The AMU is part of the TSS control loop in that the ICS will turn heaters on or off according to the heat measured by the monitored temperature sensors. The AMU will also gather housekeeping data to be transmitted to Earth in the DCAX data packets.

Detector bias supplies will be identical, voltage programmable, 1-kV output power supplies. Each supply will be capable of operating either detector via a crossover network operated by th ICS, thereby achieving redundancy. Each bias supply will be voltage programmed with an ICS-controlled D/A converter.

The small ion pump on the HiRes detector requires a 3.5-kV power supply for operation. The ion pump power supply should be able to provide up to 1 mA (maximum load) to handle outgassing of a new detector. However, the ion pump load should drop to a few microamps after launch (as the detector vacuum cleans up). The only control required for the ion pump supply is power ON/OFF provided by the ICS. The ion pump will require keep-alive power from launch until the beryllium window is removed during rendezvous with the target comet.

Thermal analysis. The most important element of the temperature control system would be the two-stage cryogenic radiator and heat pipe system used to maintain the high resolution x-ray detector cooling capability required under adverse environmental conditions.

The temperatures of the DCAX and its associated high-resolution x-ray sensor radiation panel are affected by:

1) Conduction and radiation from the main spacecraft body;
2) Radiation from the cometary coma, and tail;
3) Direct solar heating;
4) Radiation from the spacecraft solar array;
5) Conduction and radiation of power required to operate the various components of the DCAX.

A cometary nucleus temperature of 222^{o} K (-51°C) was assumed as worst case. Using a nucleus radius of 1.5 km, a view factor of 0.0009 for radiation heat transfer between the comet and the DCAX was determined for a distance of 46 km. Use of this value is conservative because operation of the DCAX would typically occur at greater distances from the comet nucleus, approximately 100 km.

Sizing of the radiator panel to achieve minimum weight was performed by an iterative procedure. The high-resolution x-ray detector heat dissipation of 20 mW plus the parasitic heat loads from the DCAX housing to the x-ray detector are transferred via two heat pipes, connected in series by a thermal switch device, to the second stage of the radiator system.

The surfaces of the first and second stages of the radiator were assumed to be silver-kapton with an emissivity of 0.75 and a solar absortivity of 0.14. It was conservatively assumed that worst-case dust accumulation would lower the emissivity to 0.30 and increase the solar absorptivity to 0.50. All external surfaces of the DCAX were assumed to be covered with 5 layers of multi-layer insulation.

A 0.25 watt (nominal) Stirling-cycle cryogenic cooler developed by Martin Marietta Orlando Aerospace has been selected to ensure that the 125^{o} K (-148°C) high-resolution x-ray detector cooling requirement is achieved in adverse operating conditions such as dust accumulation on the radiation panels or worst-case solar-array orientation. Because the cryogenic cooler is a split-cycle device, the cooler motor, which dissipates about 30 W, can be mounted on the outside face of the DCAX, far removed from the detector.

The thermal switch was developed by Martin Marietta Denver Aerospace. Its function is to minimize heat flow from the radiator panel to the high resolution x-ray sensor during conditions under which the temperature of the radiator panel would exceed 125° K (-148°C). This would occur if the spacecraft were oriented with the radiator panel pointing toward the Sun or during worst-case solar-array orientation. The cryogenic cooler would operate during these conditions.

H. Low Atomic Number Elemental Analysis

Extensive tests conducted with the collaboration of Dr. Ron Musket and Duwayne Spence of the Kevex Corporation have demonstrated the feasibility of also analyzing cometary dust by coupling Cm-244 alpha excitation with a "windowless" detector. The sensitivity of detectors to the x-rays fluoresced from the low atomic number elements -- such as carbon, oxygen, and sodium -- is usually limited by the poor transmission of the low energy x-rays through the protective beryllium window and the dead layer of the detector itself. To operate in the "windowless" mode, the sample must be placed inside a vacuum chamber where the source and detector are colocated. In the tests to be described in this section, the detector was a special Si(Li) device selected for minimum dead layer and for good response characteristics for low-energy x-rays. The radiation's source arrangement relative to the detector and sample is a special, patented geometry developed for this type of low-energy fluorescence analysis.

Many of the samples we wished to analyze were in powder form, and since the arrangement of the equipment demanded an upright sample, it was necessary to find a method of holding the powder grains with some material which contained no light elements (e.g., no organics could be allowed) and which would not outgas in vacuum. This requirement led to the development of the technique of making gallium mounts. This technique is described in general in section B above, and in greater detail in New Idea Report number 696 submitted by Martin Marietta to NASA.

Altogether, over 80 different runs of 29 different samples were made. Certain of these runs were pathfinder tests to evaluate sample preparation methodology, count-rate systematics, and pure element responses. Both artificial mixtures and natural meteorite specimens were run. This discussion will concentrate on the latter as being the most instructive and most germane to the problem at hand.

Elements Analyzed. In Figure H-1, an x-ray fluorescence spectrum of Murchison meteorite (type C2, or CM) exhibits peaks for not only the light elements, but also for Cr, Fe, and Ni. The copper (Cu) and gallium (Ga) peaks result not from the meteorite material, but from the gallium mounting substrate and the copper backing. The reason these heavier elements are excited is chiefly because of x-ray emissions that accompany the alpha emission from the Cm-244 source material. By far the strongest line on this logarithmic scale is oxygen (O), both because of its high concentration in the meteorite and the fact that the alpha particle excitation efficiency increases with decreasing atomic number of the target element. This is also made clear by observing that the Mg and Si peaks are approximately the same in height, whereas under Fe-55 excitation (see Fig. F-4), the Mg x-ray signal is much less than that of Si. Also resolved and at a good yield is the very diagnostic aluminum (Al) line, sandwiched between Mg and Si. On the other hand, it is also apparent why Fe-55 is a superior source for excitation of medium atomic number elements such as K, Ca, Ti, and Cr. Inspection of Figure F-3 shows superior peak definition for these elements than is seen in Figure H-1.

Light Element Detection. In addition to superior excitation and detection of Mg and Al, the windowless detector assembly also allows analysis of several elements not ordinarily analyzed by x-ray emission. These elements are carbon (C), oxygen (O), and sodium (Na). In Figure H-2, the higher C, Mg, and S content of Orgueil meteorite (type CI) as compared to Murchison (type CM) are apparent. In this magnified linear representation of the two overlaid spectra, the carbon signals are clearly detected from both meteorites. Because of the magnification, the oxygen peaks are off scale.

Similar results are evident in Figure H-3, where the more carbon, sulfur, and oxygen-rich Murchison meteorite is plotted as dots for comparison with the Allende meteorite material, whose spectrum is plotted as bars. This time, the vertical scale is a logarithmic representation, so that the high oxygen content (relative to Si, the normalization element) is apparent, as is the high C and S, but lower Al. It is important to note that the C content of Allende is only 0.3% for the bulk material, yet the peak in this region is clearly discerned from background.

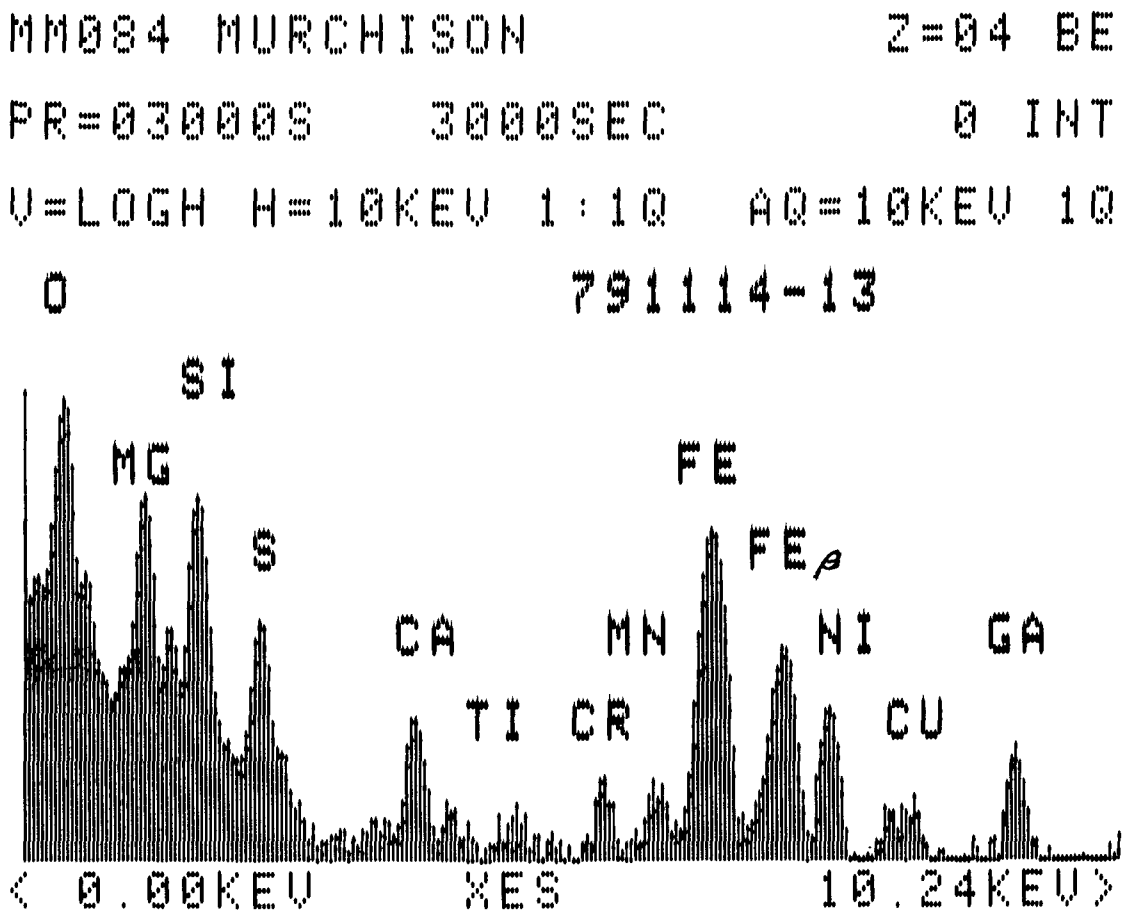

Figure H-1
Spectrum of Murchison meteorite under Cm-244 excitation.

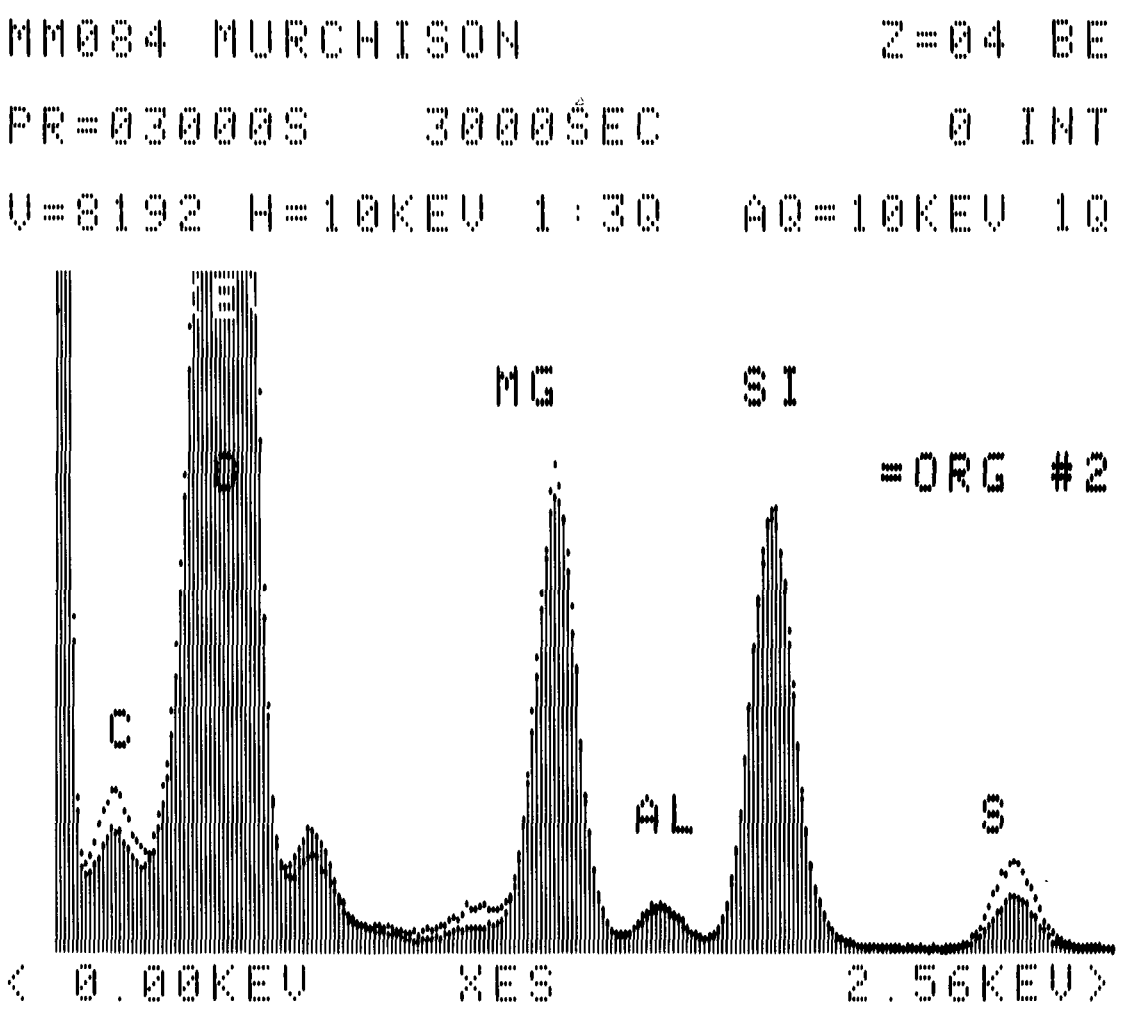

Figure H-2
Comparison of spectra for Murchison and Orgueil (Cm-244 excitation)

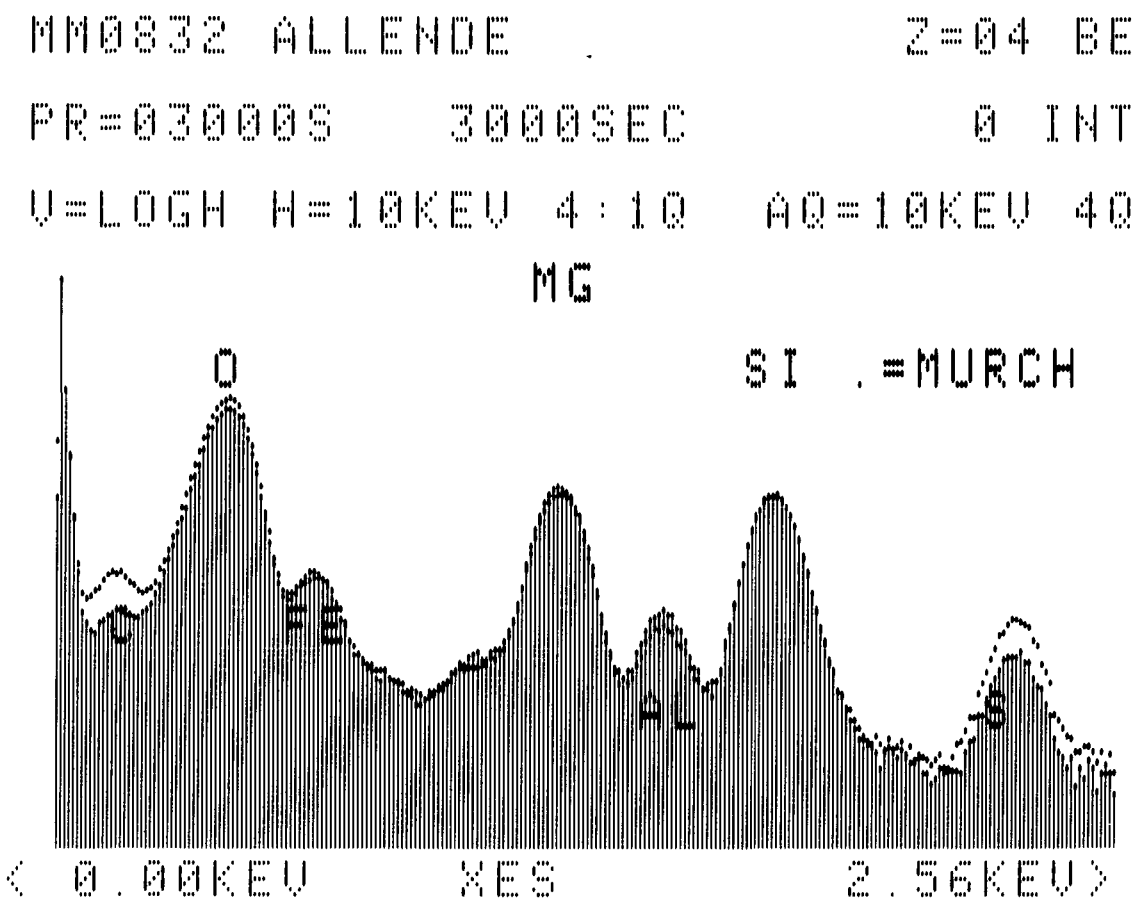

Figure H-3
Comparison of spectra for Murchison and Allende (Cm-244)

A final most interesting example is the comparison of two separate Orgueil samples, Figure H-4. Orgueil #1 had been extracted with water, which removed the magnesium sulfate salt contained in the sample. This explains the much lower Mg, O, and S peaks compared to Orgueil #2, which had never been exposed to an extraction procedure.

The measurement of sodium cannot be satisfactorily done when the sample is collected on a gallium substrate. This is because the Ga and Cu L lines overlap the K emission lines from Na. This problem is avoided, however, by collection of the sample on a surface free of these and other elements of similar atomic number. Organic viscid materials are acceptable, but they do, of course, then interfere with C and O measurements. The solution to this dilemma is simply that comet dust must be collected simultaneously on two separate substrates, with one substrate being analyzed especially for Na, Ga, and Cu, and the other for C and O. All other elements will be analyzed accurately on both collectors. As brought out in section C above, there are ample advantages for using several different collection substrates anyway.

Analytical Accuracy. It is thus determined that the proposed system does discriminate successfully and accurately the known geochemical differences between meteorite classes, including even some of the subtle trends among carbonaceous meteorites. As examples of concentration trends, in Figure H-5 the net integrated peak counts (i.e., backgrounds subtracted) versus element concentrations for the three major carbonaceous groups are presented. These calibration curves for two very difficult but important elements -- oxygen and aluminum -- demonstrate the performance of the method.

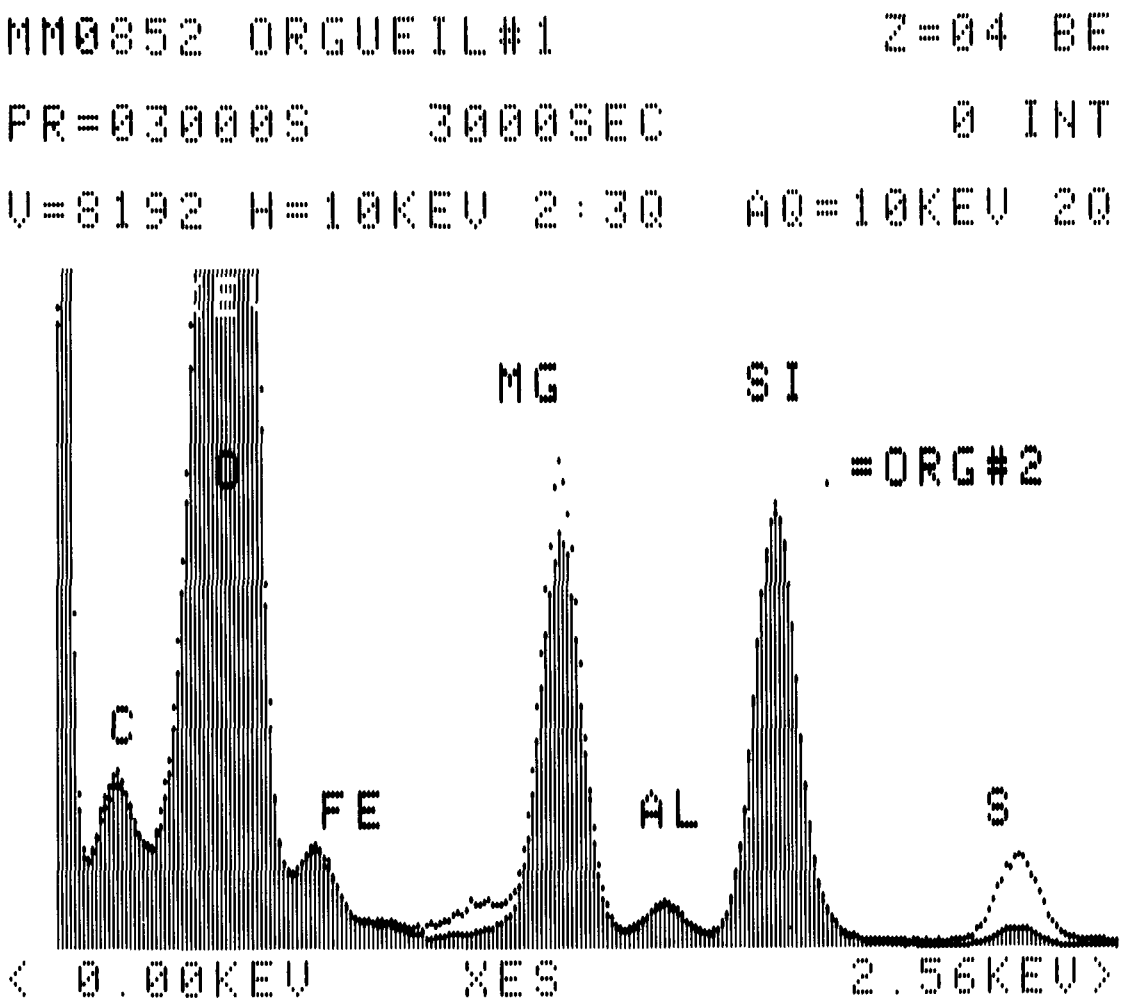

Figure H-4
Comparison of two Orgueil samples. Orgueil #1 (shaded peaks) underwent water extraction.

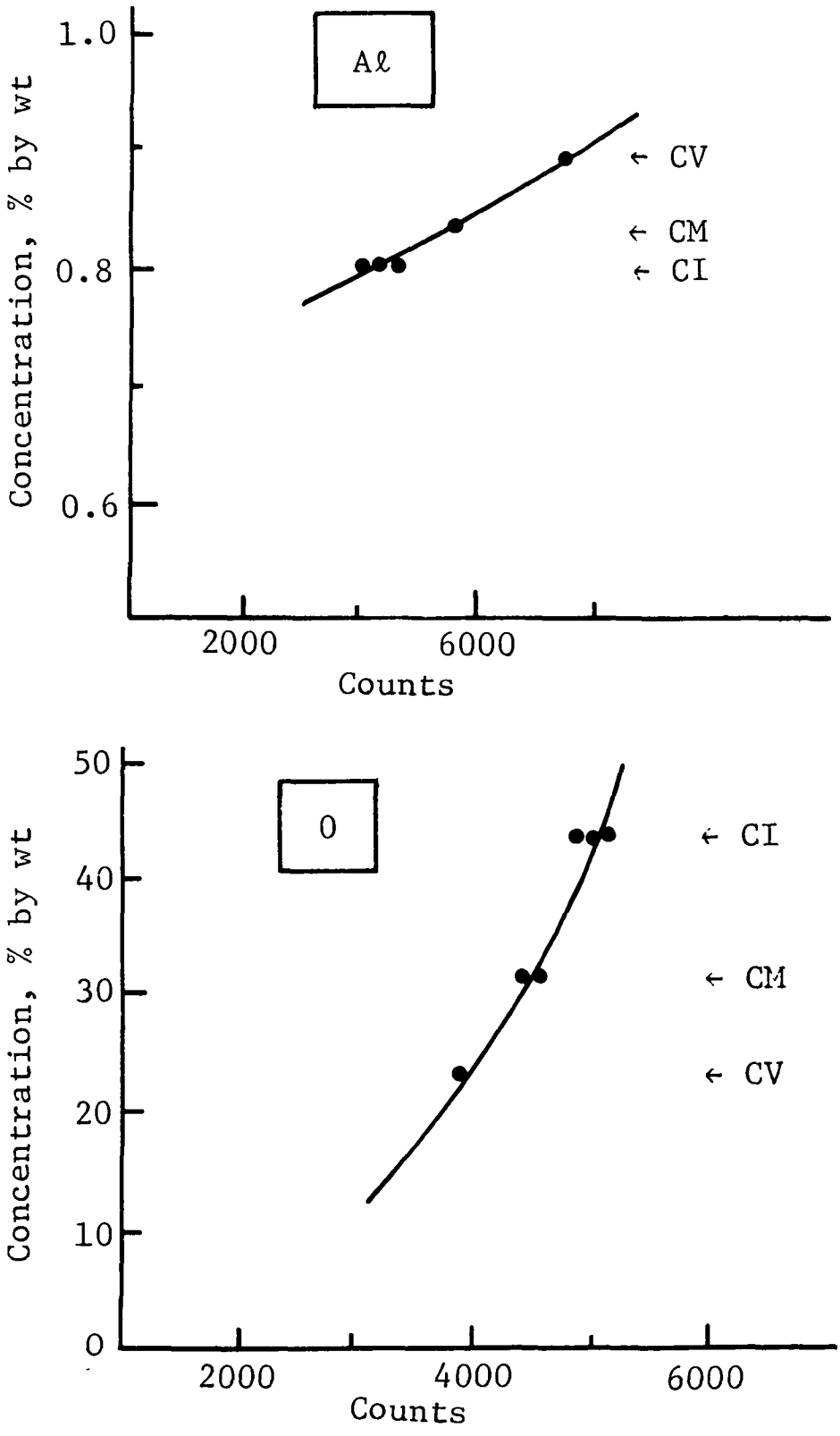

Figure H-5 Quantitative correlation of aluminum and oxygen concentrations in Orgueil (CI), Murchison (CM), and Allende (CV) chondrite samples with x-ray fluorescence peak intensities (corrected for background).

I. X-Ray Diffractions of Cometary Material

The type of analysis made by x-ray fluorescence can elucidate the bulk elemental composition of dust grains to a high degree of accuracy, but cannot uniquely infer the abundances of the various chemical compounds, i.e., mineral phases, which are included in the sample. Another technique, x-ray powder diffraction, yields information on the ordered internal structure (crystalline form) of the various constituent phases. These data, when combined with the element composition data, can greatly improve the reconstruction of the mineralogic make-up of the sample.

To investigate the types of data which might be obtained, we have taken x-ray powder diffraction patterns of two meteorite samples prepared as thin layers. A Philip's laboratory diffractometer was used. The source radiation was the Cu K-alpha-1 line. Over 40 distinct diffraction peaks were observed from the two samples, as delineated in Table I-I. Murchison meteorite represents type CM meteorite material, and contains the very interesting line at about 7.2 Angstroms, indicating presence of a phyllosilicate mineral, such as chamosite (iron-rich member of the chlorite series). Type CI meteorites are very rich in phyllosilicates, presumably due to secondary alteration reactions (weathering) of the original minerals. Establishing whether or not cometary grains include phyllosilicate minerals is of great interest because they imply the prior existence of an aqueous phase (liquid water) or else some mechanism for direct formation of hydrated minerals during nebular condensation. Evidently, chamosite is missing from the diffraction pattern obtained for the type CV meteorite, Allende (see Table I-I).

It should be said at this point that unless a sample contains crystallized mineral grains, no diffraction peaks will be produced. Amorphous material gives one bland, broad-humped pattern. There is certainly some reason to believe that the cometary grains may be poorly crystallized, amorphous material in

Table I-I. X-Ray Diffraction Data for Murchison and Allende Meteorites (d-spacings in Angstroms)

d-Spacing (A)	Meteorite	Peak Height(s)	Mineral
7.24	M*	27.4	CH, CM**
6.56	A	6.8	
6.03	M	9.2	
5.96	A	7.9	Sodalite
5.46	M	8.6	
5.21	A	11.3	
5.18	M	8.2	
4.73	M	8.0	CH, CM
4.55	M	8.4	CH, CM
3.97	M,A	12.1, 14.0	CH, CM
3.82	A	7.0	
3.66	M	16.6	CH, CM
3.61	A	19.6	Sodalite
3.26	M,A	10.6, 5.8	
3.15	A	7.5	
3.11	A	10.3	
3.08	M,A	10.8, 13.9	Gehlenite
2.97	M,A	18.8, 9.7	Diopside, CH
2.91	M	8.4	
2.88	M,A	13.9, 36.0	Diopside, Geh.
2.82	M	8.6	
2.69	A	6.6	
2.66	M,A	16.8, 7.2	CH, CM
2.63	M,A	17.2, 26.8	
2.60	M	12.2	
2.58	M,A	15.6, 29.8	Diopside
2.49	A	8.9	
2.39	M,A	8.4, 11.2	
2.33	M,A	8.2, 11.8	CH, CM
2.25	M,A	7.4, 9.3	

Table I-I. (Cont)

d-Spacing (A)	Meteorite	Peak Height(s)	Mineral
2.19	M	7.2	CH
2.00	A	7.7	Sodalite
2.06	M	6.4	CM
1.96	M,A	7.9, 25.5	
1.89	A	8.1	
1.87	A	6.8	
1.86	A	7.5	
1.80	M,A	8.8, 6.7	CH
1.77	M	8.5	
1.74	M,A	7.2, 14.5	Gehlenite
1.68	A	6.8	
1.67	M,A	6.3, 7.3	
1.65	A	6.3	
1.63	M,A	5.3, 5.8	
1.56	A	4.6	

* M = Murchison meteorite
  A = Allende meteorite

**CM = monoclinic chamosite
  CH = hexagonal chamosite

view of the characteristics of many of the Brownlee particles. On the other hand, some of these particles are indeed well crystallized, as is obvious from their morphology when viewed with the scanning electron microscope. Although an x-ray diffraction experiment should be considered of lower priority than a primary measurement experiment, such as for elemental composition, it is nonetheless of considerable interest for missions which can afford a more comprehensive instrument complement.

Feasibility of a space-borne diffractometer has been proven through testing and concept studies in this and other laboratories. In our work, the objective was to develop a miniaturized, low-power diffractometer system suitable for use on an advanced spacecraft missions to Mars. The first science breadboard of this diffractometer was fabricated and tested in 1973. Results with the first breadboard revealed desirable further improvements and these were incorporated in a second unit. The second unit utilizes the conventional x-ray optical arrangement, the nonfocusing Bragg-Brentano geometry in which a highly collimated monochromatic beam is directed at an angle to the surface of a fine-powdered sample and the diffraction maxima observed at the same takeoff angle. Rotation of the sample and detector about a common center, but with the detector moving at twice the angular rate, preserves the equal-angle geometry throughout the sweep from 0^{o} to 45^{o}. This geometrical arrangement is shown in Figure I-1.

Movement of the goniometer system is controlled by a single stepper motor that drives both gears. This stepper motor is in turn driven by a specially designed diffractometer control unit. With the controller, it is possible to step-scan in various increments from 0.8^{o}/step all the way down to 0.01^{o}/step. The scan time is also variable and covers the working range in as fast as 4.5 minutes or, for high-precision work, as slow as 10 hours. The slower scan range is particularly useful for detailed study of diagnostic peaks in a particular angular range of interest.

The x-ray tube is a fully sealed device with an electron beam source and an indirectly heated oxide cathode formed as a triangular-sectioned annulus.

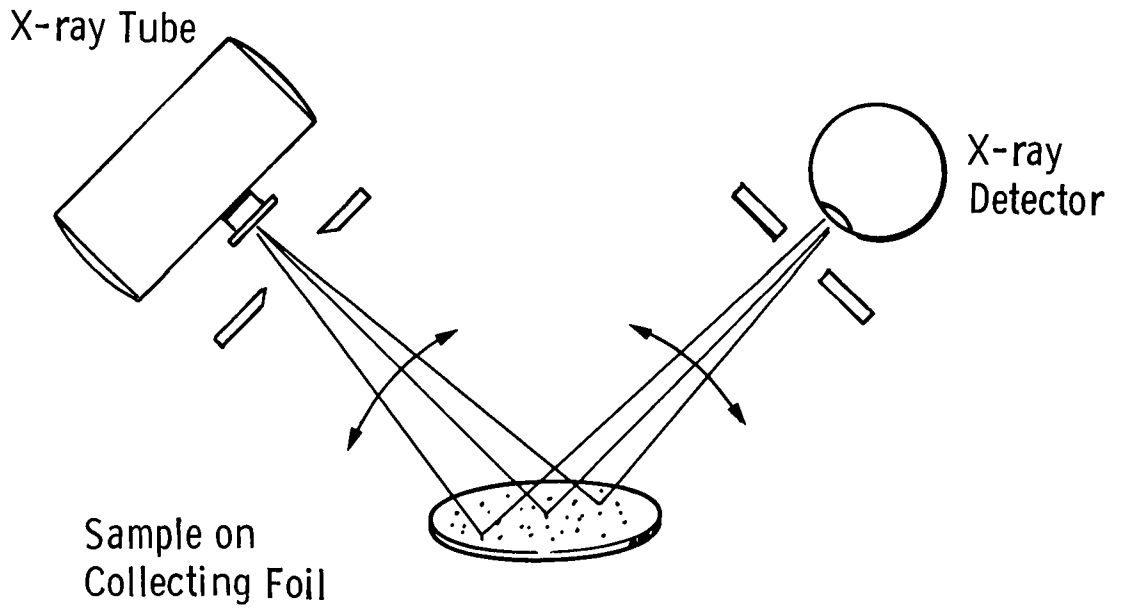

Figure I-1
Geometrical Arrangement for X-Ray Diffraction Analysis

Shaping electrodes produce a tightly focused beam that may be turned on and off at a high frequency, if desired, by a current-control electrode. Combined with a monitor and feedback circuit, this electrode is used to adjust for constancy of beam current, and hence tube output. The basic tube is inherently rugged and was selected because many of the design characteristics and fabrication techniques have been successfully applied in spacecraft microwave communication systems. Because this unique design employs a point source of x-rays rather than the conventional line source, the need for complicated Soller slit assemblies is eliminated. A number of other features of the diffractometer design are given in Table I-II.

As an example of the discriminatory power of this miniature diffractometer, the patterns shown in Figure I-2 are of three types of clay minerals, two of which have prominent peaks at the high d-spacing, low angle limit. Note in particular the detection of the montmorillonite peak at about 5 degrees (two-theta), which is diagnostic of these and other large d-spacing phyllosilicates found in type CI carbonaceous chondrites.

Table I-II. Features of Diffractometer Design

Point Source Obviates Need for Soller Slits

Tight Geometry Produces High Count Rate

Both Low and High Angles Can be Scanned

Monitoring Incoherently Scattered Component Eliminates Requirements for Stringent High-Voltage Stability

Amenable to X-Ray Fluorescence Modes

High Energy (Cu K) Minimizes High-Angle Limit

X-Ray Tube Derived from Flight-Proven Microwave Tube Design

Detectors Flight-Proven on Viking

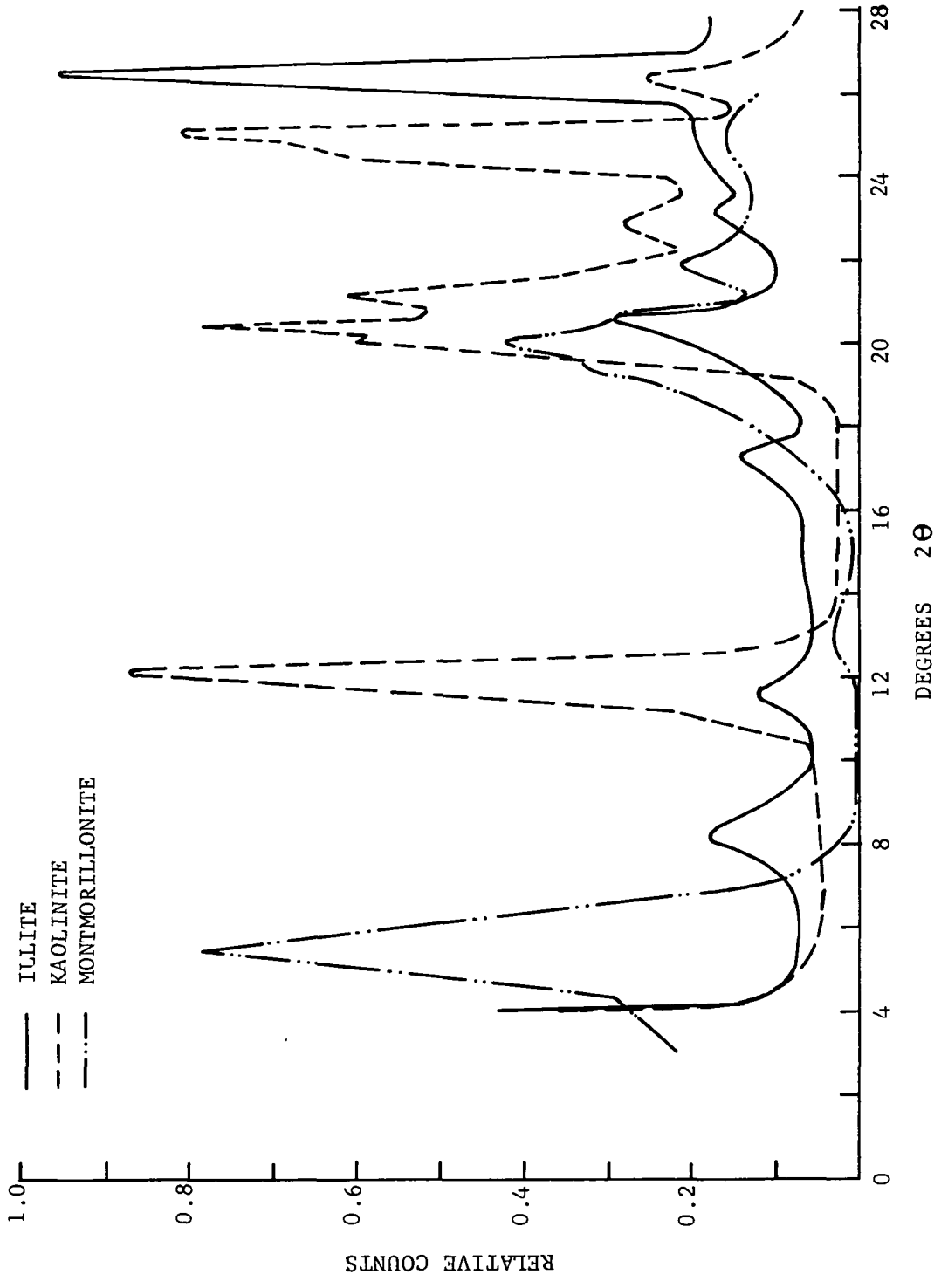

Figure I-2
X-Ray Diffraction Patterns from Miniature Diffractometer

J. Direct Beam Excitation of the Nucleus

In 1978, it was suggested jointly by this author and Dr. J. I. Trombka that an electron beam directed toward the nucleus might be sufficient to stimulate x-ray fluorescence and thus probe directly the composition of the nucleus without the necessity of a physical docking by the spacecraft. Some of the advantages over just analyzing collected dust are that it should provide some idea of the compositional heterogeneity of the nucleus as well as a direct indication of the ice-to-dust ratio.

There are, however, certain scientific disadvantages as well as technical challenges associated with this scheme:

a) Lack of sensitivity may prevent determination of any but the major and high-minor elements.
b) Electron beam operation could lead to differential charging of spacecraft components causing, in turn, electrostatic discharges damaging to onboard electronics.
c) The electron beam will naturally diverge during free flight to the cometary nucleus; this beam blow-up will limit achievable spatial resolution.
d) Very high voltages are required; the resulting system could be very large and heavy.
e) Target charging could cause defocusing or rejection of the beam.

We have subsequently studied these and related problems to examine the feasibility of this suggested experiment.

Beam Parameters. In the laboratory, we have conducted an experiment using the defocused beam of an electron microprobe to quantitatively measure the stimulated fluorescence from Allende meteorite material. Scaling from these results, an adequate counting rate should be achievable even at a distance of 1 km from the surface of the nucleus if the electron gun is operated at 10mA and 20kV. Since the observed intensity varies as the inverse square of the

range to the nuclear surface, moving closer has a very beneficial effect on counting rate (hence, on signal-to-background ratio; and/or stay time required for adequate measurement). On the other hand, the feasibility of accomplishing such a measurement from a distance of greater than 10 km seems low.

Beam Spreading. Even for a perfectly parallel beam in free space, divergence will occur because of charge repulsion. Using the equations of motion, readily derived from first principles, the spreading of an initially parallel beam has been calculated. Some results are summarized in Table J-I. These estimates pertain to the comet in its quiescent state, i.e., they neglect the halo effects of electron scattering by gas, plasma, and micron-sized dust. Dust becomes a problem at particle desities (integrated along the line of site to the target) of about $10^7/cm^2$ (for average particle diameter of 1 micrometer).

Though most cometary nuclei are only 1 to 5 km in diameter, the beam diameters are small enough to do useful mapping. At a range of one kilometer, it may be possible to achieve 50 m resolution, and hence mapping of the nucleus to roughly 300 pixel elements per hemisphere. Since comet nuclei rotate, in general, a mapping strategy could simply involve station-keeping at a low latitude point and allowing the comet to slowly (period of typically 5 hours) rotate. The map would be completed by taking up a new position at the diametrically opposite latitude.

Table J-1. Electron Macroprobe Spreading Characteristics

Electron Energy (keV)	Beam Current (mA)	Range to Nucleus (km)	Beam Diameter at Nucleus (m)
20	1	0.1	1.3
20	1	1	16.3
20	1	10	190
20	10	1	56.8
30	10	1	41.0

Target Charging. Cometary dust is quite likely a poor conductor. It is difficult to usefully bound the expected migration rate of built-up charges. Under worst-case conditions of no charge losses, a one milliampere beam current with 50 m pixel diameter would charge up to the 20kV accelerating voltage in much less than one second. Mechanisms by which charges could be lost include neutralization by ambient plasmas, lateral and penetrating charge migration, ablation of particles and surface layers, and sublimation of negative ions. If these processes are found to be slow compared to the charging rate, a mission strategy of sequential pulsed irradiation of different surface elements could be adopted, with allowance for charge dissipation between re-pulses of the same target element.

Spacecraft Charging. It is now well known that charging of spacecraft can cause significant damage to onboard electrical circuits when localized discharges occur. A recent NASA program, the SCATHA satellite, was dedicated to the study of this problem. This satellite included a number of monitoring devices as well as electron and ion guns.

On previous satellite missions, high power electron guns have been successfully operated for the purpose of studying energetic electron propagation in the geomagnetic field. There are therefore ample precedents for operation of equipment of this type on spacecraft missions. It will be important to carefully consider the maintenance of charge balance on the spacecraft if hazardous charge/discharge transients are to be avoided. One technique that has been used in the past involves the use of a compensating ion beam to balance overall charge. If the comet mission is to be accomplished using an ion drive engine, then the ion source might be used in conjunction with the electron gun to achieve the desired control over the spacecraft potential. Also, the minimization or protection of exposed insulating surfaces on the exterior of the spacecraft might be a sufficient safeguard.

Device Size and Weight. Electron gun design is sufficiently versatile and advanced that the gun itself could be as small as 1200 cubic cm, weighing

1.5 kg. The necessary high voltage supply is a somewhat greater problem, although recent advances have made possible a supply which is 15x15x6 cm, weighing less than 2.5 kg, and providing 30kV at 1mA. Application of available technology satisfies expected spacecraft constraints on size and weight. Power consumption is approximately 40 watts, but could be as high as 500 watts if the higher currents (10mA) were found necessary. On solar-electric driven spacecraft, this is still a small fraction of the available power.

K. Prototype Housing for Cryogenic Detector

A key component of the recommended instrument system is a cryogenically-cooled high resolution detector. In laboratory tests, a detector housing of special design was coupled with a miniature Stirling cycle refrigerator. Although the test successfully demonstrated operation of the detector in the complete absence of liquid nitrogen coolant, the ultimate performance was not achieved because of excessive heat leaks through the housing. We have consequently re-designed the detector support and housing assembly, using high-vacuum components and materials with high thermal impedance. The new detector front-end system includes all the normal electronic components, plus a thermocouple temperature sensor. To keep costs down, only an inoperative detector and a low-cost, medium thickness beryllium window have been used.

A cross-section of the prototype housing is shown in Figure K-1. The three support braces for the copper rods are low thermal conductivity isolation "spiders". At the end for connection to the refrigerator, the copper rod coldfinger is sealed to a highly convoluted, thin bellows. The main purpose of the bellows is to provide a long heat path and hence a high thermal impedance to transport of heat into the copper rod from the outside structure. Maintaining a high vacuum within the housing prevents heat loss by other convection. We have also studied the amount of heat loss via radiation coupling to the copper rod, and find it to be small enough to not represent a major problem.

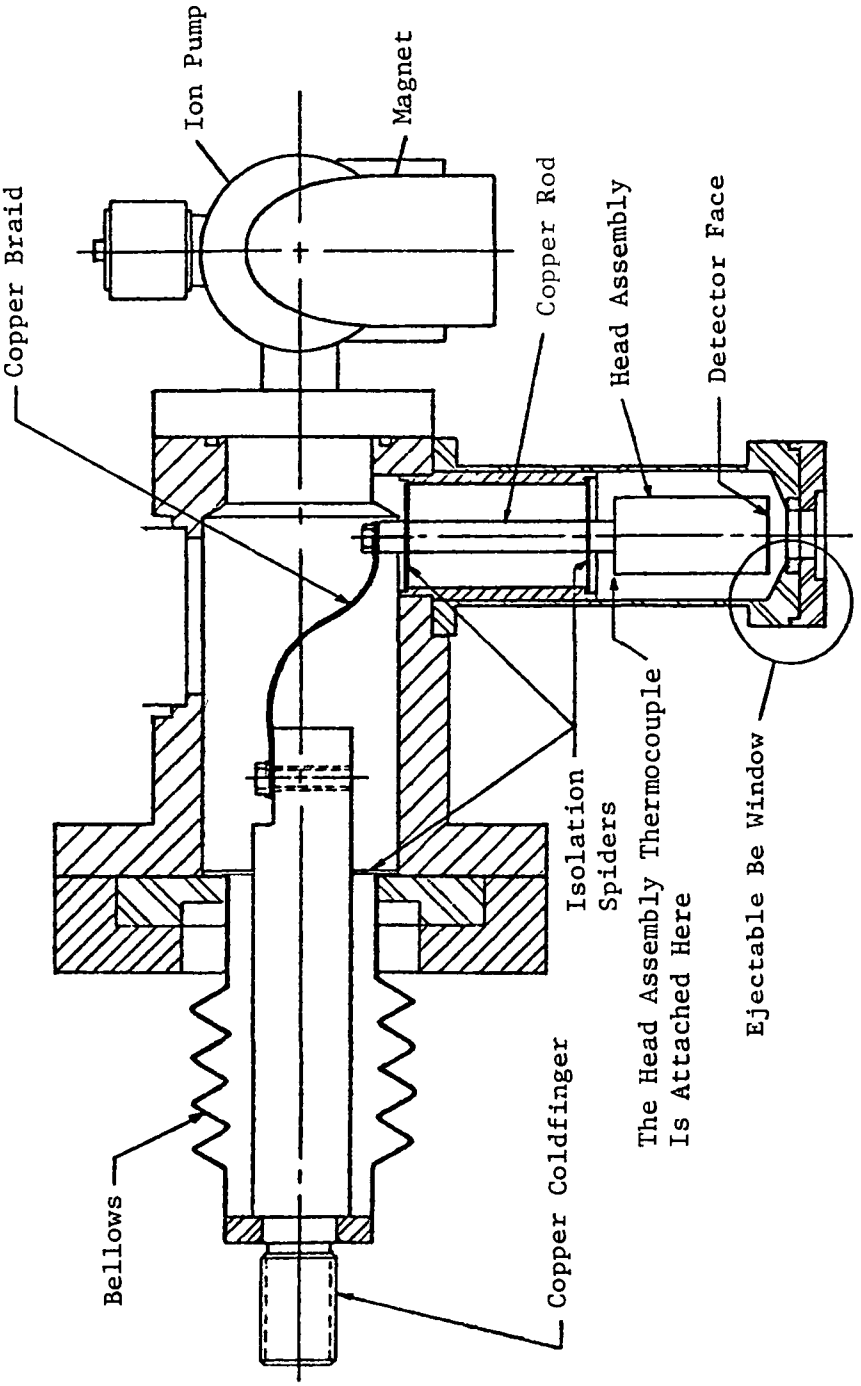

Figure K-1 Prototype Detector Housing

Calculations of heat flow across the bellows indicates only 370 mW at a temperature differential of 215 K between copper rod and housing. However, actual experiments indicate that much greater heat fluxes are probably occurring. One source of error in the calculation might be the use of a room-temperature conductivity value for stainless steel, whereas a value at cryogenic temperature is more appropriate.

In the tests, a closed cycle Stirling cryocooler rated at 250 mW at 80K temperature was used. At higher temperatures, it can accommodate many times more than a 250 mW heat load. The cooler operates off 17.5 VDC, consuming 24 watts of power. The cobalt alloy coldfinger of the cryocooler was thermally coupled to the copper rod coldfinger of the prototype detector housing using both a compressed copper fuzz button and a copper sleeve held in place by a Kapton oversleeve. Chromel-alumel thermocouples were used to monitor temperature. In a separate experiment, a copper rod of 140 g mass was similarly connected, and supported within a vacuum housing by Kapton rings. The resultant time-temperature profile is shown in the data plotted in Figure K-2. In the first one hour of cryocooler operation, the rod was at a temperature of -52 deg C, and had reached a temperature for satisfactory operation of the detector (-140 deg C, or 133 K) by 2 hours, 34 minutes. After 5 hours, the temperature began to stabilize at -202 deg C (73 K). After removing power from the cooler, the copper rod stayed below -140 deg C for two hours.

With the prototype housing, the cooling of its approximately 60g copper mass was much slower. Because it was suspected that a major source of heat influx might be through the bellows, an isolated test on just the bellows and its mounted copper rod was performed. This copper rod has an estimated mass of only 32g, and if the bellows were an adequate insulator, should cool down much faster than the rod in the preceding test. Results are given in Figure K-3. This rod did indeed cool more rapidly, achieving the -50 deg C point in only 30 minutes. However, after 2 hours, it reached only -115 deg C, and began cooling at a rate slower than for the more massive isolated copper rod. The ultimate temperature that could have been reached is estimated at -130 C

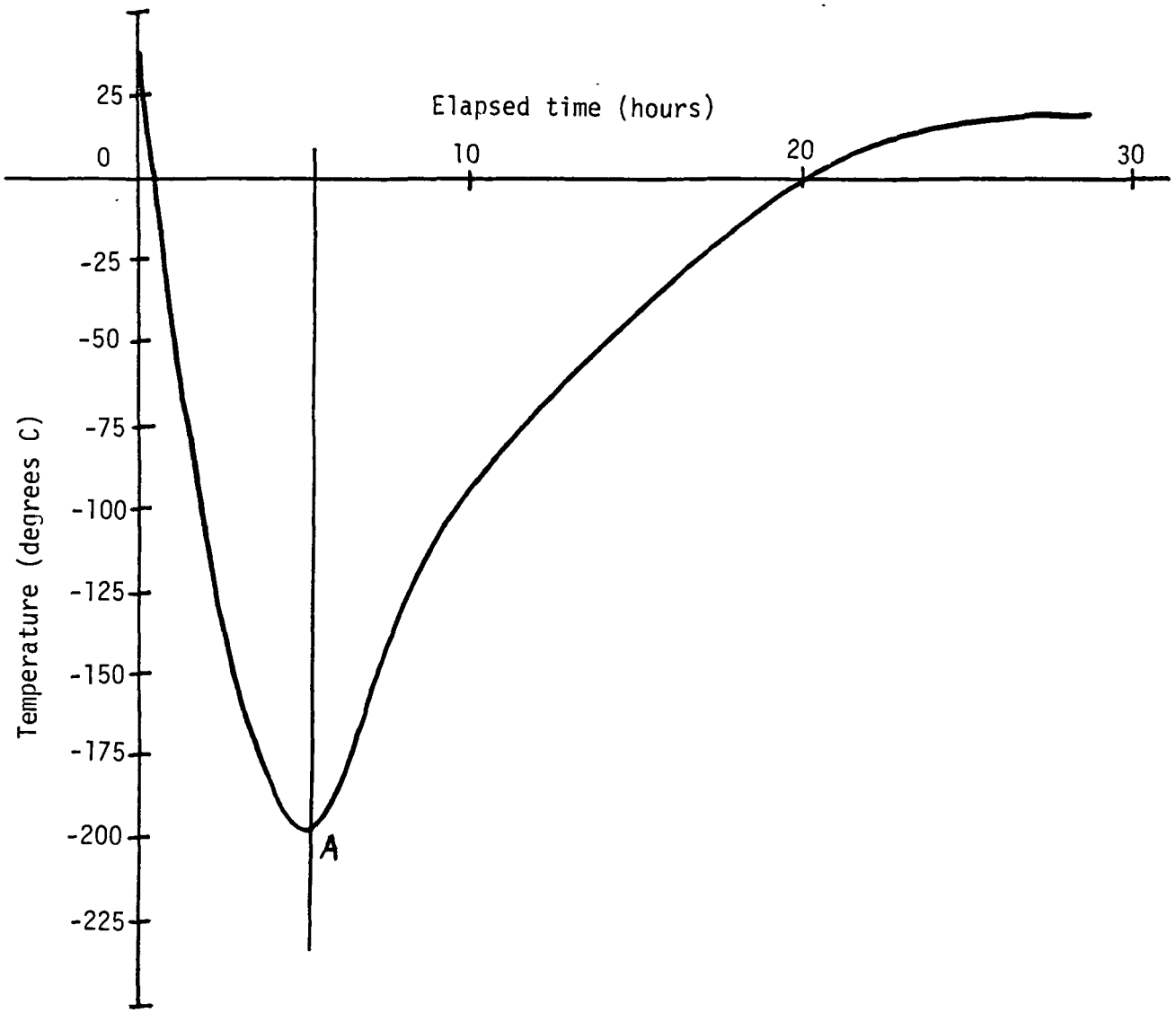

Figure K-2
Cooling and warm-up of a copper rod cooled by the Stirling cycle cryocooler. Power to the cryocooler was removed at time A (5 hrs, 30 min).

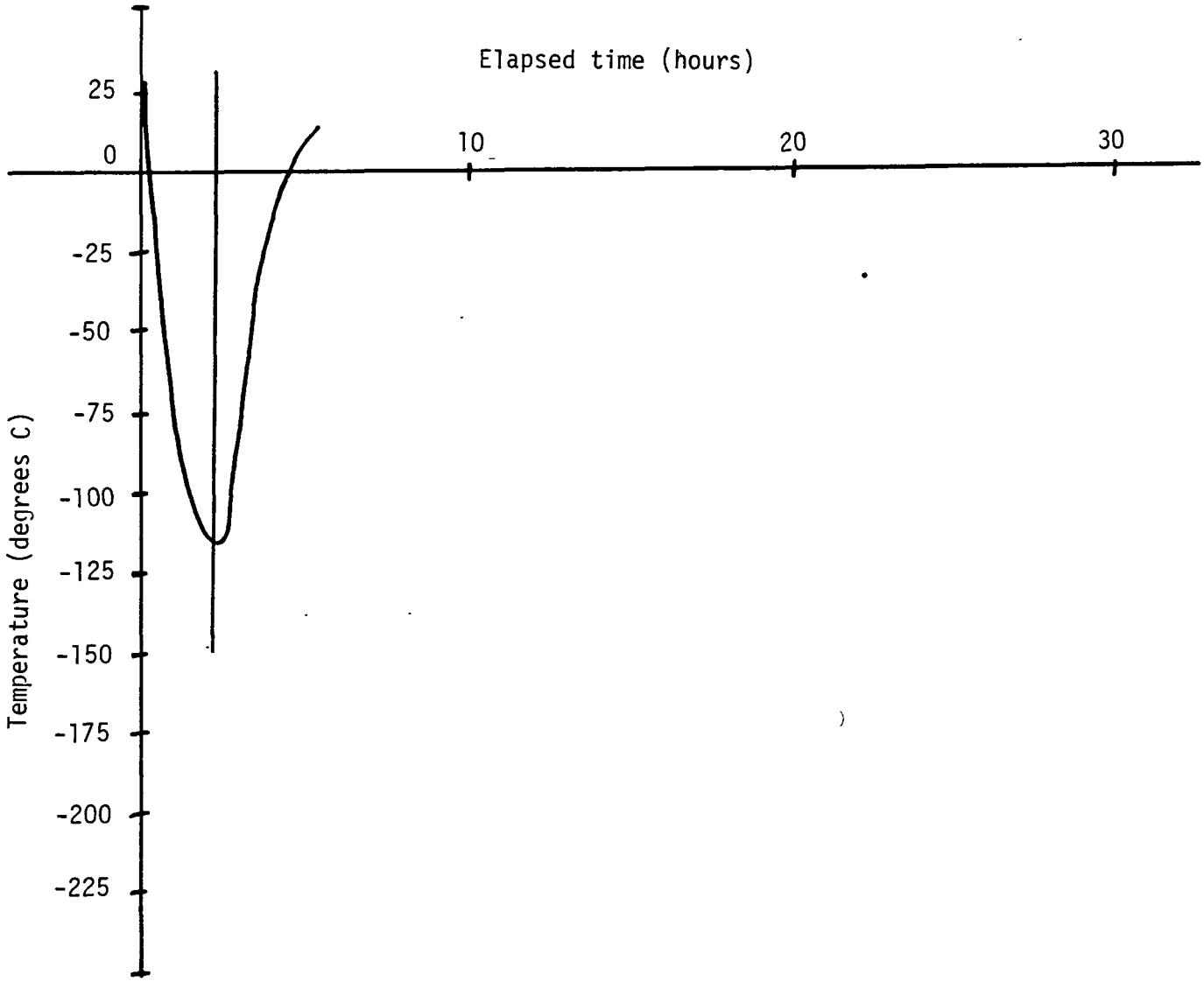

Figure K-3
Cooling and warm-up curves for the bellows and copper rod assembly of the prototype detector housing.

(143 K), some 70 degrees higher than the ultimate temperature of the larger rod. In addition, once power was removed, the bellows-mounted rod increased 20 degrees in temperature in only 15 minutes. This performance is close to, but not satisfactory for the operating conditions needed by the Si(Li) detector. Since the bellows is quite long (about 8 cm in convoluted length) and thin (5 mils), it is probably not feasible to reduce its conductance by adjusting the L/A ratio. A much more satisfactory solution, both in terms of weight and reliability, would be to find a material of suitable low conductivity and yet with good vacuum sealing and low outgassing properties. The latter requirements arise from the critical susceptibility of the silicon x-ray detector to exogenous contaminants. One possible solution worth pursuing is the micro-dewar using a convex, thin glass wall, similar to the approach taken for cooling of certain infrared solid-state sensors.

The mass properties of the prototype housing are as follows:

Item	Mass
Aluminum housing (ind. detector)	25 g
Bellows ass'y (w/o SS flange)	53 g
Ion pump (w/o magnet)	140 g
Magnet	60 g
Total	503 g

L. Particle Size Distribution Effects

The x-ray fluorescence emission from a material is, in general, a nonlinear function of sample composition and thickness. For most elements and comet dust particle sizes envisioned, this generalization holds. There are two extremes--the "thin" and "thick" approximations--in which applicable equations become greatly simplified.

Where the specimen or particles are "thin," i.e., relatively transparent to the excitation and fluorescence x-rays, the counting rate in the fluorescence detector will be proportional to the concentrations of the element in the sample and to the thickness of the sample. On the other hand, if either excitation or fluorescent x-rays are strongly attenuated within the specimen (or the sample is several grains thick), the "thick" approximation is valid and the counting rate becomes independent of further increases in thickness of the sample. It is interesting that for both relations, the ratio of counting rates, R_i/R_j, between two elements i and j, is independent of thickness. However, if the grain is thin for one element and thick for another, the ratio becomes linearly dependent on thickness.

Calculations we have performed show that neither extreme can be assumed for the wide range of elements of interest in comet dust. In the field of x-ray fluorescence analysis of microparticles and aerosol droplets, the occurrence of particle sizes that satisfy neither the thick nor thin approximations is termed the "intermediate region." For this situation, the ratio of observed intensities for two different elements does depend on grain thickness.

Sensitivity Calculations. To examine this problem, we have calculated values of the ratio R_i/R_j for various particle sizes and integrated over particle size distributions such as the Sekanina-Miller distribution and straight power-law functions. The computer program, entitled COMETD, models the absorption of both excitation and fluorescent components as a function of sample thickness. The dust composition is taken as that of bulk CI carbonaceous material. Some of the results are plotted in Figures L-1 through L-3. These figures demonstrate the theoretical change in relative counts, expressed as the ratios between selected elements. For ease of presentation, all ratios have been plotted normalised to 1.0 in the thin approximation (in reality, the absolute values of these ratios can be much different than one, but this has the effect of merely sliding the curve up or down on the plot).

In Figure L-1, we note the strong functional dependence of observed Fe/Si; and S/Fe ratios, especially for particles greater than 10 um in thickness. On the other hand, the ratio of two elements which are closer in atomic number (and hence with closer x-ray emission energies) is much less dependent upon particle thickness. The example of this is the S/Si ratio. This figure also illustrates the point that if the comet dust is self-adhesive, so that more than one monolayer can be collected, it is possible that by monitoring the change in apparent ratios of certain elements, one can infer the thickness of the collected sample.

Figure L-2 and L-3 provide more examples of ratio dependencies. In Figure L-2, we have plotted with a + symbol the average result obtained if the dust is distributed in size according to the Sekanina-Miller formula. Fortunately, the small grains predominate so that "effective" thickness is only around 10 um, a portion of the curves where ratios are not strongly sensitive to thickness.

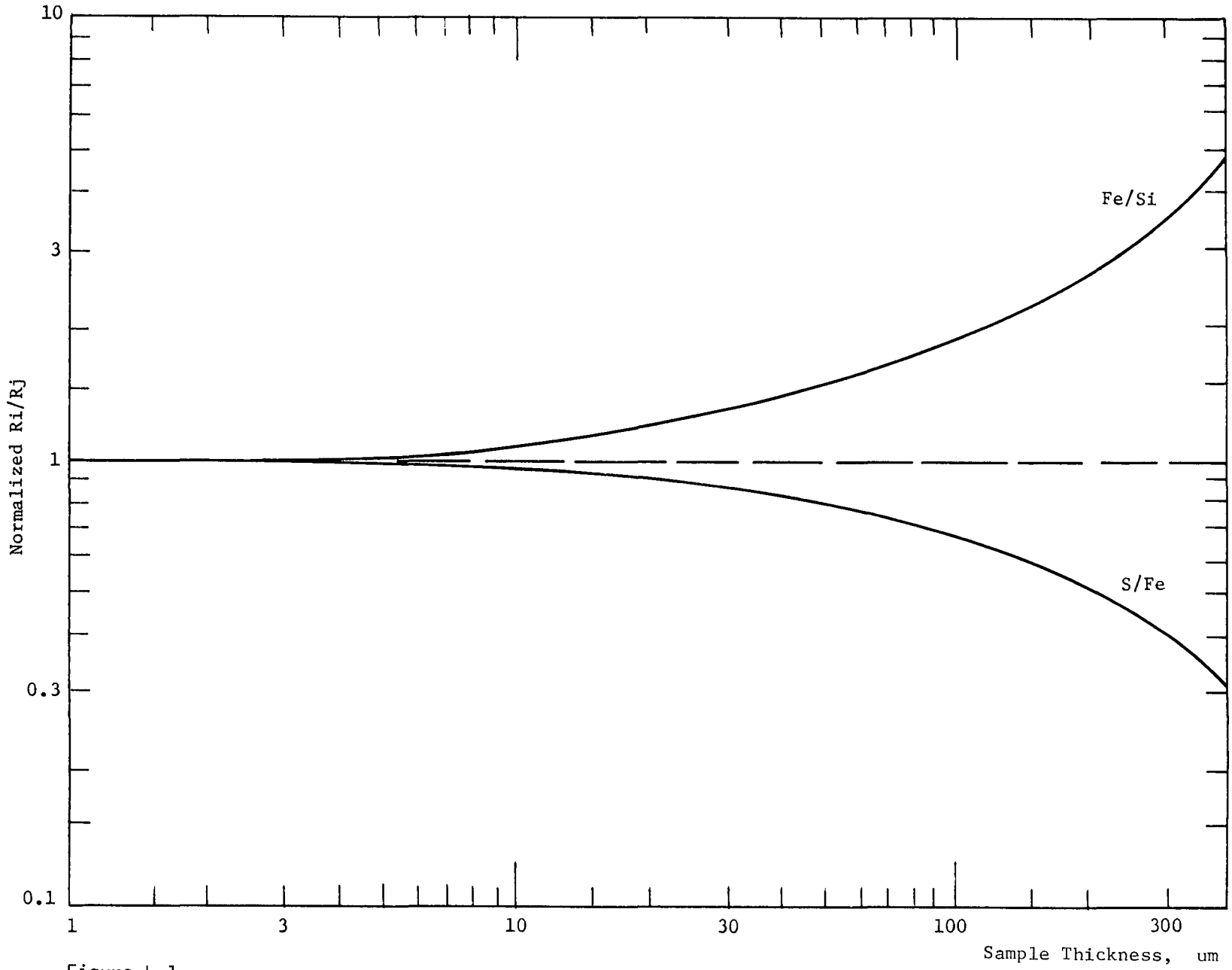

Figure L-1
Normalized Ri/Rj Ratio vs. Sample Thickness
for Fe/Si and S/Fe (see text)

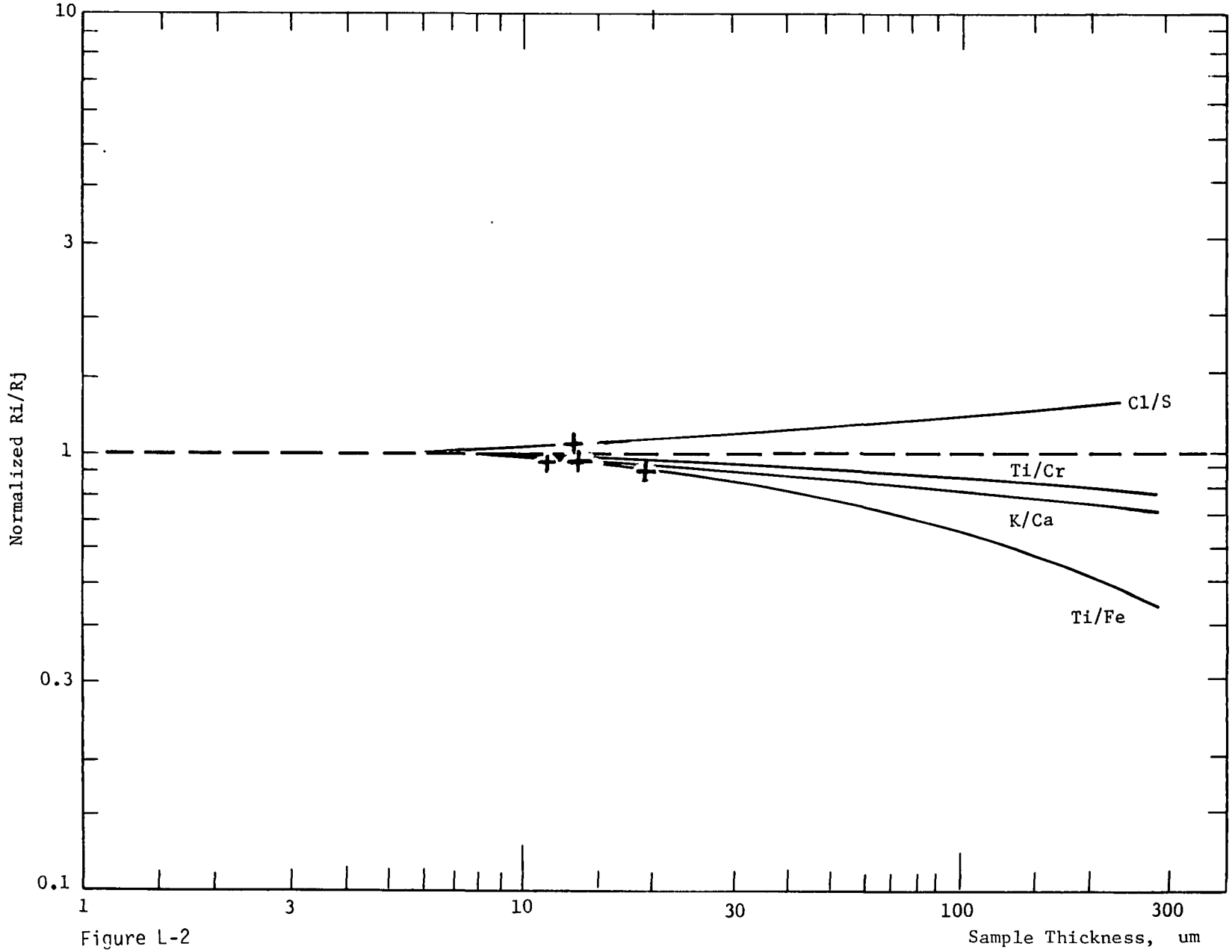

Figure L-2
Normalized Ri/Rj Ration vs. Sample Thickness for Various Element Pairs (+) symbols indicate average result if distribution is according to Sekanina-Miller formula.

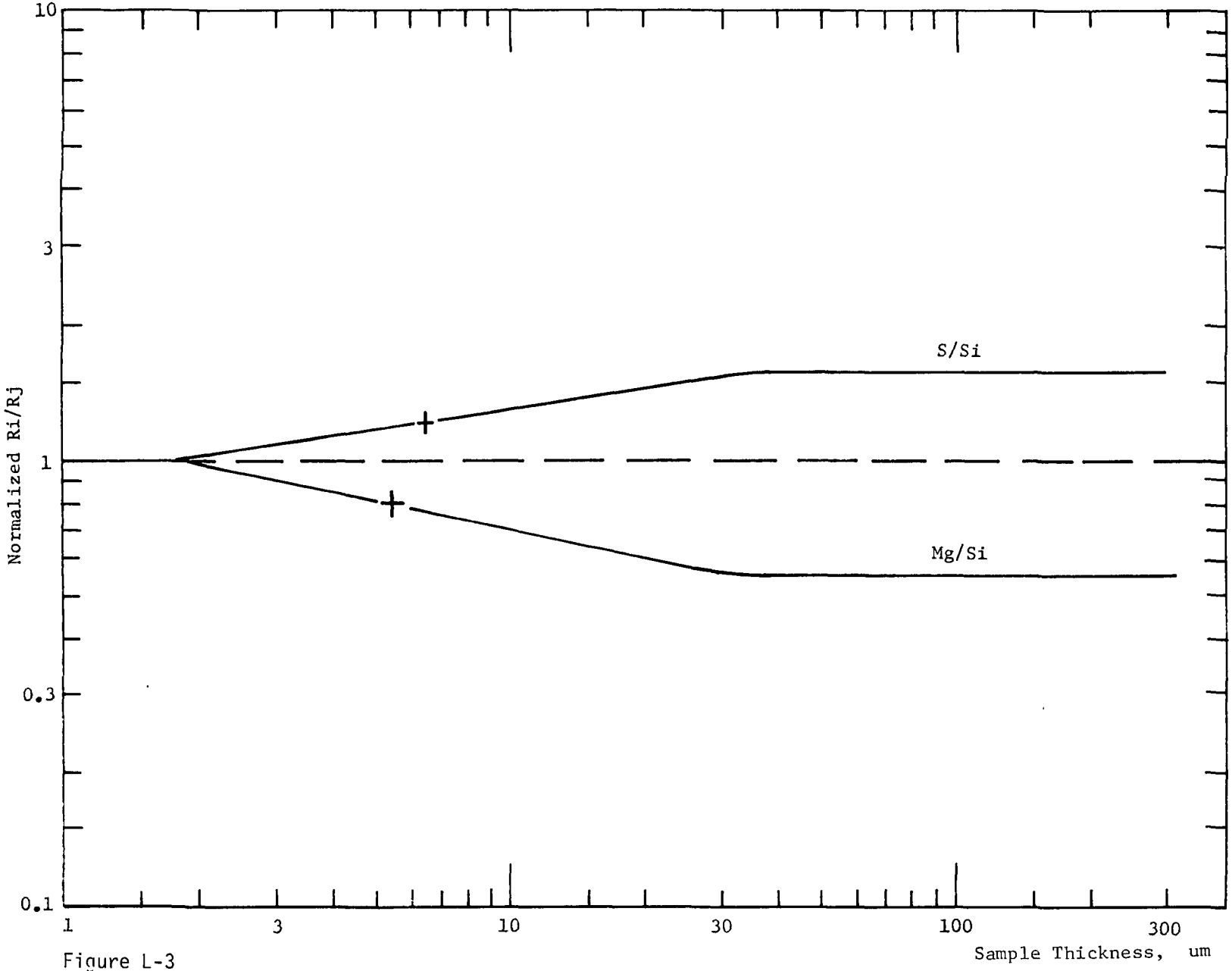

Figure L-3
Normalized Ri/Rj Ratio vs. Sample Thickness for S/Si and Mg/Si. (+) symbols indicate average result according to Sekanina-Miller formula.

In Figure L-3, we also show results of calculations with other size distributions. Ratios are in general only very weakly dependent upon the detailed or even the gross shape of the distribution curve, as the wide range of exponential shapes demonstrates. Although we give results only for S/Si, the dependency for other elements (selected as near-neighbor pairs) are quite similar. The key conclusion is that ratios can be most accurately determined for elements with similar x-ray emission energies. By a process of "bootstrapping," i.e., finding best ratios for a string of overlapping pairs, the total composition of the sample can be found. Note also that knowledge of the actual sample thickness within even a factor of two can nearly eliminate any uncertainty of element ratio values.

Independent Assessment of Factors. Knowledge of particle size distribution and/or sample thickness could greatly reduce any residual uncertainties regarding the correction of the data for sample thickness. Perhaps the most useful auxiliary data would be that from experiments designed to measure particle size distributions. Many techniques have been proposed for this type of experiment, including rather sophisticated laser-based optical scattering equipment. An important distinction that must be made is between dust and ice grains, since the distributions could be different.

One of the most technically challenging but precise techniques would be to image individual dust grains in a miniaturized scanning electron microscope. This has the advantage that chemical homogeneity between particles and within particles might be evaluated via a fluorescence emissions monitoring mode. On the other hand, it is doubtful that a sufficient statistical sample (number of images) could be obtained to result in as accurate size distribution information as can be obtained by other methods.

In addition to size data, it will be quite useful to know the amount of material collected, i.e., the thickness of the dust deposit or the percent area coverage of a monolayer. Various special experiments can be conceived for this. Radiation gauging by alpha particles or x-rays is one obvious technique. Indeed, the proposed experiment can obtain such data by two different phenomena just from x-ray interactions: (1) thickness, by changes in intensity of the backscattered radiation; and (2) areal coverage and thickness, by the obscuration of the emissions from two marker elements placed in the collection substrate. The first technique will not be highly accurate because the mean particle size of one to a few microns is less than the minimum thickness required for the collection substrate. But the second technique could be quite accurate, especially using non-interfering markers such as F, Sc, and As; or, by CsI L and M lines, or by Pd L lines.

Other approaches include measurement of the mass of dust collected on a given exposed area by the quartz crystal microbalance or the oscillating fiber microbalance. Extensive experiments with the latter have been conducted in this laboratory and elsewhere to demonstrate the feasibility of its application to this problem.

M. Analog Particle Preparation

Much of our experimental work has used samples of the types described in section B above, and meteorite powders. Unfortunately, there are no naturally-occurring materials on earth which are equivalent to "primitive" elemental composition, i.e., containing relative abundances of elements paralleling that of the sun and the presumed proto-solar nebula. The CI carbonaceous chondrite meteorites do indeed provide this kind of material, but with two drawbacks: 1) the elemental match holds on a bulk scale, not on the microscopic scale, where significant elemental variations occur, and 2) this material is very rare and not available in appreciable quantities for studies of this kind.

It would be of considerable value, therefore, to have available a homogeneous material of primitive-like composition for instrument calibration as well as laboratory testing of instrument susceptibility to particle size effects, such as those covered in section L above. To achieve the desired composition, about 12 to 15 different elements need to be included. Ideally, one would simply combine the necessary chemical ingredients, heat them to melting, then quench the mixture quickly to form a homogeneous glass. However, depending upon the selection of component, there can be a very wide range of melting points (m.p.) so that as the temperature is increased, the lower m.p. components will melt and begin to vaporize. By the time the high m.p.'s are reached, significant losses via vaporization of several components could occur.

Two techniques are available to try to prevent such losses. The first employs a fluxing agent, such as lithium tetraborate, which melts at a relatively low temperature but will fuse silicates and many other oxides at temperatures below their pure-state m.p.'s. The problem with this approach is that the fluxing agent must generally be in excess of the material being processed. Typical ratios are 4:1. Thus, the resulting glass is predominantly composed of foreign atoms (especially Li and B), and would not have the same x-ray absorption characteristics or the same impact vaporization characteristics as the presumed comet dust. Thus, although this approach could be of some value in certain studies, e.g., trace element detection sensitivities, it would not provide satisfactory material for most experimental purposes.

A second approach is an adaptation of the technique originally developed by R. W. Brown for producing glass pellets of uniform composition as calibration standards for election microprobes. In this approach, the fusion of components is accomplished rapidly by heating the mixed materials in a molybdenum "boat" strip heater. Use of the rapid heating and an inert cover gas (such as argon or nitrogen) at high pressure to help suppress vaporization losses seems to make possible the nearly quantitative incorporation of even the more volatile elements, including the alkalis (Na, K, Rb). Known problems associated with this technique include inhomogenities within the glass, contamination by molybdenum, and some loss of Ti and Fe by diffusion into the foil. Problems two and three are not of concern because the degree to which they occur is both small and subject to calibration. The first problem is of serious concern because we desire that the material be homogeneous on a fine scale so that after grinding into powder, the resulting particles will be compositionally identical. Our recommended approach to ensure the latter, based upon previous laboratory experience in sample preparation, is to premix the starting ingredients very thoroughly, and then grind them either in a ball mill or with an automatic mortar and pestle for a very long period of time (3 or 24 hours, respectively) to achieve microscale particle mixing.

A problem not addressed by Brown is the three volatile elements sulfur, chlorine, and carbon. These elements must be incorporated into our melts, but were not required in previous work because the intent was to simulate igneous materials which typically are very low in these volatile elements. Because of the high volatility of several forms of these elements, we consider their incorporation as relatively refractory compounds such as sulfates (for S), chlorides (for Cl), and carbides or carbonates (for C). For most other elements, their oxide forms are considered the appropriate starting material.

A laboratory apparatus has been assembled to make preliminary test fusions. The extent to which this apparatus may be used depends upon the further development of comet dust analytical instrumentation. However, the feasibility of this device has been demonstrated.

The apparatus, which we have termed "Rock Fusion Test Chamber," consists of a hollow metal cylinder constructed of aluminum with 16 mm thick walls. The chamber has inside dimensions of 120 mm diameter by 125 mm high. Feedthroughs for gas, thermocouples, and electrical heating of the molybdenum boat are also provided.

A schematic of the operating controls of the rock fusion apparatus is shown in Figure M-1. In brief, the operating procedure is as follows:

1. The sample is placed in the molybdenum "boat" and the chamber lid is tightened.

2. The chamber is degassed under vacuum for approximately thirty minutes to remove water and other impurities.

3. The chamber is pressurized with argon to approximately 60 psi.

4. The aron is valved out and current is sent through the molybdenum boat.

5. When the boat temperature has reached the desired level, the current is shut off. The melting process may be observed through the quartz viewing window.

6. The valve is opened by a fast-acting valve to quench the sample, then the chamber is backfilled with argon.

7. After cooling, the sample is removed.

Tests accomplished to date demonstrate the unit can readily achieve silicon dioxide melting temperatures, in excess of 1600°C. Future work is planned under the auspices of the Giotto Co-Investigator support contract (JPL-956214)

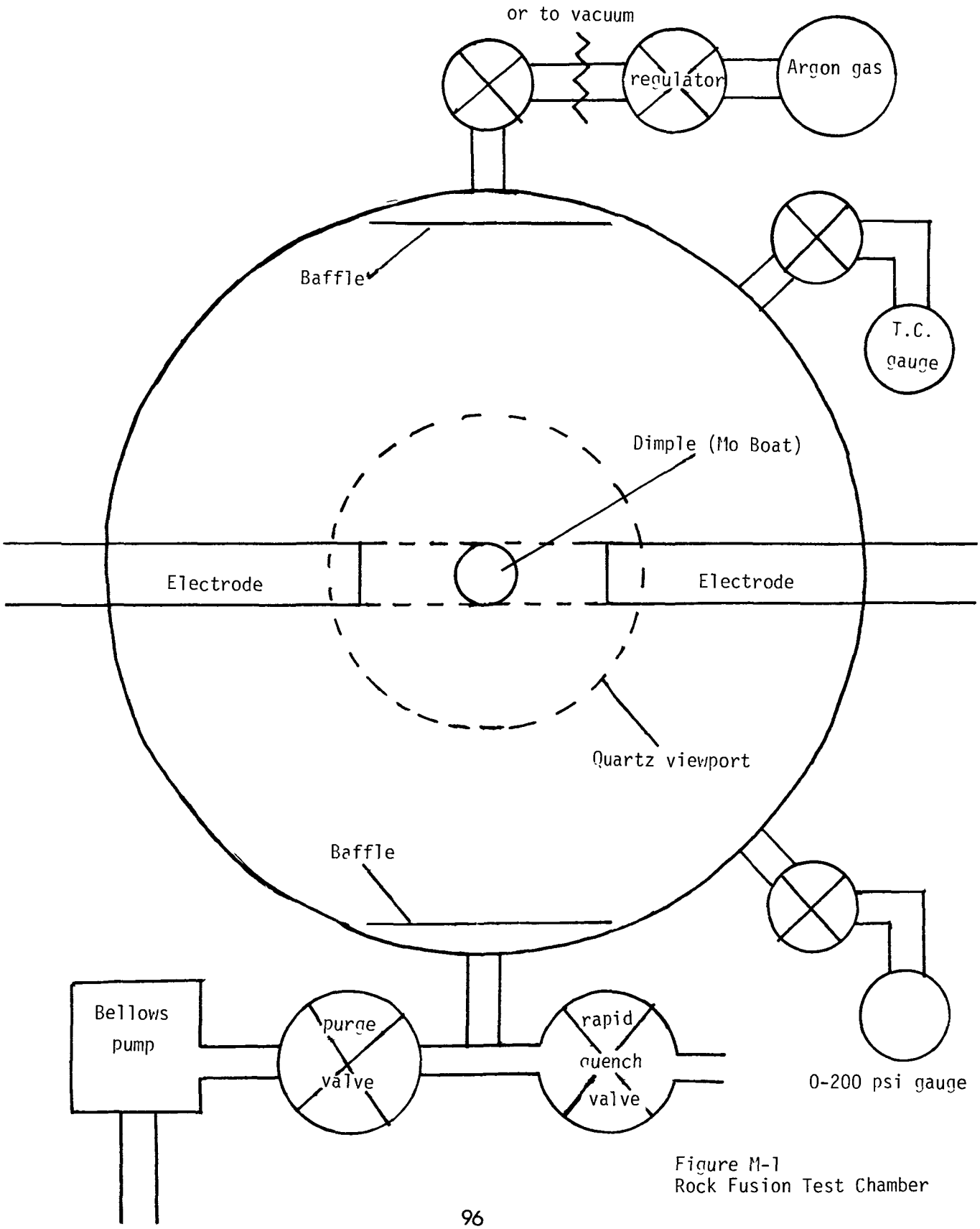

Figure M-1
Rock Fusion Test Chamber

N. Time of Flight Mass Spectrometer Subsystems

During a very first encounter of a comet, such as a flyby mission, it would be very difficult to efficiently collect dust because the kinetic energy is sufficient to completely vaporize the particle upon impact with the collecting material. For these types of missions, an approach being developed by the Max Planck Institute for Nuclear Physics at Heidelberg seems to provide the best possibility for analyzing the chemical composition of individual dust particles. This approach employs a time of flight mass spectrometer (TOFMS), which determines the relative composition of the ions formed by the impact process. An examination of the potential scientific performance of this type of experiment is given in Section O below. An instrument based upon this concept, named the Particle Impact Analyzer (PIA), has now been accepted for the European Space Agency's Giotto mission to fly by Comet Halley.

A number of electronic subsystems and sensors for this instrument deserve special consideration because of the unusual requirements, especially for high operating speeds, of this type of analysis. This includes the possible use of a channeltron multiplier for ion detection, signal buffering using a charge coupled device array, a flash pulse-height converter and analyzer system, and an impact light flash sensor.

Channeltron Multiplier. In previous developments, an electron multiplier sensor has been used to detect and measure the pulse train of ions that emerges from the TOFMS drift tube. Although the electron multiplier has adequate performance for this application, it suffers from a high susceptibility to contamination. Exposure to either humidity or vapors of any substance can lead to a drastic loss in sensor amplification. With fixed electronics, this can lead to reduction of signal to the point that intrinsic noise causes errors in signal measurements, or even that the signal is lost completely due to electronic thresholds. Protection of the electron multiplier means a dry, inert cover gas must be provided at all times until achieving orbit. During cruise, the spacecraft must not outgas so much as to contaminate the delicate sensor surfaces. This could especially be a problem for a long during solar-electric powered mission, where mercury ions are being continuously produced.

The channeltron is a special type of electron multiplier where a continuous strip resistor is formed on the inside wall of the multiplying tube. The resistive material can be made suitably inert to the degrading influences of moisture so that reasonable amounts of exposure to air can be tolerated with only minor effects on sensor gain and sensitivity. Channeltrons have been successfully flown in a number of space-borne instrument packages. Most such devices are produced by Galileo Electro-Optics Corporation.

We have conducted a study of the performance requirements for a channeltron applied to TOFMS readout. Critical parameters are rise time, duty cycle, collector size, input pulse strength, and dynamic range. It is concluded that none of the available models can meet these requirements. However, by careful selection of geometrical and resistive strip properties, it appears feasible to produce a satisfactory device. Our analysis is based upon the concept of modification of the design of a Galileo model 4800 channeltron.

The channeltron utilized must have a high capacitance output stage. The capacitance must be sufficiently high so that enough charge can be stored to

provide a linear output current for a single event. The conductivity of the channel must also be high enough to allow the channeltron to recharge before the next event. Assuming a maximum event rate of one hundred events per second the channel will have 10 ms to recharge.

With these design parameters in mind, what is required is a high conductivity device whose physical parameters allow a 50% increase in capacitance. The device would have an inner wall diameter of 3 mm and outer wall diameter of 5 mm and a length of 20 mm. The calculations show that the device should have a capacitance of 18 pf, and a gain of ten. If this section were used as the output stage of the channeltron it would store 3.6 nC, assuming an effective voltage of 200 volts. With a total channel (entire tube) gain of a thousand, over one million ions could be processed before the section becomes discharged. The dynamic range of the channel will still be limited by instantaneous space charge saturation if too many ions of a single species are present (10^4-10^5 at a single mass unit will cause space charge saturation at a total channel gain of one thousand). The high conductivity allows the channeltron to recharge in 1.8 ms or 555 events/second. Each event may have up to one million ions.

Another possibility for increase the dynamic range of the instrument beyond 1000 for a single event would be to utilize a two stage channeltron. We have discussed this with Galileo but the design of a two stage channeltron has not yet been finalized. Galileo has previous experience in fabricating two stage devices. All the devices being considered would be curved to inhibit ionic feedback. The power consumption of the channeltron would be 5 to 15 mW.

Charge Coupled Device Array for Signal Buffering. One of the chief technical challenges of measurement of the ions after separation in the TOFMS drift tube is the close spacing, in time of arrival, of the ion bunches. For example, the time difference between the potassium mass line and the first calcium mass peak is only 0.3 microseconds. The spread between silver calibration lines can be as small as 0.18 microseconds. These timing problems are discussed further in Section 0 below.

One approach would be to completely analyze each pulse, or ion burst, as it arrives at the detector. This requires very high speed electronics, and this possibility is examined in latter paragraphs. An alternative is to somehow store the sensor output signals at high speed, then read them out at slower speed to allow processing. This is feasible for an experiment of this type because measurement of only 100 particles per second is considered quite adequate from a scientific performance point of view. This would allow up to 10,000 microseconds for electronic processing of the pulse train, about 100 times longer than the duration of the event itself. Reduction of performance speed on the electronics by a factor of 100 is quite significant from a power and complexity standpoint.

We have conducted experimental and design analyses of the application of a charged coupled device (CCD) array for accomplishing the data buffering task. The device selected is the Fairchild 321A. This device has undergone an extensive study for reliability by Martin Marietta Denver Aerospace under NASA contract NAS8-33194. It is capable of operating over a wide range of clocking rates, up to 20 MHz. The CCD device has a published signal-to-noise (SNR) ratio near 1000, but this dynamic range is achieved only when the averaging technique specified by the manufacturer is followed. With averaging the SNR is as poor as only 15 to 1. With suitable layout and circuit operation precautions, we have found that SNRs near 200 are achievable. The larger overall dynamic range required for this experiment can be accommodated by cascading CCD devices, either through attachment of devices to different dynodes (if an electron multiplier is used) or by connection to different pre-amplifier channels who share the sensor output signal (if a channeltron is used).

The CCD units consists of two 455 bit analog shift registers. To store the maximum value during each sampling period, the signal is inverted and the CCD is operated in a mode which initially fills each charge bucket by pulsing the input diode for a short time to a low potential to inject charges across a barrier formed under the first shift register electrode into the following shift register electrode. Then, the input diode is reverse biased and drains all excess charge until the remaining surface potential under the electrode is

equal to the barrier potential under the next electrode. The stored charges can be a measure of the minimum, maximum, or average value of the signal during the sampling interval, depending on the manner in which the CCD controls are connected.

During analysis, the sampling periods of the CCD would be determined as a function of time after start of the impact signal. The sampling times would primarily be determined by a read-only memory (ROM). Values stored in this ROM can readily be altered. Table N-I shows suggested sampling periods between various mass numbers. Sampling would start 3.7 microseconds after the rise of impact signal.

Table N-I Sampling Periods Between Detector Arrival Times for Various Atomic Mass Units

Range of Mass Numbers in AMUs	Sampling Periods in nano seconds
1 to 10	240
10 to 20	120
20 to 60	60
100 to 120	60
120 to 250	20,000

After storage of all samples of one spectrum, the analog values of the CCD would be read out and digitized at a constant rate of approximately 50 kHz. This frequency is primarily determined by the conversion time of the analog-to-digital converter (ADC) which is 15 microseconds. For each sample, an electronic range switch would select the most sensitive unsaturated channel by testing consecutively which of the most sensitive CCD channels has an unsaturated output. This can be accomplished by testing with an AND-gate which of the three more sensitive ADCs has eight high digital outputs. The range switch could also identify the range selected for each signal with a two bit word. Because which time period after particle impact each sample of the spectrum was taken is known, only storage of 512 ten-bit words are required to store one spectrum.

The eight-bit words from the range switch can also be conducted to a digital type of linear-to-logarithmic converter, which is basically a ROM with eight address lines and five binary outputs.

A digital peak valley selector would compare the values of consecutive measurements to determine if the difference is negative, positive, or equal. Additional logic would be used to determine at which sampling intervals a peak or a valley occurred. The respective logarithmic amplitude data would be combined with range and time information, and then stored in buffer locations reserved for groups of valleys or peaks respectively.

Since the CCD is based on technology that is very similar to CMOS technology, the device itself consumes little power. However, the CCD presents a reactive load to the driving circuit. Unless the driving circuit is impedance matched, an excessive amount of power will be lost. Impedance matching may not be a workable solution in this case because two clock rates are needed. An alternative may be found in power switching the CCD since the duty cycle at the fast clock frequency is very small. The power consumption is proportional to the frequency.

The signal processing electronics must be capable of compressing the data in the mass spectrum. With the CCD data processing scheme, it becomes feasible to detect the peaks, valley, and inflection points of the spectrum using a digital differentiation scheme. This can be done either by a series of logic gates, or by operation of microprocessor-driven decision logic. Preliminary studies indicate that the RCA 1802 microprocessor operated at 2 mHz could accomplish the necessary decision code within the processing time available.

Flash Analog-to-Digital System. The alternative approach to the CCD buffering technique is to employ a high speed electronics system capable of processing all signals in real time. This places difficult constraints on several circuits. One of these is the pulse-height measuring circuit. TRW is a manufacturer of high-speed converters, but these devices consume large amounts of power. RCA has just introduced a 6-bit CMOS flash analog-to-

digital converter. This device consumes 35 mW at sampling rate of 11 MHz. Features on the chip allow paralleling two devices to double the sampling rate or one may connect two devices in series to allow for a 7-bit converter. RCA presently has a flight certification program underway for this part. We have received a sample of the new 8-bit version. However, this device has several known defects, which are scheduled for correction in August 1982. At the time of writing, this device is considered the best candidate for pulse analysis of a TOFMS comet experiment.

A second portion of the instrument requiring very high speed operation is the digital logic for storing and processing the converter output. We have a concurrent program in design of very high speed random access memory (RAM) elements based upon CMOS silicon-on-sapphire (SOS) manufacturing technology. Individual units can achieve 4,000 bit storage in 55 nanoseconds. The part is supplied under a special contract by RCA. The device designation is TCS-246, and is currently undergoing a military qualification test program. A power consumption budget is given in Table N-II.

Light Flash Detector. The purpose of the light flash detector is to measure the initial event of impact. Light generated during the impact plasma flash would be detected and the resultant signal used to time-sequence the electronics of the TOFMS analyzer. The two main requirements on this detector are that it may have very fast rise time (10-30 nanoseconds minimum) and sensitivity adequate to detect the impact flash.

Table N-II. Power Profile for High Speed Analysis Subsystems

Section	Power
Channeltron	15 mW
Charge-Integrator	200 mW
Wide Band Log Amp	800 mW
Flash A/D Converter (4 ea.)	140 mW
Clock, pulse arrival and Misc circuits	500 mW
TOTAL	1.7 Watts

The two principal sensors we considered are the silicon photodiode and the vacuum-tube photomultiplier. An EG&G model MHz-016 photodiode having risetime of 12 nanoseconds was selected for testing. Pertinent characteristics of this photodiode are listed in Table N-III. The selected detector was mounted together with a pre-amplifier onto a small electronics board which could be inserted into a target vacuum chamber. Tests were performed at the dust particle accelerator at the Max Planch Institute in Heidelberg. Iron microspheres of one micrometer diameter were accelerated to velocities up to 4 km/sec. No light flashes were detected. Since the absolute light yield has neither been measured for fast sampling intervals nor for very high speed particles, it is not known how much below the photodiode noise threshold the light flash signal was. Comet flyby velocities are typically 50-70 km/sec, so that easily 100 times the energy compared to the 4 km/sec experiments might be available for plasma heating and light emission. Because of the fourth-power relationship of black-body radiation with temperature, several orders of magnitude greater light intensity might be available.

A second approach is to use a miniature photomultiplier tube (PMT). The most reliable such device for space application is a ceramic-construction type manufactured by EMR, Inc. However, during the past year, the EMR miniature-sized tubes have been phased out of production. A candidate replacement would be the PMT miniature series manufactured by Hamamatsu, Ltd. A typical device is 14 mm in diameter, 84 mm long, and has an electronic gain of one million at 1000 VDC bias. These tubes are available with bialkali or CsTe photocathodes, the latter being a solar-blind, UV sensitive cathode.

Table N-III. Photodiode Characteristics

Active Area	133 mm sq.
Spectral Range	350 to 1150 nm
Sensitivity Limits	
at 800 nm	6 microwatts
at 350 and 1150 nm	70 microwatts
ultimate (full bandwidth)	0.01 microwatts
Rise Time	
intrinsive	12 nsec
with miniature pre-amplifer	25 nsec
Operating Temperature	0 to 70°C

0. Scientific Performance Criteria for the TOFMS

The Time of Flight Mass Spectrometer (TOFMS) is a proposed experiment for analysis of the composition of comet dust particles. On a rendezvous mission, an intense ion beam or energetic laser pulse would be used to vaporize and ionize comet dust collected on a suitable substrate. For a fast flyby mission, the dust particles are simply allowed to strike a target; their extremely high kinetic energy resulting from high flyby velocity will then be transformed into heat sufficient to vaporize and ionize the constituent atoms.

An electrostatic time of flight mass spectrometer then collects, separates, and analyzes the resulting ions. Many factors can affect the scientific performance of such an instrument, but a fundamental limitation is associated with the overlaps from element-to-element because of isotope effects. First, we should consider the possible range of particle types.

Data relevant to particle compositions derives from our knowledge of the compositions of the sun, meteorites, asteroids, extraterrestrial particles collected from the atmosphere, and what little we know so far about comets. Possible particle types include:

(1) Solar-like grains, with bulk composition approximately that of the sun or CI meteorites. Such grains are especially rich in Si, Mg, Fe, S, and O.

(2) Mafic silicate grains, similar or identical to olivine or pyroxene compositions (Mg, Si, Fe, O).

(3) Fe-rich grains, often containing S, Ni, and minor elements.

(4) Aluminosilicate grains, with Al, Si, and O, but also possibly Ca, Fe, Mg, Na, etc.

(5) Ice grains, probably mostly H_2O, but possibly also containing C and N-based molecules.

(6) Carbonaceous grains, containing organics rich in C and H, with also O and N.

(7) Volatile-rich grains (with high Zn, Hg, S, Cl or other volatile species).

Heterogeneous combinations of almost any of these are possible. For example, carbonaceous material or ice may well be an intimate mixture or coating of the rocky or metallic types of particles. We should also consider the possibility, however remote, of secondary alteration processes, resulting in amorphous or mineral species quite unlike the seven types given above. For example, the composition of a typical CI meteorite is as given in Table O-I. These include:

(8) Magnetite (Fe_3O_4)

(9) Salt grains, especially sulfates (S, O, Mg, Ca, Fe, Na, Cl, Br)

(10) Oxides of various elements

(11) Reduced compounds (carbon black, SiC, native Fe, sulfides, etc.)

(12) Hydrated silicates

Table O-I. Calculated Amounts of Minerals in Orgueil, %

Clay minerals	62.6
Magnetite	6.0
Troilite	4.6
Sulfur	1.7
Limonite	0.5
Merrilite	0.8
Breunnerite	2.8
Magnesium Sulfate	6.7
Gypsum	2.9
Sodium Sulfate	0.6
Carbon	2.9
Remaining Metals	1.1
	93.2

(Bostrom and Fredriksson, 1966)

Of all of these particle types, the most difficult to analyze to high accuracy will be the grains which are also the most important, viz., the solar-like grains. In Table O-II, we have determined the mass levels expected in a TOFMS spectrum if the particle were solar-like and if all elements are ionized and detected with equal efficiency. This analysis is based upon the relative isotope abundances for the elements on the earth. A plot of this spectrum is shown in Figure O-1.

Table O-II. Mass Spectrum for Solar Composition

(Assumes unit efficiencies)

Mass spectrum for: Solar comp 'CI' 'Rel to 1 um part'

Particle diameter = 1.0 microns

Mass No.	Tot Intensity		Contributors	Z	Sym	Comp: '%'	ppm
1	199.9700	2.000E+02	H				
2	.0300	3.000E-02	H	1	H	2.000	20000
12	306.5590	3.066E+02	C	6	C	3.100	31000
13	3.4410	3.441E+00	C				
14	25.9038	2.590E+01	N	7	N	.260	2600
15	.0962	9.620E-02	N				
16	4588.9140	4.589E+03	O	8	O	46.000	460000
17	1.7020	1.702E+00	O				
18	9.3840	9.384E+00	O	9	F	.025	251
23	51.0000	5.100E+01	Na				
24	755.5200	7.555E+02	Mg	12	Mg	9.600	96000
25	97.2480	9.725E+01	Mg				
26	107.2320	1.072E+02	Mg	13	Al	.850	8500
27	85.0000	8.500E+01	Al				
28	968.2050	9.682E+02	Si	14	Si	10.500	105000
29	49.3500	4.935E+01	Si				
30	32.4450	3.245E+01	Si	15	P	.100	1000
31	10.0000	1.000E+01	P				
32	560.5000	5.605E+02	S	16	S	5.900	59000
33	4.4840	4.484E+00	S				
34	24.8980	2.490E+01	S	17	Cl	.044	440
35	3.3233	3.323E+00	Cl				
36	.0829	8.294E-02	S,Ar	18	Ar	.001	10
37	1.0767	1.077E+00	Cl				
38	.0001	6.300E-05	Ar	19	K	.044	440
39	4.1228	4.123E+00	K				
40	106.7667	1.068E+02	Ar,K,Ca	20	Ca	1.100	11000
41	.3027	3.027E-01	K				
42	.7040	7.040E-01	Ca	21	Sc	.001	5
43	.1595	1.595E-01	Ca				
44	2.2660	2.266E+00	Ca	22	Ti	.043	430
45	.0500	5.000E-02	Sc				
46	.3446	3.446E-01	Ca,Ti	23	V	.005	49
47	.3130	3.130E-01	Ti				
48	3.3774	3.377E+00	Ca,Ti	24	Cr	.240	2400
49	.2369	2.369E-01	Ti				
50	1.2652	1.265E+00	Ti,V,Cr	25	Mn	.190	1900
51	.4888	4.888E-01	V				
52	20.1024	2.010E+01	Cr	26	Fe	18.400	184000
53	2.2920	2.292E+00	Cr				
54	107.6592	1.077E+02	Cr,Fe	27	Co	.050	500
55	19.0000	1.900E+01	Mn				
56	1686.5440	1.687E+03	Fe	28	Ni	1.100	11000
57	40.2960	4.030E+01	Fe				
58	80.7400	8.074E+01	Fe,Ni				
59	5.0000	5.000E+00	Co				
60	28.8530	2.885E+01	Ni				
61	1.3090	1.309E+00	Ni				
62	4.0260	4.026E+00	Ni				
64	1.1880	1.188E+00	Ni				

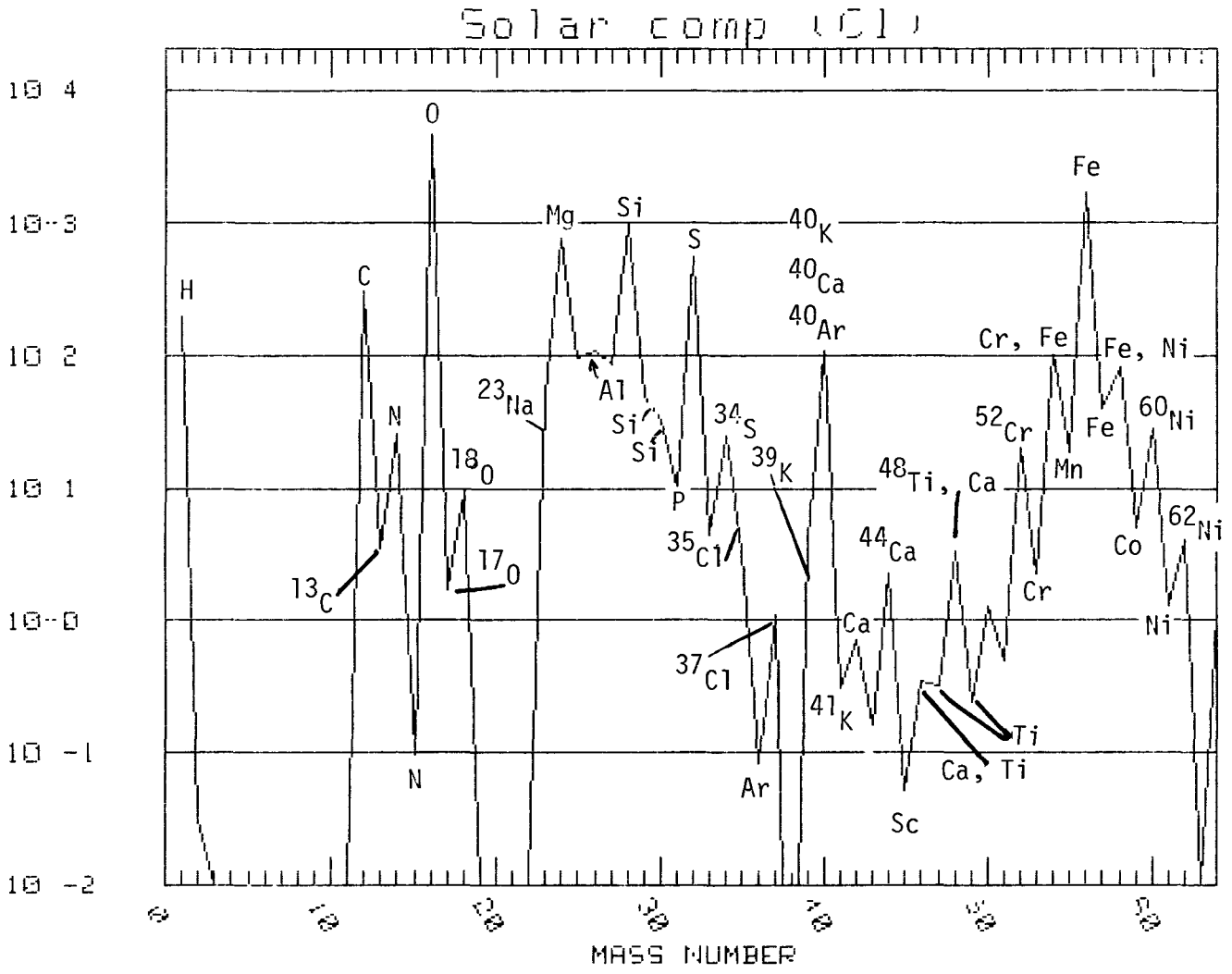

Figure 0-1
Plot of TOFMS spectrum of ideal solar compositon particle(assumes unit efficiency for all masses)

This analysis shows that several elements may be difficult to resolve because they produce small peaks in the neighborhood of much larger peaks. One example is aluminum. At the position of 27 AMU (Atomic Mass Units), Al is alone. However, both Mg and Si are much higher peaks. If smearing occurs, either because some Mg ions arrive late or Si ions arrive early down the drift tube, they can erroneously be counted as Al ions. Another difficult element may be phosphorus, in danger of being overridden by the much more abundant Si and S in the particle. Chlorine may also be a problem, although Cl-37, less abundant than Cl-35, is three mass numbers away from the likely interferents, S-34 and Ca-40. Potassium and sodium are also likely to be difficult; K-39 and K-41 may be swamped by Ca; Na-23 may be hard to resolve accurately in the presence of background from Mg-24. Manganese is alone at 55 AMU, but sandwiched between the Cr-54 and very strong Fe-56 peaks. Cobalt (Co-59) will probably be completely obliterated by Ni-59, second most abundant isotope of nickel.

On the other hand, elements such as H, C, N, O, Mg, Si, S, Ca, Ti, Cr, Fe, and Ni may all be detected readily, in some cases by two or more peaks. In addition, the alkalis (Li, Na, K, Rb) are very readily ionized, so that their signals may become relatively much higher, thereby making their detection easier. Note also that the total intensity range of interest is almost five orders of magnitude. Since particles may easily cover the range of 0.4 um to 30 um in size, there are an additional 8 orders of magnitude in particle mass which can be encountered. Limitations in ion collection efficiency due to space charge limiting may further constrict these 8 magnitudes to perhaps 4. Nonetheless, the total range desired is still 5 + 4 = 9 orders of magnitude in sensitivity. Accurate measurements over this entire range is unlikely to be achievable in a flight instrument, but if enough particle data is obtained it may be possible to classify different groups and then pool the data within each group to obtain overall composition for a large number of elements.

III. SUMMARY AND CONCLUSIONS

X-ray techniques have been devised for comet dust composition and flux analysis. Sample collection techniques have been designed and tested to demonstrate feasibility. A number of detailed engineering studies have been applied to the major problems anticipated for conducting an x-ray based experiment on a comet rendezvous mission. It should be possible to not only collect adequate dust sample for analysis, but to discriminate to some degree between particle types and to monitor temporal changes in dust emission.

The chemical analysis based upon x-ray fluorescence will be sufficiently accurate to distinguish whether the dust is compositionally similar to any of the known meteorite classes, or whether it is unique. Some 15 to 25 major, minor, and trace elements will be susceptible to analysis, depending upon the exact composition of the dust. These elements include Si, Fe, O, Mg, S, Ca, C, Ni, Na, Al, Cr, Mn, N, Cl, K, Ti, Zn, V, Ge, Zr, and Sr.

X-ray diffraction and direct electron beam excitation of the comet nucleus ("electron macroprobe") are feasible, but technically more difficult experiments which could provide additional scientific information of fundamental significance. A time-of-flight mass spectrometer analysis is feasible for flyby modes, but unlikely to provide as accurate analyses as can be achieved with dust collection and detailed analysis during a rendezvous mission.